Philemon's Thesis_Report .pdf

📋 My Files

🖥 My Files

🎓 Delhi Technological University

Document Details

Submission ID

trn:oid:::27535:74683339

Submission Date

Dec 23, 2024, 6:44 PM GMT+5:30

Download Date

Dec 23, 2024, 7:12 PM GMT+5:30

File Name

Philemon's Thesis_Report .pdf

File Size

59.8 MB

161 Pages

31,071 Words

169,127 Characters

3% Overall Similarity

The combined total of all matches, including overlapping sources, for each database.

Filtered from the Report

- Bibliography
- Cited Text
- Small Matches (less than 10 words)

Exclusions

- 89 Excluded Matches

Match Groups

72 Not Cited or Quoted 3%
Matches with neither in-text citation nor quotation marks

0 Missing Quotations 0%
Matches that are still very similar to source material

0 Missing Citation 0%
Matches that have quotation marks, but no in-text citation

0 Cited and Quoted 0%
Matches with in-text citation present, but no quotation marks

Top Sources

1%   🌐 Internet sources

2%   📖 Publications

1%   👤 Submitted works (Student Papers)

Integrity Flags

1 Integrity Flag for Review

🚩 **Replaced Characters**
67 suspect characters on 14 pages
Letters are swapped with similar characters from another alphabet.

Our system's algorithms look deeply at a document for any inconsistencies that would set it apart from a normal submission. If we notice something strange, we flag it for you to review.

A Flag is not necessarily an indicator of a problem. However, we'd recommend you focus your attention there for further review.

Match Groups

72 Not Cited or Quoted 3%
Matches with neither in-text citation nor quotation marks

0 Missing Quotations 0%
Matches that are still very similar to source material

0 Missing Citation 0%
Matches that have quotation marks, but no in-text citation

0 Cited and Quoted 0%
Matches with in-text citation present, but no quotation marks

Top Sources

1% 🌐 Internet sources

2% 📖 Publications

1% 👤 Submitted works (Student Papers)

Top Sources

The sources with the highest number of matches within the submission. Overlapping sources will not be displayed.

1	Publication	
Singh, Mukhtiar. "Adaptive network-based fuzzy inference systems for sensorless...		0%

2	Internet	
dspace.dtu.ac.in:8080		0%

3	Internet	
escholarship.mcgill.ca		0%

4	Submitted works	
University of Hong Kong on 2024-05-16		0%

5	Publication	
Chu Sun, Syed Qaseem Ali, Geza Joos, Francois Bouffard. "Virtual Synchronous Ma...		0%

6	Publication	
Gaurav Yadav, Mukhtiar Singh. "Unveiling the Superiority: Comparative Analysis ...		0%

7	Internet	
dr.ntu.edu.sg		0%

8	Publication	
Mehdi Sajadinia. "An adaptive virtual inertia control design for energy storage de...		0%

9	Publication	
"Automatic Control and Emerging Technologies", Springer Science and Business ...		0%

10	Internet	
unsworks.unsw.edu.au		0%

11 Submitted works

Queen's University of Belfast on 2022-03-08   0%

12 Submitted works

University of Edinburgh on 2022-04-28   0%

13 Internet

onlinelibrary.wiley.com   0%

14 Submitted works

University of Leeds on 2016-08-25   0%

15 Publication

Begum, Mahmuda. "Distributed Cooperative Control for Autonomous Microgrids"...   0%

16 Publication

Mohammad Reza Babaei, Ali Ghasemi-Marzbali, Soolmaz Abbasalizadeh. "Control...   0%

17 Publication

Pedro Jose dos Santos Neto, Tarcio Andre dos Santos Barros, Joao Pedro Carvalho ...   0%

18 Submitted works

Indian Institute of Technology, Madras on 2016-04-08   0%

19 Submitted works

Mississippi State University on 2020-03-03   0%

20 Internet

anavidal.webs.uvigo.es   0%

21 Publication

Fang Lin Luo, Hong Ye. "Power Electronics - Advanced Conversion Technologies", ...   0%

22 Submitted works

Greater Noida Institute of Technology on 2022-12-13   0%

23 Submitted works

Institute of Technology, Nirma University on 2018-09-24   0%

24 Submitted works

University of Hong Kong on 2020-04-07   0%

25	Submitted works	
Veer Surendra Sai University of Technology on 2016-06-06		0%

26	Internet	
digitalcommons.du.edu		0%

27	Internet	
gtusitecirculars.s3.amazonaws.com		0%

28	Submitted works	
Anna University on 2024-05-09		0%

29	Publication	
Debouche Naamane, Habib Benbouhenni, Ali Chebabhi, Zarour Laid, Dalal Zellou...		0%

30	Publication	
Hassan Bevrani, Hêmin Golpîra, Arturo Román Messina, Nikos Hatziargyriou, Fed...		0%

31	Publication	
Jaipal Saroha, Mukhtiar Singh, Dinesh Kumar Jain. "ANFIS Based Add-on Controlle...		0%

32	Publication	
Mahmoud M. Elwakil, Helmy M. El Zoghaby, Soliman M. Sharaf, Magdi A. Mosa. ""...		0%

33	Publication	
Majid Mehrasa, Abdolreza Sheikholeslami, Mohammad Rezanejad, Jaber Alipoor e...		0%

34	Submitted works	
National Institute of Technology, Silchar on 2018-07-20		0%

35	Publication	
R. Navanietha Krishnaraj, Jong-Sung Yu. "Bioenergy - Opportunities and Challeng...		0%

36	Submitted works	
RMIT University on 2024-10-28		0%

37	Submitted works	
Victoria University on 2018-04-15		0%

38	Internet	
upcommons.upc.edu		0%

39 Submitted works

Anna University on 2024-11-09 0%

40 Publication

Hae-Gwang Jeong, Ui-Min Choi, Kyo-Beum Lee. "Control strategies for wind powe... 0%

41 Publication

Hu, Jiefeng. "Advanced Control in Smart Microgrids", University of Technology Sy... 0%

42 Submitted works

IIT Delhi on 2018-02-21 0%

43 Publication

Kassiane de S. Medeiros, João Marcus S. Callegari, Lorrana F. Da Rocha, Danilo I. B... 0%

44 Publication

Kesara Wimal. "A Truly Decentralized Consensus Protocol that Eliminates Tenden... 0%

45 Publication

Khadkikar, Vinod. "Power quality enhancement at distribution level utilizing the ... 0%

46 Publication

Mariem Y. Yousef, Magdi A. Mosa, Said M. El Masry, A.M. Abdel Ghany, A.A. Ali. "D... 0%

47 Publication

Thongchart Kerdphol, Fathin Saifur Rahman, Masayuki Watanabe, Yasunori Mita... 0%

48 Submitted works

Victoria University on 2017-11-29 0%

49 Internet

backend.orbit.dtu.dk 0%

50 Internet

openprairie.sdstate.edu 0%

51 Internet

spiral.imperial.ac.uk 0%

VIRTUAL SYNCHRONOUS MACHINE CONTROL STRATEGIES IN LOW INERTIA MICRO-GRID

A Thesis Submitted
In Partial Fulfillment of the Requirements
for the Degree of

DOCTOR OF PHILOSOPHY

by

PHILEMON YEGON

(Roll No. 2K21/PHDEE/24)

Under the Supervision of
Prof. Mukhtiar Singh
Department of Electrical Engineering
Delhi Technological University, Delhi - 110042

Department of Electrical Engineering

DELHI TECHNOLOGICAL UNIVERSITY

(Formerly Delhi College of Engineering)
Shahbad Daulatpur, Main Bawana Road, Delhi - 110042. INDIA

October, 2024

DELHI TECHNOLOGICAL UNIVERSITY
(Formerly Delhi College of Engineering)
Shahbad Daulatpur, Main Bawana Road, Delhi-42

CANDIDATE'S DECLARATION

I hereby certify that the work which is being presented in the thesis entitled **VIRTUAL SYNCHRONOUS MACHINE CONTROL STRATEGIES IN LOW INERTIA MICRO-GRID** in partial fulfillment of the requirements for the award of the Degree of Doctor of Philosophy and submitted in the Department of Electrical Engineering of the Delhi Technological University is an authentic record of my own work carried out during the period from August, 2021 to October, 2024 under the supervision of Prof. Mukhtiar Singh, Department of Electrical Engineering

The matter presented in this thesis has not been submitted by me for the award of any other degree of this or any other Institute.

(Philemon Yegon)

This is to certify that the student has incorporated at the corrections suggested by the examiners in the thesis and the statement made by the candidate is correct to the best of our knowledge.

Signature of Supervisors

Signature of External Examiner

DELHI TECHNOLOGICAL UNIVERSITY

(Formerly Delhi College of Engineering)
Shahbad Daulatpur, Main Bawana Road, Delhi-42

CERTIFICATE BY THE SUPERVISORS

Certify that **Philemon Yegon** (2K21/PHDEE/24) has carried out their work presented in this thesis entitled "**VIRTUAL SYNCHRONOUS MACHINE CONTROL STRATEGIES IN LOW INERTIA MICRO-GRID**" for the award of **Doctor of Philosophy** from Department of Electrical Engineering, Delhi Technological University, Delhi, under my supervision. The thesis embodies results of original work, and studies are carried out by the student himself and the content of the thesis do not form the basis for the award of any other degree to the candidate or to anybody else from this or any other University/Institute.

(Mukhtiar Singh)
    Supervisor

Date:

v

Abstract

In the recent past, energy sector has undergone significant transformations. On one hand, world demand is rising, while tradition power sources, mostly reliant on fossil fuels, are fast phased out by de-commissioning of old power plants. Furthermore, these conventional methods lack ecological sustainability. The combustion of coal releases greenhouse gases (GHGs), which pollute the environment and endanger the surrounding ecosystem. Furthermore, they emit carbon dioxide, methane gas and nitrogen dioxide which are the highest contributors of global warming. The hazardous effect of global warming includes melting of mountain ice caps, extreme weather pattern alterations, flooding, storms, and droughts. This scenario has compelled policymakers from various countries to reconsider how to address the always increasing energy demand while mitigating the adverse effects of traditional energy sources. To tackle these difficulties, renewable energy sources (RES) have assumed a more significant role. However, high penetration of RES reduces inertia in the system due to their integration with power electronics devices which lack rotational mass for kinetic energy. Reduced inertia contributes heavily on frequency instability. The modern power system easily loss synchronism over the slightest disturbance because of low inertia. Microgrid concept is taking shape as the alternative sources of energy. It can be either grid connected or islanding mode. Grid forming voltage converters enable islanding mode due to their designed to participate in regulation of voltage and frequency at the point of common coupling (PLL). Its contained energy storage system in the cluster of energy sources. The grid-connected is commonly grid following voltage converters, it only delivers power and does not participate in voltage or frequency control. Microgrid provide power to specific group of consumers. It can be hospital, school or residential areas. Microgrids comprises of diverse sources energy, such as energy storage systems, fuel cells, solar PV panels, and wind turbines. Notwithstanding the intermittent nature of RES, the microgrid frequency control

vi

take into account the changes from both the source and load sides, the control of microgrid frequency becomes more important for maintaining reliable operation and energy security. To simulate the isolated microgrid, a complex technique is used to address the requirements of the secondary controller and the primary frequency regulation of the diesel engine generating unit. In addition, the isolated microgrid is connected to a diesel power plant, wind turbine, solar plant and battery/ultracapacitor to conduct experiments on load fluctuations, wind speed variations and solar radiation variations and their total shutdown. In best practices, integrated microgrid with the diesel power plant allows possibility of distributing the economic load demand between the microgrid and the diesel power units. The thermal unit only provides power during periods of high demand. The baseload needs are met by other units within the integrated microgrid. The investigations are conducted in different scenarios to determine the viability of energy storage devices in isolated and integrated microgrids. The primary difficulties in microgrid voltage and frequency regulation for converter regulation. Microgrid distributed generation incorporates the use of the Virtual Synchronous machine (VSM), droop controller, optimisation technology, and RES to increase the transient and small signal responsiveness in the microgrid (MG). The purpose of the power converter is to deliver voltage and current in a way that is appropriate for consumer loads in order to process and regulate the supply of power. In order to enhance the frequency responsiveness of the microgrid during disturbances such as significant frequency deviations. Typically, the PI controller or PID controller utilizes as a secondary controller in the frequency control of the microgrid. Further research was conducted on the control architecture of combining standard secondary controllers in a cascading manner to create innovative combinations of cascaded controllers. The effectiveness of this cascaded controller is evaluated by implementing improved swam optimization algorithm, genetic algorithm and model predictive control (MPC). The novel modified PSO techniques was formulated and implemented in the system to fine tune PID controller. The purpose of modified PSO technique is to maximise the control parameters in order to regulate the disturbances occurred in the microgrid such as frequency, RoCoF as well as voltage due to inertia variation. The results were compared with conventional techniques. Hybrid energy storage system that's battery and ultracapacitor were

vii

incorporated in the microgrid to supplied the needed energy during the disturbances and also during the normal working of the microgrid. Battery is known for its high energy density but low power density (slow response) while ultracapacitor has high power density and low energy density (quick response). The two energy storage devices complement each other while responding to the disturbances. The control seeks to simulate inertia and damping using ultracapacitor which replicate prime mover of synchronous generators (kinetic energy). In this thesis, energy needed for inertia and damping is determined to compensate for energy loss. MATLAB Simulink environment was used to test effectiveness of the proposed techniques consequently, the comparison was conducted with the conventional methods and the results clearly demonstrated the efficacy of the proposed strategies microgrid frequency response. Finaly, real time validation was conducted on OP4510 OPAL-RT emulator.

viii

Acknowledgements

This thesis is the final results of my Ph.D. endeavour, and I would like to express my gratitude to all those who have provided assistance and contributed to making this trip an indelible and remarkable experience for me. First and foremost, I express my sincere thanks to the heavenly father, God, for bestowing upon me blessings; life, good health, and the incredible vigour that has enabled me to accomplish my educational aspirations. I would like to express my greatest appreciation to my guide, Prof. Mukhtiar Singh, Professor in the Department of Electrical Engineering at Delhi Technological University (DTU), for his exceptional guidance, research assistance, patience, encouragement, extensive expertise, and unwavering support during my studies. This thesis would not have been completed without his unwavering dedication and mentorship. The guidance he provided was invaluable in doing research and writing my thesis.   He is really the most exceptional guide and mentor, demonstrating his exceptional competence in leadership and unwavering dedication. I would like to express my gratitude to Prof. Uma Nangia, the previous head of EED, and Prof. Rachana Garg, the current head of EED, as well as all other academic and staff members, for their invaluable support as well as cooperation during my research and coursework. I express thanks to the Department of Electrical Engineering for providing me with the essential resources to work with maximum efficiency within the given time constraints. I would like to extend my sincere gratitude to my senior and colleagues, Dr. Aakash Seth, Nimmi, Ashutosh, and Gaurav in the microgrid operation & control Research facility. Their scientific contributions, meaningful discussions, encouragement, and enjoyable experiences have been instrumental throughout this challenging yet remarkable journey. I express my gratitude to them for their significant scientific contributions, productive talks, inspiration, and enjoyable experiences. I would like to express my sincere thanks to the staff members of our Power Electronics Laboratory, notably Ms. Renu, Ms. Vandana, and Mr. Raju, for their unwavering support and assistance during my research work. Their personal and professional assistance, motivation, and moral support have contributed to my increased sense of tranquillity. The time I spent with them will

ix

forever be one of the most unforgettable and pleasurable moments of my life. I would like to show my appreciation to my mum Mrs Jane Cherop Cheruiyot, as well as my siblings Joan, Abigael, Purity, Tabitha and Denis, for their love, continual care, and emotional support they gave me during my study. Their unwavering trust in me and confidence have always been driving forces in pursuing my goal. I would like to express my gratitude to my wife, Mrs Faith Chepngeno Yegon, and my sons; Adrian Kiplangat Kirui, Ivan Kiprotich Kirui and Harry Kipkoech Kirui for their love, emotional support, understanding, cooperation, patience and encouragement they gave me throughout my Ph.D. studies. I am indebted. Thank you. I would like to express my gratitude to Indian council for cultural relations (ICCR) and Kenyatta University (KU) for their kind financial assistance throughout my research endeavour.

Date: Philemon Yegon

x

This thesis is dedicated to my beloved father
Late Mr. David Kipyegon Cheruiyot

Contents

xii

xiii

xiv

List of Figures

xvi

List of Tables

xviii

List of Abbreviations

VSM	Virtual Synchronous Machine
VI	Virtual Inertia
VSC	voltage Source Converter
SC	Synchronous Condensers
EV	Electric Vehicles
IBR	Inverter Based Resources
RES	Renewable energy sources
ESS	Energy Storage System
HESS	Hybrid Energy Storage System
RoCoF	Rate of Change of Frequency
DG	Distributed Generation System
PSO	Particle Swarm Optimization Technique
MPSO	Improvised Particle Swarm Optimization
GHG	Greenhouse Gas
THD	Total Harmonic Distortion
VSMs	virtual synchronous machines
KNDGC	Kenya National Grid Distribution Code
NERC	North American Electric Reliability Corporation
MG	Microgrid
PID	Proportional (Kp), Integral (Ki) and Derivative (Kd) controller
ANFIS	Adaptive Neuro-Fuzzy Inference System
FOPID	Fractional Order PID
MCP	Model Predictive Control
PQ	Active and Reactive Power
FFR	Fast Frequency Response
IGBT	Insulated-Gate Bipolar Transistor
ITAE	Integral of Time-Weighted Absolute Error

xix

IAE	Integral of Absolute Error
ITSE	Integral of Time-weighted Squared Error
ISE	Integral of Square Error
PWM	Pulse Width Modulation
PLL	Point of Common Coupling
SPV	Solar PhotoVoltaic
SoC	State of Charge
FAESS	Fast-Acting Energy Storage System
SAESS	Slow Acting Energy Storage System
RPM	Ragone Plot Method
SBM	Search-Based Methods
AM	Analytical Methods
PAM	Pinch Analysis Method
SM	Statistical Methods
VSG	Virtual synchronous generators
VOC	Voltage-Oriented Control
UPF	Unity Power Factor
SMC	Sliding Mode Control
VFOPID	Variable fractional order PID
PTS	Power Transformation System
MOSFET	Metal Oxide Semiconductor Field Effect Transistor

1

Chapter 1

Introduction

This chapter provides a brief synopsis of the subjects examined in this thesis. This work outlines the research dimensions arising from a critical review of Virtual Synchronous Machine Control Strategies in Low Inertia Micro-Grids, thereby laying out the contributions presented in this thesis.

1.1   Background

Recently, the worldwide power sector is going through lot of transformations. On the one side, global demand is on rising side while conventional power generation primarily dependent on fossil fuel is declining very rapidly. Moreover, these conventional techniques lack ecological sustainability. Coal combustion emits greenhouse gases (GHGs), which pollute the environment and poses a threat to the local ecosystem. In addition, they release carbon dioxide, which has resulted in global warming. The global warming is causing several environmental challenges such as severe weather changes patterns, flooding, droughts, storms, and melting of ice caps in mountains. Several countries throughout the globe are grappling with the issue of increasing energy consumption. As these scenarios continue to grow in number, the traditional means of generating electricity, such as coal use, are being surpassed by necessity. This scenario has forced the policy makers to rethink about meeting the everlasting growing energy demand while combating the ill effect of conventional generation. In order to address these challenges, renewable energy sources (RES) such as solar power and wind power plants have taken on a more prominent role.   However, the increasing penetration of RES has caused

Chapter 1. Introduction
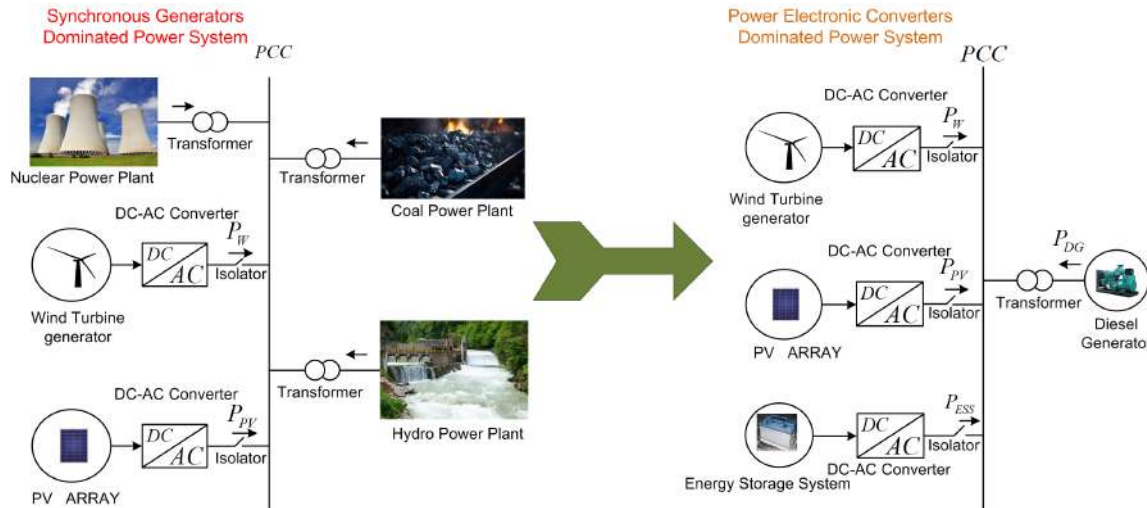
FIGURE 1.1: Modern Power System

instability in the system due to their intermittency and increased power electronics interface [3]. Power electronics equipment lacks inherent inertia energy which is readily available in case of synchronous machine based traditional network. The dominance of power electronics power system causes reduction in inertia, resulting in frequency instability and low inertial response. With such evidential challenges, several methods have been put forward to solve this threat in modern power system grid. Here are some techniques: The modern wind turbines include Permanent Magnet Synchronous Machines (PMSMs), fixed and variable speed induction generators and synchronous generators. Due to variation of wind in speed and direction during energy transformation, power electronics converter interface plays a crucial function. The power electronics converters are required to regulate grid frequency and voltage and stabilised them since the wind turbines operate at varying speeds due to change of weather. It ensures optimal power conversion over a given range of wind speed. These converters are designed in various topologies according to their applications.

Synchronous condenser (SC) is a rotating electrical machine which operates as a motor with no load or generator without a driver. The SC is regulated through excitation control just like synchronous generator. Traditionally, it has been utilized to consume or produced reactive power through varied excitation. It is also found to be very suitable for some sort of frequency support thanks to

the kinetic energy stored in its inertia. Hence, the SC outperformed static VAR compensators as it can provide reactive power compensation and also participates in inertia control through short circuit power. Further, it is not only the high penetration of RES but also the de-commissioning of old thermal power plants which is resulting into the reduced inertia. As a results of weak grid, challenges like low short circuit level, high frequency variations, high rate of change of frequency (RoCoF), and problems of voltage sags and swell are becoming great headache for power system operators. To address the above-mentioned challenges, SC are getting renewed interest. However, the higher installation cost, high rotational energy losses and regular maintenance requirement are some of the hindrances.

Currently, energy storage systems (ESS) are also used to provide grid support, playing a crucial role in managing power fluctuations from unstable renewable energy sources. Battery and ultra-capacitor energy storage systems are increasingly important for frequency control [4]. Batteries have desirable characteristics such as moderate cost, moderate response time, and high energy density, discharge times from seconds to hours, moderate power density, lifetimes of 3 to 15 years (250 to 1500 cycles), and efficiencies between 75% and 90% [5, 6]. In the charging state, battery voltage is fixed and cannot be easily regulated; however, output power can be controlled to manage this limitation. Battery storage systems can also be used for inertia emulation by applying proportional gain and combining it with the RoCoF. Frequency improvement is possible with ESS which has fast response frequency characteristic and has a flexible quality in terms of charging and discharging [7].

On the other hand, ultra-capacitors are used when the DC-link inertia emulation is insufficient due to their superior energy storage capacity. Ultra-capacitors offer advantages such as high-power density and a relatively long lifespan. Lifespans of 4 to 12 years (over 50,000 cycles), and efficiencies between 85% and 98%. A well-designed controller enables a DC-DC converter to precisely regulate the ultra-capacitor voltage to align with the reference voltage. Furthermore, specific techniques centered around Partial loading have been suggested to leverage the available capacity for inertial response. Operating a power plant under partial load conditions is very inefficient and results in a higher per unit cost of energy output. Recently, the concept of virtual

Chapter 1. Introduction

synchronous machines (VSMs) emulated through power converter is gaining lot of popularity [8, 9]. The basics working principle of VSM is to emulate swing equation in synchronous machine, in most power electronics-dominant power system VSM is becoming popular. With tuning and best optimization techniques continuously improving, VSM has outsmart conventional synchronous generator. Damping and inertia is large in VSM and has fast frequency response. Since its parameters are purely out of programmed system, it is flexible hence easily adjusted. Micro-grid and distributed energy resources can graciously utilize this VSM quality [10]. The purpose of the power converter is to deliver voltage and current in a way that is appropriate for consumer loads in order to process and regulate the supply of power. In order to enhance the frequency responsiveness of the microgrid during disturbances such as significant frequency deviations. Typically, the PI controller or PID controller utilizes as a secondary controller in the frequency control of the microgrid. Further research was conducted on the control architecture of combining standard secondary controllers in a cascading manner to create innovative combinations of cascaded controllers. The effectiveness of this cascaded controller is evaluated by implementing improved swam optimization algorithm, genetic algorithm and model predictive control (MPC). The novel modified PSO techniques was formulated and implemented in the system to fine tune PID controller. The purpose of modified PSO technique is to maximise the control parameters in order to regulate the disturbances occurred in the microgrid such as frequency, RoCoF as well as voltage due to inertia variation. The results were compared with conventional techniques.

1.1.1 Microgrid

The microgrid concept is emerging as an alternate energy source. It can function in either grid-connected or islanding mode. Grid-forming voltage converters facilitate islanding mode as they are engineered to regulate voltage and frequency at the PLL. It incorporates an integrated ESS among the group of energy sources. Grid-connected mode typically consist of grid-following voltage converters, which solely provide electricity without engaging in voltage or frequency regulation. Microgrids supply electricity to designated groups of

consumers. It may pertain to hospitals, educational institutions, or residential zones. Microgrids consist of many energy sources, including energy storage systems, fuel cells, solar photovoltaic panels, and wind turbines.

Key Characteristics of Microgrids

The main key characteristics of microgrids are:

1. Location of utility

2. Distributed generation (DG)

3. Control systems

4. Grid integration mode and islanding mode

5. Load management

Microgrid control system

Hierarchical Control methods

Hierarchical control techniques consist of 3 distinct levels of control.

Primary Control

It is developed with the following key components:

- Maintaining the stability and reliability of frequency and voltage.

- Mitigating the presence of circulating currents that may result in excessive levels of current in power electronic components.

- Offering plug-and-play functionality for Distributed Energy Resources (DER) and efficiently distributing both active and reactive power across them, ideally without the need for physical connections.

The primary control system creates set points for the lower-level control system, which includes the inner and outer control loops for the distributed energy resource.

secondary control This control often operates within a time range of seconds to minutes, indicating a slower response compared to the first control. It confirms the independent behaviour of the main and secondary control loops and enables their distinct designs. The secondary control, such as a centralized controller, establishes the reference point for the main control. It reestablishes the
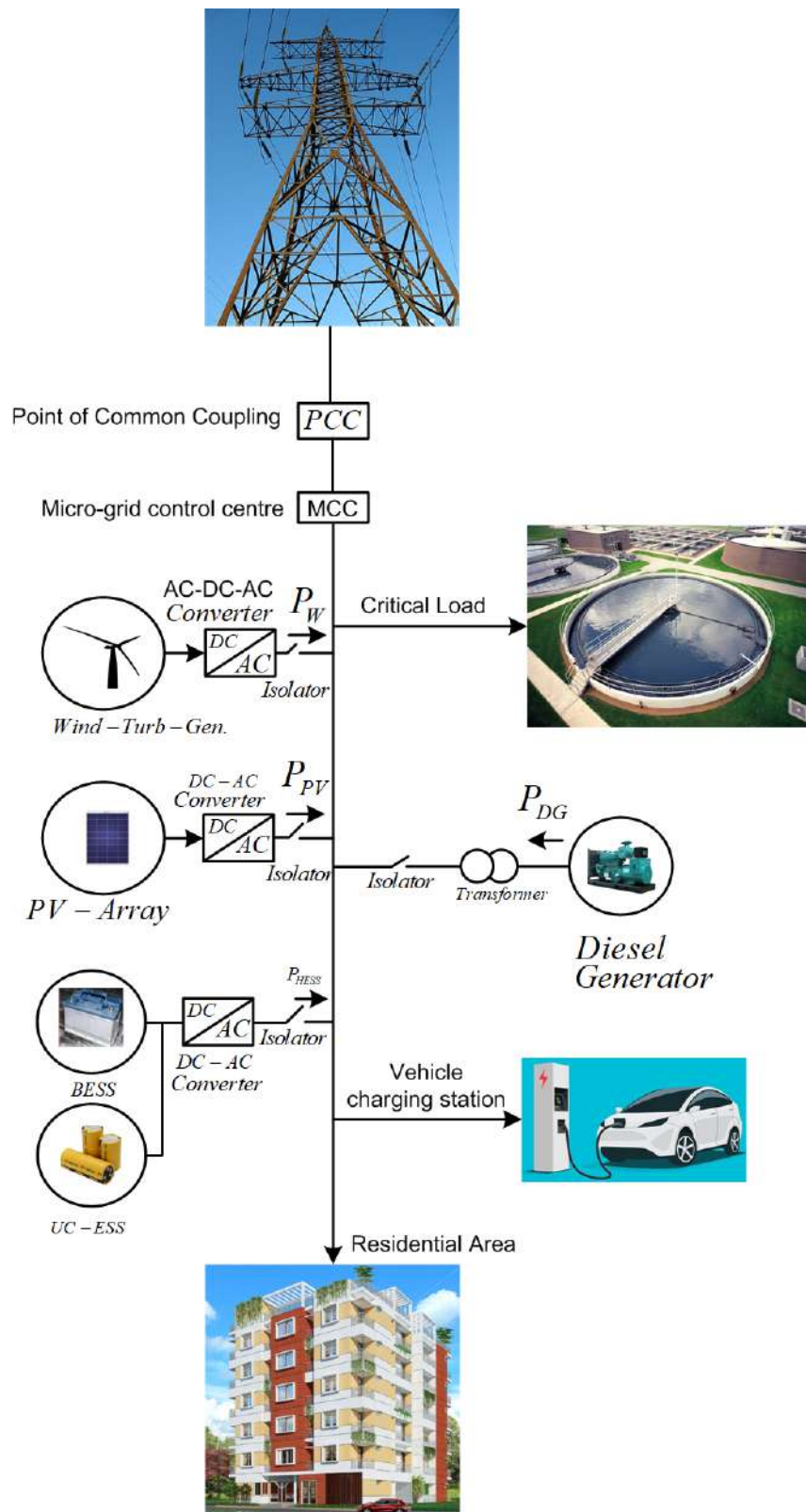
FIGURE 1.2: Diagram of microgrid with renewable generation

microgrid frequency and voltage and counteracts the power variations caused by fluctuations in loads or RES. This secondary control may be designed to satisfy specific power quality criteria, such as maintaining voltage balance on essential busses.

Tertiary control It operates on a timescale of minutes to hours, is the control level that considers economic factors to optimize the performance of the microgrid and regulate the power flow between the microgrid and the main power grid. In the times of emergencies, such as blackouts, this control system may function as a virtual power plant known as microgrid clustering. It is capable of managing linked microgrids and ensuring the delivery of electricity to the most essential loadsare several intricate control mechanisms that provide challenges for small microgrid (MG) and home DER users in establishing power management and control systems. Specifically, the cost of communication updates and data collection systems has increased.

1.1.2   Frequency Control Challenges

The heightened incorporation of renewable energy sources typically diminishes the overall system's inertia. The graph depicts the system frequency profile. The system's frequency deterioration results from sudden disturbances induced by generating tripping or load shedding. The frequency is controlled in order to prevent excessive deviation beyond the permissible limit.The frequency of the power grid is regulated by the rotational speed of synchronous generators and remains steady when there is equilibrium between mechanical input and electrical output.Whenever there is an excess of electricity in the grid, there will be a transient increase in frequency (frequency zenith). When a power deficit in the grid results in a transient frequency decline (frequency nadir), the RoCoF denotes the time derivative of the power system frequency.

1.1.3   Voltage Source Converters Regulation

Voltage source converters have very instrumental in integration of renewable energy to the grid. In grid network, it can be classified as voltage-controlled converters and current-controlled converters [11]. Voltage-controlled converters
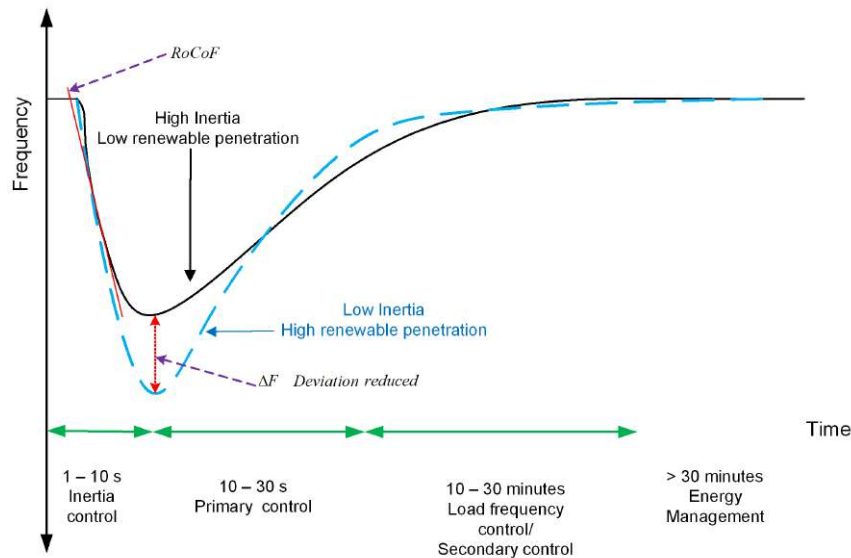
FIGURE 1.3: Frequency response in high and low-RES penetration after disturbance

is also categorized as grid-forming while current-controlled converters are grid-following. They perform grid supporting tasks like power, frequency and voltage control. Current-controlled VSCs (CC-VSCs), is mostly used to control PQ of the system, it's commonly referred to as inner loop control. It also ensures, at the PCC the power factor is unity. It is synchronized with PLL to provide grid reference quantities of voltage, current, phase angle and frequency. Voltage-controlled VSC (VC-VSC), this is a grid former as it generates its frequency and voltage. It forms part of the grid where the output active power and reactive power affects frequency and voltage magnitude respectively [12].

Grid forming inverters are designed for controlling voltage and frequency in microgrids by establishing the grid frequency and voltage, and they possesses the capability to function in island mode. The grid-following inverters synchronize with the grid's voltage and frequency to deliver an exact quantity of electrical power to the grid. It controls the phase angle and magnitude of the delivered current [13].
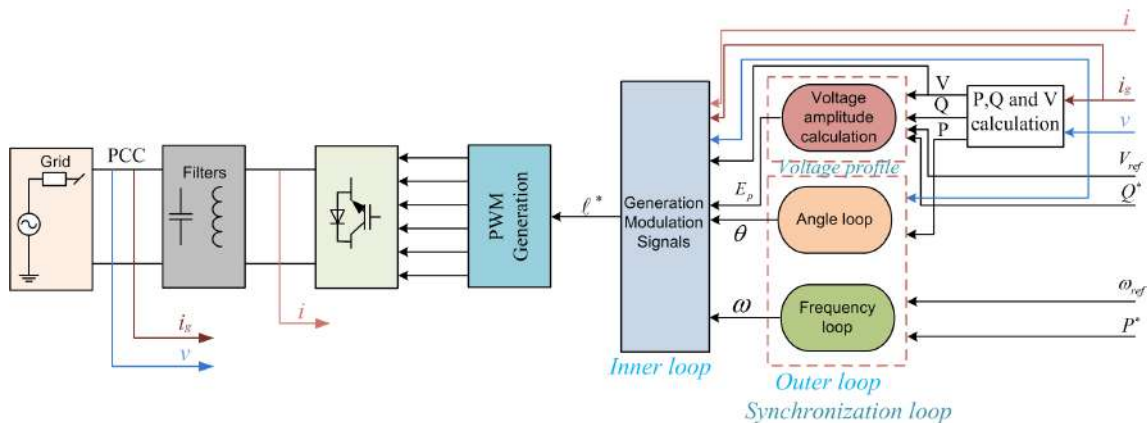
FIGURE 1.4: Grid forming converter

1.1.4 Power grid Integration

The contemporary electric power sector has experienced substantial reorganization from conventional systems, particularly with the incorporation of RES. Today, many power grid utilities have substantial RES interconnections. The integration primarily affected local transmission systems and did not impact the reliability of regional or national grids. In the current power system landscape, standardization has become crucial. Countries and utilities implement bilateral agreements and standardization through electricity regulatory agencies and bodies responsible for overseeing them. Today's renewable energy sources integration must comply with critical grid connectivity regulations and transmission constraints. Most of these standards share common concerns.

Frequency control: The consistent functioning of an interconnected power system depends on a prompt equilibrium between electrical load and supply. The system frequency acts as a key measure of this equilibrium. In small isolated systems, the integration of RES can significantly impact grid frequency, making the interconnection a critical issue [14].

Control of Active and Reactive Power: RES facilities frequently need to regulate their reactive power to sustain voltage at a designated level. The required is essential to minimize voltage fluctuations in the system, thereby reducing any negative impact on the transmission grid's voltage performance. The voltage at the PCC should be maintained at 0.15 per unit (15% of normal)

voltage [15].

Stringent Power Quality Requirements: A key concern in all international standards for grid-connected systems is the quality of the distributed power [16]. According to these standards [15], the current injected into the grid must not exceed a total harmonic distortion of 5

Grid harmonics: Periodic distortions in the supply voltage, known as voltage harmonics, can lead to overheating in equipment like transformers and motors. Power electronic elements are frequently associated with current distortion.

Voltage Flicker: It refers to brief sags or surges in line voltage, which may be classified as either periodic or non-periodic. The intensity of this effect increases when control systems for RES activate several machines simultaneously.

Voltage Control: Contemporary renewable energy sources possess the capability to regulate power factor and voltage at the generator terminals. Nonetheless, even with the power factor and voltage maintained consistently across each microgrid as actual power varies, the imaginary power consumption of the RES may still experience fluctuations due to reactive losses within the grid system. As a result, the RES reactive power consumption generally increases with real power output unless supplementary reactive support equipment is installed [17–19]. In such situations, software simulations are necessary to evaluate the RES impact on the system [20]. If it is determined that the RES installation negatively affects system stability, additional auxiliary equipment may be required to mitigate the issue.

1.2 Literature Review

This section presents an analysis of inertia control systems utilizing power electronic converters, with a particular emphasis on VSM control. The thesis is centered on the challenges of actual VSM implementation, optimization strategies, and associated control stability difficulties.

In reference [3], the authors proposed an in-depth overview of methods for enhancing inertia. This reference discussed the balance of power between supply and demand, especially in light of growing demand and the increased use of power electronics, which shifts the focus to inertia. In [21], batteries and

ultracapacitors are considered as alternative sources of inertia. In future power systems, control and power electronics devices are seen as key enabling technologies. Furthermore, a HESS that integrates a battery with an ultra-capacitor is utilized to regulate power in virtual synchronous generators (VSGs). With the gradual reduction or complete phasing out of synchronous generators, power converters are increasingly used to function as VSGs. [22]. Power management strategy (PMS) for regulating power flow in a DC microgrid functioning in grid-connected mode. The microgrid model is composed of the ac utility grid interfaced with a voltage source inverter operating as a grid-forming converter (VSC), an energy storage system (ESS) formed by a battery bank and a bidirectional dc-dc converter operating as a grid-supporting unit, a distributed generation acting as a grid-feeding unit, and the customer loads with strict voltage regulation [23].

Xin Meng, Jinjun Liu, and Zeng Liu [24] proposed A Generalized Droop Control, it is a well-designed controller, Generalized Droop Control (GDC) can achieve effective control performance and, unlike traditional droop control, it can offer virtual inertia and damping in stand-alone mode. The researcher contrasts Virtual Synchronous Generator (VSG) with traditional droop control, delineating their different merits and drawbacks. Both methods incorporate proportional-integral (PI) controllers and filters. The GDC parameters are designed in a flexible and intuitive way, resulting in relatively fast and precise restoration times. In [25], Elyas Rakhshani and Pedro Rodriguez proposed a method for analysing the dynamic effects of virtual inertia in two-area AC/DC interconnected automatic generation control (AGC) power systems. The growing incorporation of RES is leading to a rise in virtual inertia in contemporary power networks. This study uses storage devices to control active power and frequency, emulating inertia to address the dynamic behaviour of the power system. A PLL is incorporated into this technique. Reference [26], the article analyzes the maximum virtual inertia of DC-link capacitors based on a multi-timescale model of power converters. The Power-Internal Voltage (PIV) model is proposed for converters exhibiting varying dynamic timeframes. It is an open-loop model that is independent of grid variations and parameters. During the analysis, the system consists of many cascaded converters for convenience.

Thorough analysis of virtual were proposed in [27] where it proposed

Chapter 1. Introduction

optimal controller ameliorates VI dynamics and brings system frequency faster to the nominal value and allows more penetration of Inverter Interfaced Distributed Generation (IIDGs). The primary difficulty in the power system is frequency variation, resulting from a discrepancy between power generated and demand. In [28], the concept of distributed power system virtual inertia, which can be implemented by grid-connected power converters. Chu Sun and colleagues in [4] proposed an improved virtual synchronous machine control, considering the limitation of energy storage in response speed and energy capacity. Another comprehensive virtual generator control method for the full converter wind turbine, with a minute-level energy storage in the dc link as the energy buffer was proposed in [29]. In [30], investigation of potential issues associated with the system-wide integration of the technology at scale. The capacity of wind generation to offer frequency support via mimicked inertia is evaluated, together with the feasibility of adjusting this dispersed response resource to guarantee prompt and efficient frequency recovery across varying system conditions. Additionally, references [31], [32] and [33] explained in details on virtual inertia and parameters tuning.

Model predictive control techniques were analyzed in [34] where a simple model predictive direct power control (MP-DPC) of single-phase pulse width-modulated rectifiers with constant switching frequency using modulation function optimization. The instantaneous active and reactive power theory for single-phase converters is discussed, on the basis of a second-order generalized integrator while in [35] a model predictive control (MPC) strategy based on virtual synchronous machine (VSM) for the grid-connected converter was proposed. The controller coordinates precise switching of gates while evaluating cost function of the system. Power quality is also regulated.

1.3 Research Gap

1. From the literature review, hybrid energy storage systems (HESS) have not been exploited in terms of the maturity of ESS for rapid inertial response and ultracapacitor sizing.

2. In the current work in the literature, most system parameters are obtained with the assumption of linear and classical control strategies. However, in practice, system parameters need intelligent tuning since most systems are nonlinear and uncertain.

3. It is evident that most of the controllers are sensitive to frequency variation, especially in weak inertia systems, and there is a lot of scope for the design of suitable frequency adaptive control techniques.

4. The DC link size is very crucial for the regulation of system voltage and frequency. However, very limited work has been reported on the optimal sizing of DC link capacitance.

1.4   Research Objectives

The primary research problem is to regulate the voltage and frequency in power electronics-dominated micro-grid or power system using an automated/intelligent control system based on the virtual synchronous machine concept for optimal fast frequency response.

1. To design a Hybrid ESS comprising of a battery and ultra-capacitor. Here, the main objective is to optimize the size of the ultra-capacitor in terms of energy storage capacity needed to emulate rotational mass (kinetic energy) as per the swing equation of a conventional synchronous generator.

2. To design a combined hierarchical control strategy for the faster response of the ultra-capacitor and slow responding energy storage system (SRESS) emulating a slack bus.

3. To optimize DC link capacitance under linear modulation conditions with the aim of minimizing frequency nadir, frequency zenith, RoCoF while regulating the voltage by exploiting a model predictive controller for active as well as reactive power control.

4. Development of a prototype of a Hybrid ESS-based micro-grid for experimental validation of proposed control strategies.

1.5   Thesis Structure

The following sections of the thesis are organized as follows. In Chapter 2, Introduction to Virtual Synchronous Machine Concept and Its Control. An adaptive inertia control system utilizing optimization techniques is offered to address this difficulty. The enhanced particle swarm optimization (PSO) and genetic algorithms (GA) optimization techniques-based PID controller have been employed to determine the suitable virtual inertia coefficient for efficient inertia emulation in conjunction with an energy storage system.

In Chapter 3, Hybrid Energy Storage Systems for Inertial Response in Micro-grid. The chapter presented a method for optimizing and quantifying the energy required to function as virtual inertia support. HESS integrates a battery and an ultra-capacitor, with the ultra-capacitor addressing quick power swings by functioning as inertia, while the battery regulates long-term power variations.

In Chapter 4, Performance analysis of Various Control Strategies for Micro-grid. This chapter discusses the incorporation of a buck-boost converter into a bi-directional system, complemented by adaptive control based on reference values, as an efficient approach for regulating Electric Vehicles. This chapter does a comparative examination of PI, FOPID, and ANFIS during battery charging and discharging.

Chapter 5, Performance Enhancement using GA Based Model Predictive Control for VSM. This chapter presents enhanced MCP controller for active and reactive power regulation. Constant switching frequency is obtained through optimization of PWM. The effectiveness of the adopted optimization technique is confirmed by its validation using MATLAB/Simulink environment.

In Chapter 6, Conclusion and Future Scope.The main emphasis is on articulating the essential findings and contributions resulting from the research. The chapter delineates prospective avenues for future research, offering insights into domains that require additional investigation and advancement.

15

Chapter 2

Introduction to Virtual Synchronous Machine Concept and Its Control

2.1 Preamble

In recent times, a drastic change in energy sector has been witnessed at global level. Due to ever-increasing number of consumers and the improvements in living standards among consumers, energy demand is escalating continuously. With these situations becoming compelling day by day, the conventional methods of power generation i.e., fossil fuels are not sustainable. Also, these traditional methods are not environmentally friendly. Coal produces greenhouse gas (GHG), which pollute the surroundings and cause harm to the living organism in the area. They also emit carbon dioxide, which is a major cause of global warming. To meet this demand over a long period of time, RES, for instance, wind, biomass and solar are now becoming popular. RES has a number of benefits as they are not destructive to environment and relatively cheap. However, it is notable that they have low inertia, intermittent in nature, nonlinear and also, uncertain [36].There is a mismatch between generation and demand which cause an imbalance. The imbalance system makes introduced voltage and frequency deviations, which leads to a system's reduced reliability and resilience. It caused system collapse or even total blackout. In conventional power system, synchronous generators help to mitigate frequency deviation and RoCoF due to their ability to change speed when the system frequency changed. Kinetic energy is utilized (rotating mass) in traditional power system which is absent in the modern power system. Several power utilities companies across the

Chapter 2. Introduction to Virtual Synchronous Machine Concept and Its Control

world invest millions of dollars annually to address frequency quality problem.

The increased penetration of RES has led to system instability due to intermittent feature of converter-inverter interface [3]. In addition, renewable energy sources, energy storage system, local loads and power system applications are interconnected. Power electronics equipment lacks inherent inertia in comparison to synchronous machine in the traditional network. Due to large penetration of renewable energy sources in conventional power system network, considerable decrease in inertia is noted, causing frequency instability (frequency nadir and zenith, high rate of change of frequency). The frequency deviation is a notable problem in modern power system comprising power electronics-based energy harvesting from RES. To address these challenges, several methods have been put forward to solve low inertia problem and frequency restoration. Some of the methods are: (i) using wind turbines; active research is on wind power plants being used to generate inertia in microgrid. This method has potential but due to uncertainty of wind speed and incorporation of power electronic devices to stabilise turbine frequency and speed make it ineffective as synchronous inertia [37], (ii) using synchronous condensers; this is a type of inertia control which employs synchronous generators running under no load. However, this method is expensive and increases cost of overall system, (iii) use of ultra-capacitors; this method is recently being explored without any significant practical implementation. Reason being problem associated with the regulation of high output current. Ultra-capacitors have high power density but less energy density [38]. Use of DC-link capacitors; this method is effective in converters with variable voltages, mostly in AC system but in system with constant terminal voltages like batteries is not applicable [39]. Certain methods based on Partial loading have been proposed to utilised the spare capacity of power plant for inertial response. However, running a synchronous generator under partial loading conditions is highly inefficient and increases the per unit cost of electricity generation.

Recently, the concept of virtual synchronous machines (VSMs) emulated through power converter is gaining lot of popularity [8][9]. Several research papers have looked into the effect of MGs and non-inertia generation on the frequency reliability, resilience, and stability of bulk power systems [40][41][42][43]. Robust repetitive control (RC) is implemented in three-phase

four wire shunt active power filters (APF) [44] for power quality in power system. Furthermore, energy storage system has been employed in some instances to arrest the problem of instability in the system and hence, maintaining real power and frequency though this introduces economical factor [45]. In [46], novel fractional order controller was proposed for frequency regulation and real power fluctuation control but it did not explain how this controller is effective on offline microgrid and their cost implication if any. Further, A well-structured frequency control system based on Proportional, Integral and Derivative (PID) controller optimized through meta-heuristic techniques for micro-grid system comprising wind, hydro, solar, diesel, and Thermal systems were conducted to give ultimate quick control response to system disturbances [47][48]. A malfunction lenient supervision for frequency and voltage was brought forward for a diesel engine machine applied on a micro grid. Nikhil Paliwal [49] in his paper implemented this control approach in a multi-source system (hydro power, gas turbine and thermal plant), where the balance between power generation and demand as well as losses in microgrid has been achieved [50]. A similar control approach based on PID controller has been presented in [51] where the frequency control is implemented in hydro-wind hybrid system. The effectiveness of this method depends on the droop coefficient of synchronous generator [52]. Battery SOC time-varying properties is proposed in [53][54] for the inertia enhancement.

Recently, a robust approach been presented by Shahryar Maleki and his colleagues in [55] where they employed linear matrix inequality method for optimal and robust control. However, the issues associated with the response time and parameter variations increases overall control complexities. However, with this considerate pool of literature given, there is still insufficient report on the design and analysis of virtual inertia control techniques gaps require more attention in order to frequency deviation problem. The inertial response and damping coefficient are notable challenges in power electronic-interfaced microgrid.

In the proposed research work, an adaptive virtual inertia control is proposed to overcome such a challenge of frequency instability using optimized PID controller-based energy storage system. In this novel concept, an improvised version of PSO and GA has been utilised to achieve optimal values for tunning of

PID controller in low-inertia microgrid. Usually, a linear dynamic inertia weight updating equation is utilised for the enhanced PSO performance (LDIW-PSO) [56]. However, it suffers from the challenge of getting stuck into local optima during search space. In [57], a natural exponential with squared power term has been incorporated in weight updating equation. Although this approach is able to avoid local minima problem but inherently suffers in terms of increased number of iterations which ultimately increases the convergence time. Moreover, the reduced values of w_{start} (0.6) and w_{end} (0.1) means reducing viscosity as the search process is analogous to moving fluid. In this thesis, natural exponential term is taken strategically without squaring it in order to reduce the number of iterations. Also, the higher values of w_{start} (0.9) and w_{end} (0.2) have been taken to reduced convergence time.

The key contribution of this chapter is summarized here:

- An adaptive virtual inertia control is proposed to enhance frequency stability in a microgrid under different disturbances. During designing; performance index, ROCOF, frequency zenith and frequency nadir have been considered to improve frequency response.

- An improved particle swarm optimization algorithm has been implemented in this proposed control to deal with challenges of local optima, and offer a balance distribution of particles between exploration and exploitation.

- A brief comparison of frequency stability with traditional PSO, GA and Improved PSO under various operating conditions have been provided along with their procedural algorithm to demonstrate their performance.

- The optimal gains obtained through proposed algorithm have been simulated on the given system and same have been validated through OPAL-RT supported hardware in loop in real time.

2.2   System Description and Control

The system under consideration is shown in Figure 2.1, where the model comprises both conventional sources of energy based on steam turbines for
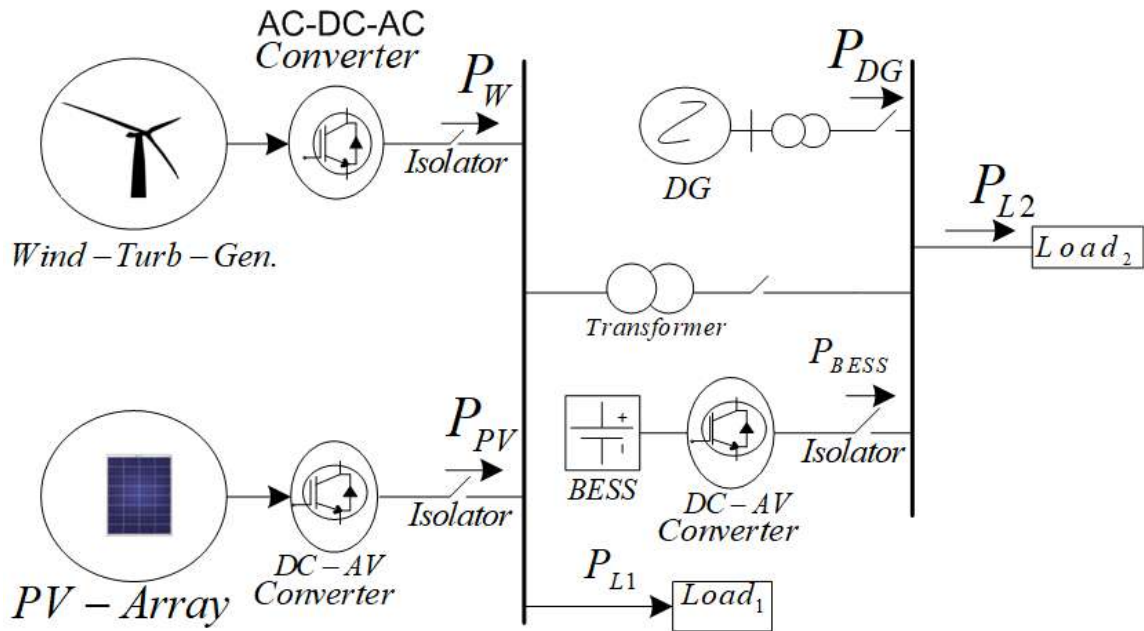
FIGURE 2.1: The block diagram of converter interfaced in microgrid

primary and secondary frequency control. Since RES is inertia-less, it needs to be regulated to avoid instability challenges. Therefore, solar and wind energy sources have also been considered for the formation of hybrid micro-grid. The system is simulated under different generation and loading conditions while ensuring the frequency control within permissible limits. The mathematical modelling of all different power sources has been done and incorporated in the development of block diagram for the simulation purpose. The detailed mathematical for different sources is as follows:

2.2.1 Modelling of Frequency Control system

In the first case, a model without virtual Inertia was conducted under the equation (2.1) given below:

$$\Delta P_m(t) - \Delta P_L(t) = \frac{2Hd\Delta f(t)}{dt} + D\Delta f(t) \tag{2.1}$$

Where
ΔP_G DG power change
ΔP_C change in power consumed

Chapter 2. Introduction to Virtual Synchronous Machine Concept and Its Control
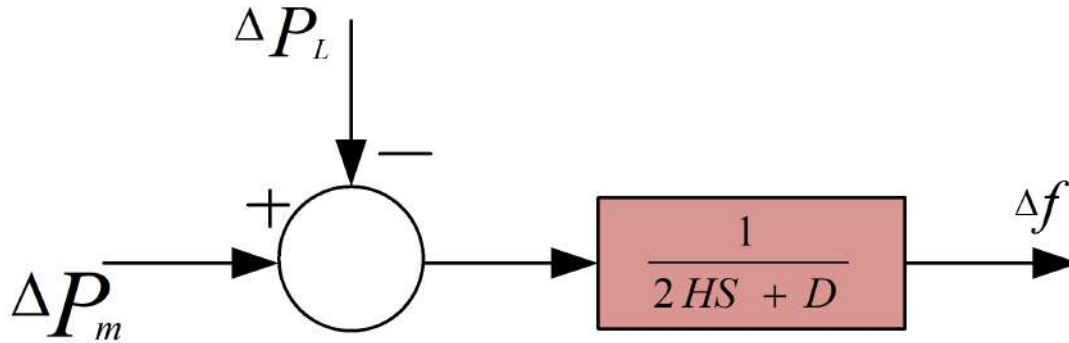
FIGURE 2.2: Frequency response model

Δf frequency change

H Inertia coefficient

D Damping coefficient

Equation (2.2) is transformed to Laplace as;

$$\Delta P_m(S) - \Delta P_L(S) = 2Hs\Delta f(S) + D\Delta f(S) \tag{2.2}$$

The equation (2.2) is represented in the Figure 2.2;

The Figure 2.3 shows the frequency deviation for both High inertia as well as low inertia system when put under certain disturbances. Here, it can be observed that in the absence of any regulating mechanism, the system droops, and it takes a long to recover. Further, the black solid line has small amplitude and it settled faster than the dotted red line. Therefore, it is always desirable to have a control system which could depict such excellent characteristics. Figure 2.3 shows hierarchical control structure with the secondary layer showing frequency restoration and control by stabilising the mismatch in load and generation.

The frequency change in a complete model is:

$$\Delta f = \frac{\Delta P_m + \Delta P_W + \Delta P_{PV} + \Delta P_{VI} - \Delta P_L}{2Hs + D} \tag{2.3}$$

Where

$$\Delta P_m(S) = \frac{1}{1 + sT_t}\Delta P_g(S) \tag{2.4}$$
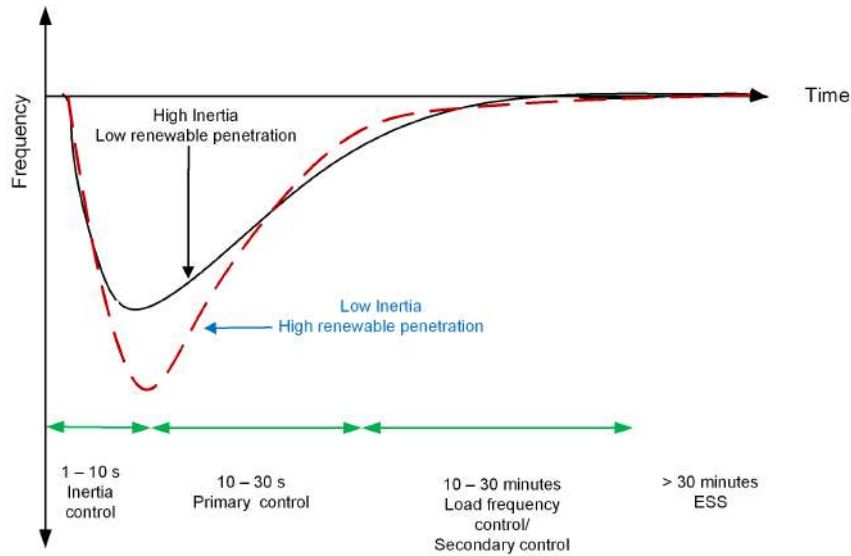
FIGURE 2.3: Inertia control, Primary and load frequency control

$$\Delta P_g(S) = \frac{1}{1 + sT_g}\left(\Delta P_C(S) - \frac{1}{R}\Delta f(S)\right) \tag{2.5}$$

$$\Delta P_C(S) = \frac{K_s}{S}(\beta \cdot \Delta f(S)) \tag{2.6}$$

$$\Delta P_W(S) = \frac{1}{1 + sT_W T}\Delta P_{\text{Wind}}(S) \tag{2.7}$$

$$\Delta P_{PV}(S) = \frac{1}{1 + sT_{PV}}\Delta P_{\text{Solar}}(S) \tag{2.8}$$

Where

ΔP_C ACE action change (signal)

ΔP_P Change in power from primary control.

ΔP_{WIND} Initial wind power change.

ΔP_W Power change in wind system.

ΔP_g The power is produced from the turbine.

ΔP_{solar} The initial change in solar power.

ΔP_{PV} The initial change in solar power.

ΔP_L Total change of load in the system.

ΔP_{VI} Change in virtual inertia power

The variable loading, load shedding, intermittent RES supply to the system caused fluctuation trend hence results in to poor frequency profile and interrupted energy supply to customer.

2.2.2 Control Description

The control part of any hybrid power system plays vital role in frequency stability, and it must be able to respond quickly to any kind of disturbances. It is always intended to have inertia control to respond first followed by primary and secondary control in case of a fault. Therefore, it is very necessary to emulate fast responding Inertia control in the RES based power system. Here, the damping coefficient plays vital role in minimizing the unwanted oscillations in the given system. A generalized virtual inertia control structure is shown in Figure 2.4 where the power disturbance may lead to frequency disturbance. Generally, a PID controller is included in a feedback close loop control mechanism [58]. PID transfer function comprise of first order derivative and integral.

$$G_{\text{Con}}(s) = K_p + \frac{K_i}{s} + K_d s \tag{2.9}$$

Where K_P, K_i, and K_d are proportional, integral, and derivative gains respectively. Further, any power disturbance can be modeled as:

$$\Delta P_{VI}(t) = \frac{\Delta f(K_{VI} + D_{VI})}{1 + sT_{ESS}} \tag{2.10}$$

Where
ΔP_{VI} change in virtual inertia power input,
ΔK_{VI} virtual Inertia coefficient,
ΔD_{VI} virtual damping coefficient
ΔT_{ESS} inverter-based energy storage system (ESS) time constant

2.2.3 System Parameters

In this chapter, the parameters used for modelling and frequency regulation has been adopted from [59], and also enumerated in table 2.1.
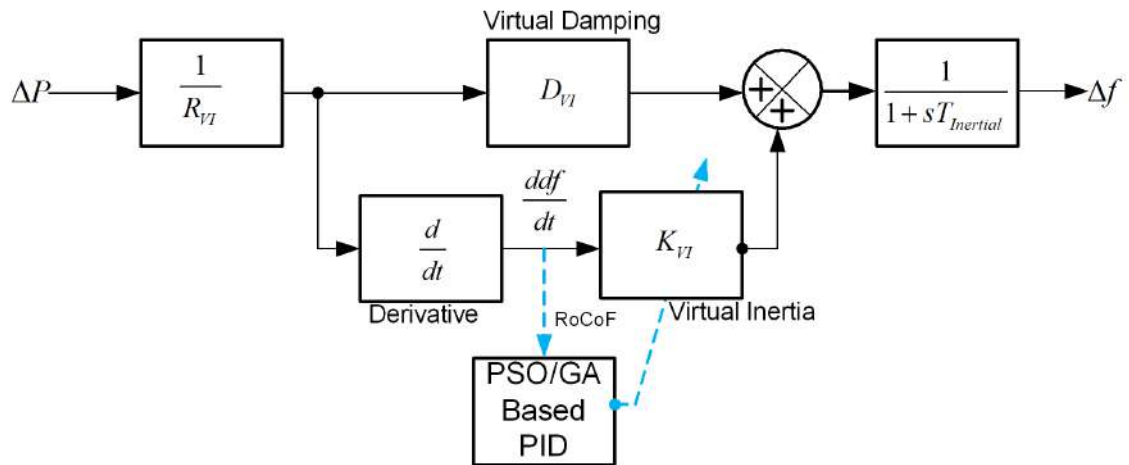
FIGURE 2.4: Virtual inertia control structure
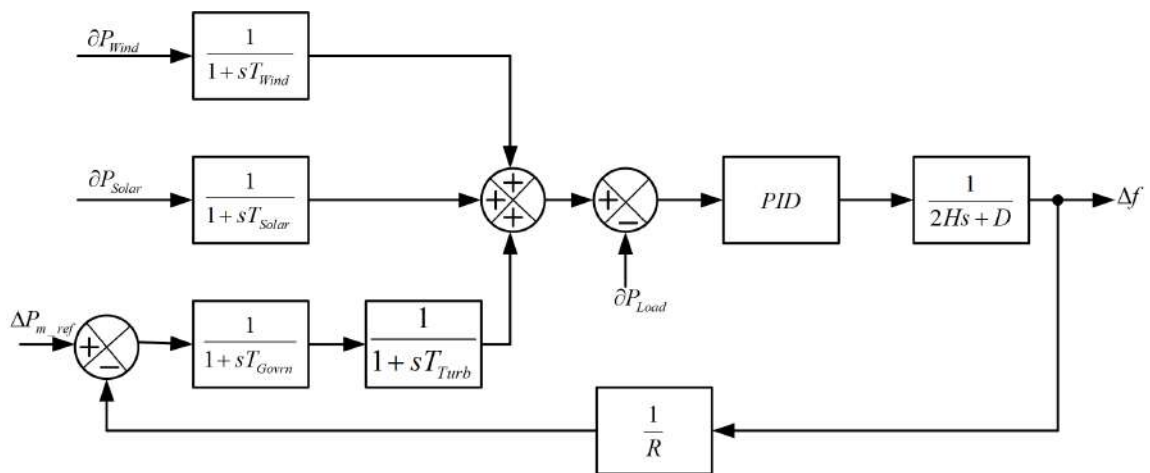
FIGURE 2.5: Micro-grid Control with PID

TABLE 2.1: System parameter values

Description	Symbol	value
Turbine Time Coefficient	$T_{turbine}$	0.5 s
Governor Time Coefficient	T_g	0.2 s
Generator Inertia Coefficient	H	5 s
Governor Speed Regulation	R per min.	0.05 s
Damping coefficient	D	0.8 s

2.3 Optimization Techniques Applied

The control performance of the given system depends on the tuning of the PID regulator. Under normal circumstances, a generalized PID may exhibit satisfactory performance. However, its performance starts deteriorating under dynamic load conditions or intermittent power generation from renewable energy sources (RES). Therefore, it necessitates searching for the optimal gains of the PID regulator that may perform under all such dynamically operating conditions. An improvised form of Particle Swarm Optimization (PSO) and Genetic Algorithm (GA) has been utilized to obtain the optimized values of PID gains for virtual inertia control under different operating conditions.

For this purpose, the control block diagram, as shown in Figure 2.5, has been modified by incorporating the frequency disturbance signal in the tuning of the PID controller using the improvised forms of the PSO and GA optimization algorithms. The whole system is simulated in MATLAB Simulink as per the block diagram shown in Figure 2.6. The simulation study is carried out for three different cases while considering different levels of disturbances, either from the load or renewable power sources that are intermittent in nature. In Case 1, a disturbance of 2% was considered at $t = 0.2$ s. In the second case, a disturbance of 3% occurred at $t = 2.2$ s, and finally, a third disturbance of 4% is introduced at $t = 4.5$ s. All three cases were considered using both optimization techniques.

FIGURE 2.6: Designed proposed layout

2.3.1 Particle Swarm Optimization (PSO)

Particle swarm optimization (PSO) was introduced in 1995 by James Kennedy and Russel C. Eberhart [60] inspired by the social behaviour of animals like flock of bird and the school of fish. It is simple but powerful optimization algorithms; it is a vigour and effective technique utilized in optimization challenges. This technique has been applied in a variety of applications. It has various advantages, for instance, efficiency in mathematical computation, simple to implement, robust, stable convergence characteristics [61], and it can also be used in online optimization due to its efficiency and simplicity [62]. The conventional Particle swarm optimization is a design based on the behaviour of a swarm of birds in search of food location [60]. The position location and speed of each particle is located by the following equation;the best local position P_i and global best G_i :

$$V_i^{(t+1)} = wV_i^t + c_1r_1(P_i^t - X_i^t) + c_2r_2(G_i^t - X_i^t) \tag{2.11}$$

$$X_i^{(t+1)} = X_i^t + V_i^{(t+1)} \tag{2.12}$$

Where r_1 and r_2 are random values in the range $[0, 1]$,
c_1 and c_2 are the social constant and cognitive constants,
w is the inertia weighting function,

wV_i^t is the inertia term,

$c_1r_1(P_i^t - X_i^t)$ is the cognitive component,

and $c_2r_2(G_i^t - X_i^t)$ is the social component.

w is the inertia weight, which is very critical for the fast convergence of the optimization process. A very effective approach based on linear decreasing inertia weight PSO has been presented in [56] to manipulate the inertia weight and update it dynamically, as represented by the equation given below:

$$w = (w_{\text{start}} - w_{\text{end}}) \times \left(\frac{T_{\text{max}}}{T_{\text{max}}} + w_{\text{end}} \right) \tag{2.13}$$

Where, w_{start} is the initial value of inertia weight, w_{end} is the final value of inertia, and T_{max} is the maximum iterations.

The linear dynamic inertia weight-PSO (LDIW-PSO) faced the challenge of falling into a local optimum during the searching process. Moreover, the performance of the optimization engine is heavily dependent on the initial and end values of the inertia constant, where values that are too small or too high may increase the number of iterations as well as the convergence time. To overcome this issue, a natural exponential is multiplied with w_{end} to enhance the velocity-updating equation. Similarly, [57] has included a square of exponential which further increases the computational burden. Therefore, in order to reduce the computational burden without compromising performance, an exponential term with a suitable value of T_{max} has been included in the weight updating matrix such that the overall convergence time reduces with a reduced number of iterations [57],[63]. The modified equation is as given below:

$$w = (w_{\text{start}} - w_{\text{end}}) \times \left(\frac{T_{\text{max}}}{T_{\text{max}}} + w_{\text{end}} \times e^{-\frac{t}{(T_{\text{max}}/10)}} \right) \tag{2.14}$$

Where $w_{\text{start}} = 0.9$ and $w_{\text{end}} = 0.2$.

Figure 2.7 illustrates that MPSO converged faster than LDIW-PSO, showing better performance.

2.3.2   Generic Algorithm (GA)

To improve system response of inertia-less micro-grid, GA has been used to optimize PID parameters so that it effectively and efficiently gives optimal
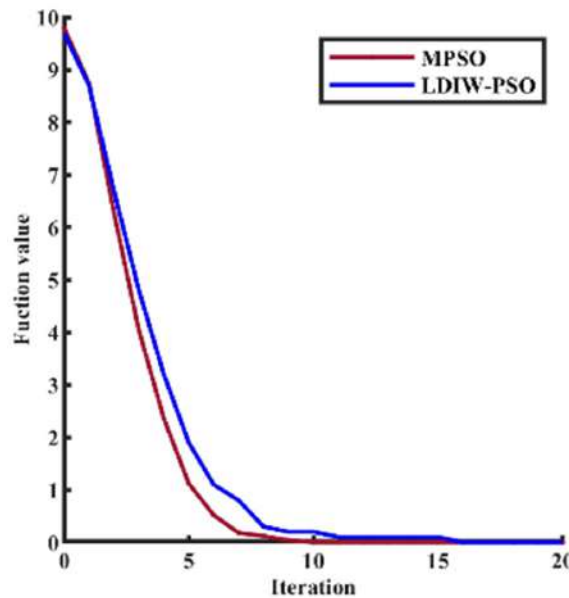
FIGURE 2.7: Comparison of MPSO and LDIW-PSO

values. With the repetitive loops, chromosomes population are iterated, in this case, each iteration is considered as a generation. The genetic material operators-choose, crossover, and mutate to form a new cluster [64]. There is an objective function for each generation. Charles Darwin's selection criteria is applied and Darwin's fitness and the struggle for survival strategy are used [65]. The probability equation is,

$$p(\eta, t) = M\frac{p(\eta, t-1)f(\eta)}{\sum f(H)} \tag{2.15}$$

Where, p is probability, η is gene, t is time, M is population, $f(\eta)$ is the fitness value of the gene, and $\sum f(H)$ is the sum of fitness values of all populations. The Genetic Algorithms (GA) is applied, and the boundary values of PID controller gains K_p, K_i, and K_d are obtained through the GA optimization process. The algorithms shown in 2.8 and 2.9 depict the step-by-step procedure of the improved PSO and GA optimization flowcharts.

28

Chapter 2. Introduction to Virtual Synchronous Machine Concept and Its Control
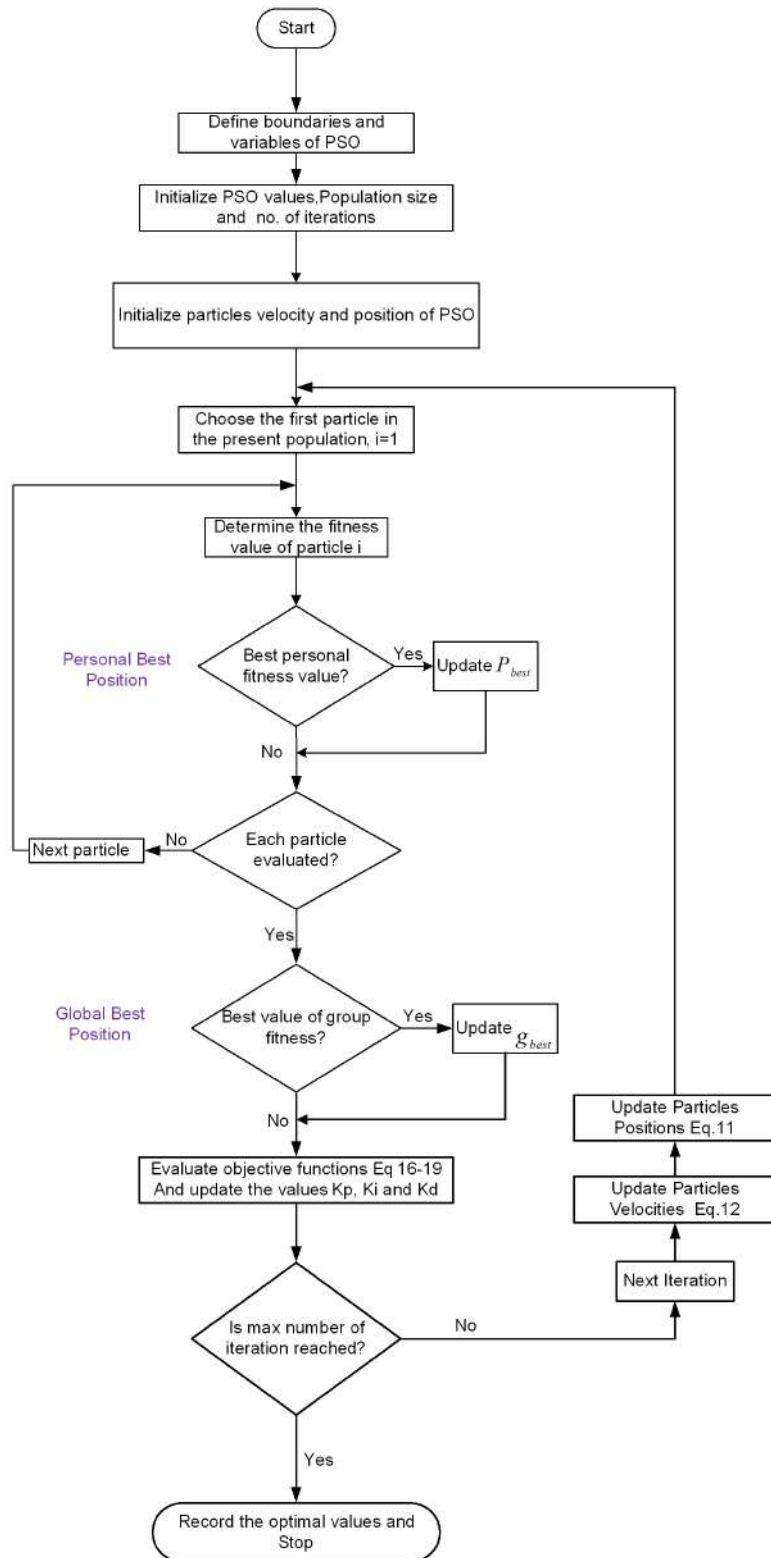
FIGURE 2.8: Particle swarm optimization (PSO) flowchart
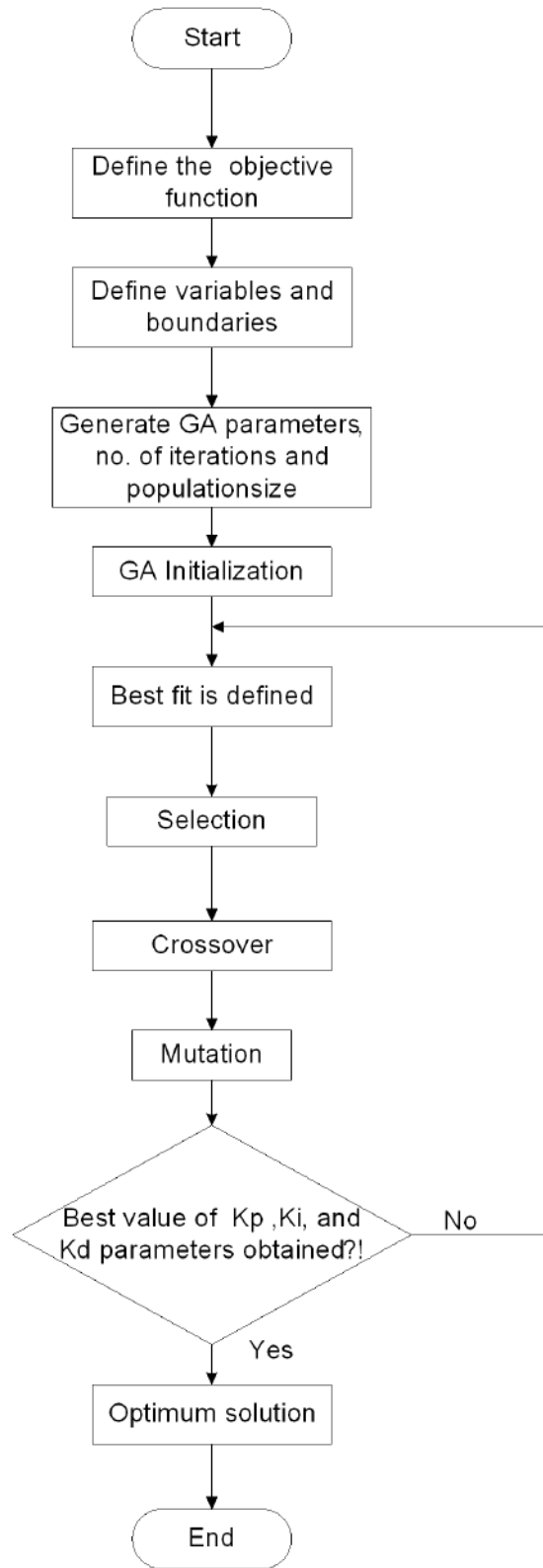
FIGURE 2.9: Genetic Algorithm (GA) flowchart

2.3.3 Formulation of four performance index (P.I)

In this chapter, improved PSO and GA is applied to minimize the error in performance index. The error, the is the deviation in frequency should be as minimal as possible. During this research, four performance indices were considered; Integral of Time-Weighted Absolute Error (ITAE), Integral of Absolute Error (IAE), Integral of Time-weighted Squared Error (ITSE) and Integral of Square Error (ISE). The following objective functions have been mathematically formulated:

Integral Time-weighted Absolute Error (ITAE)

$$ITAE = \int_0^{t_{\text{Sim}}} t |\Delta f| \, dt \tag{2.16}$$

Integral Absolute Error (IAE)

$$IAE = \int_0^{t_{\text{Sim}}} |\Delta f| \, dt \tag{2.17}$$

Integral Square Error (ISE)

$$ISE = \int_0^{t_{\text{Sim}}} |\Delta f|^2 \, dt \tag{2.18}$$

Integral Time Square Error (ITSE)

$$ITSE = \int_0^{t_{\text{Sim}}} t |\Delta f|^2 \, dt \tag{2.19}$$

The deviation in frequency Δf is due to perturbations in the power system caused by intermittent power supply and nonlinear loads. The time range for simulation is denoted as t_{Sim}. The goal is to minimize the performance index (P.I.) subject to the PID controller parameter gains K_p, K_i, and K_d as shown in 2.20.

$$
\begin{aligned}
K_{p,\text{Upper}} &\geq K_p \geq K_{p,\text{Lower}} \\
K_{i,\text{Upper}} &\geq K_i \geq K_{i,\text{Lower}} \\
K_{d,\text{Upper}} &\geq K_d \geq K_{d,\text{Lower}}
\end{aligned}
\tag{2.20}
$$

Where the Population size, iterations and boundaries size taken are provided in tables 2.2 and 2.4.

TABLE 2.2: PSO & GA Elements

Elements	Data
Population size	100
Maximum iteration	50

TABLE 2.3: PSO & GA boundary condition

Parameters	Lower boundary	Upper boundary
K_p	0	1000
K_i	0	1000
K_d	0	1000

2.4 Simulation Results and Discussion

The simulation of the 250 MW system with RES penetration is shown in 2.1. It consists of DG 200 MW, solar power plant 15 MW, wind power plant 25 MW and 10 MW of BESS, residential load of 5 MW and 10 MW industrial load [66, 67] incorporating the proposed controller with optimal gains obtained through PSO as well as GA is tabulated in Table 4. Here, all the four performance indices were considered for each case. Series of simulations were conducted in MATLAB environment to obtain optimal parameters vales for different algorithms. Given below are algorithm for improved PSO and GA showing parameter settings, initialization, termination and fitness function:

The population size is 100, the maximum number of iterations is 50, the minimum fitness is 0.0001, and the maximum and minimum allowable velocities are V_{max} and V_{min}, respectively. The acceleration constants are $C_1 = 2$ and

Chapter 2. Introduction to Virtual Synchronous Machine Concept and Its Control
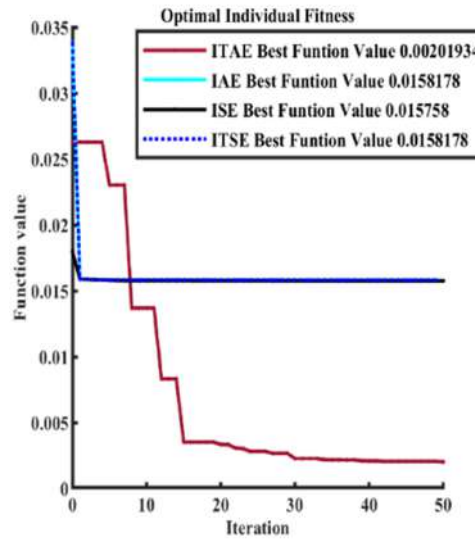
FIGURE 2.10: PSO based optimization curve

$C_2 = 2$; the other parameter is the inertia weight, which has been modified as discussed earlier.

For the Genetic Algorithm (GA), the same population size and the same number of iterations (generations) as the improved Particle Swarm Optimization (PSO) are used. The crossover probability is 0.8, and the mutation probability is 0.1. In Figures 2.10 and 2.11, the optimal individual fitness based on improved PSO and GA are illustrated with the four performance indices. The optimization curves for the PID parameters are shown in Figure 2.12, with each curve representing the optimal value of each constant.

TABLE 2.4: PSO & GA boundary condition

Parameters								
	ITAE	ITAE	IAE	IAE	ISE	ISE	ITSE	ITSE
	PSO	GA	PSO	GA	PSO	GA	PSO	GA
K_p	1000	913.6278	1000	970.5514	1000	810.4577	1000	760.6385
K_i	4.4809	1.3339	2.1039	243.1919	0.6580	0.0233	2.1041	2.7500
K_d	0	1	0	0.7023	0	1.2251	0	8.1265

The optimization techniques used above are able to minimize error, and their evaluation is carried out based on four main performance indices, where the
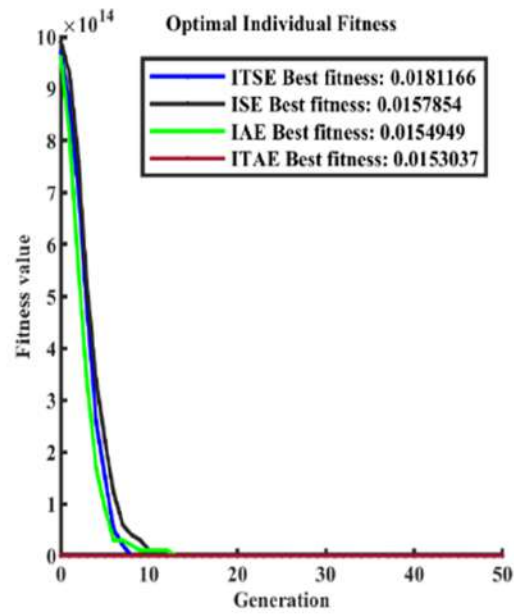
FIGURE 2.11: GA based Fitness curve
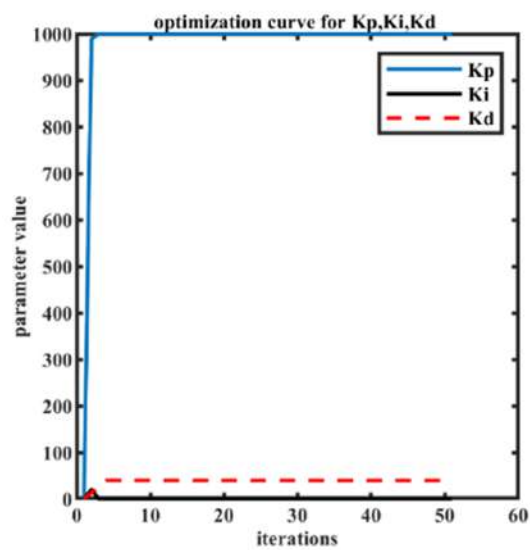
FIGURE 2.12: optimization curve

settling time, undershoot, overshoot, and oscillation have improved drastically. The Rate of Change of Frequency (RoCoF) and frequency deviation are brought to steady state within a few milliseconds, unlike the conventional rotational mass of synchronous machines, which takes up to 10 seconds to settle. The response is very fast and comes into effect well before the primary response, which sets in between 30 seconds and 30 minutes, and the secondary frequency control, which sets in after the 30th minute to shed loads or operate protective mechanisms.

The simulation study is carried out under three different operating conditions, with Case 1 considering a 2% disturbance, Case 2 a 3% disturbance, and Case 3 a 4% disturbance:

Case 1: 2% disturbance: Initially, the system is stable at a frequency of 50 Hz for the first 0.2 seconds. Then, an abrupt load demand of 5 MW is introduced, causing a frequency disturbance. The frequency oscillations take approximately 20.734 ms to damp out, and the system is restored to stable operation with a frequency of 50 Hz while feeding a load of 245 MW.

Case 2: 3% disturbance: After 2.2 seconds, a renewable energy source (RES) starts supplying 7.5 MW, leading to power and frequency oscillations. It takes approximately 23.645 ms to damp out the oscillations, and the frequency is restored to its nominal value while feeding a load of 252.5 MW.

Case 3: 4% disturbance: At the 4.5th second, another disturbance occurs due to a reduced load demand of 10 MW. This results in higher amplitude frequency and power oscillations, taking approximately 24.505 ms to damp out. The frequency is again restored to its nominal value, with the overall system load at 242.5 MW.

The simulation results for all performance indices are shown separately from Figure 13 to Figure 16. Figure 13 shows the simulation results for the ITAE performance index, Figure 14 presents the results for IAE, Figure 15 shows the simulation results for ISE, and Figure 16 presents the results for ITSE. Each diagram consists of traces of change in frequency (ΔF), frequency, power, and change in power (ΔP) for the PID controller optimized through PSO and GA. It is easy to observe that GA performs better in terms of lower peak overshoot, while PSO outperforms GA in terms of settling time. It is worthwhile to mention that in both cases, the system performs satisfactorily and stabilizes rapidly when subject to any kind of disturbance.

2.4. Simulation Results and Discussion

35
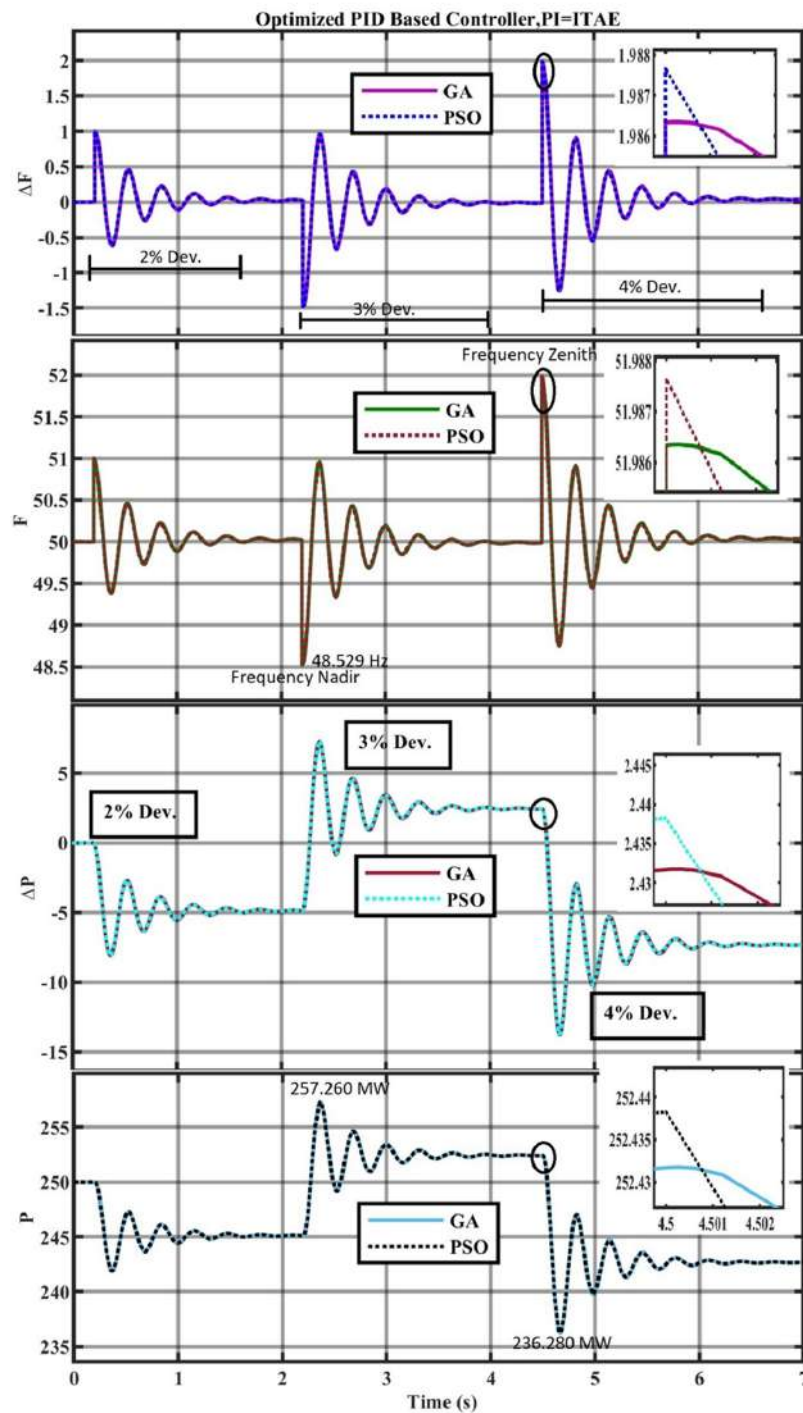
FIGURE 2.13: PSO & GA PID based, Performance Index=ITAE

Chapter 2. Introduction to Virtual Synchronous Machine Concept and Its Control
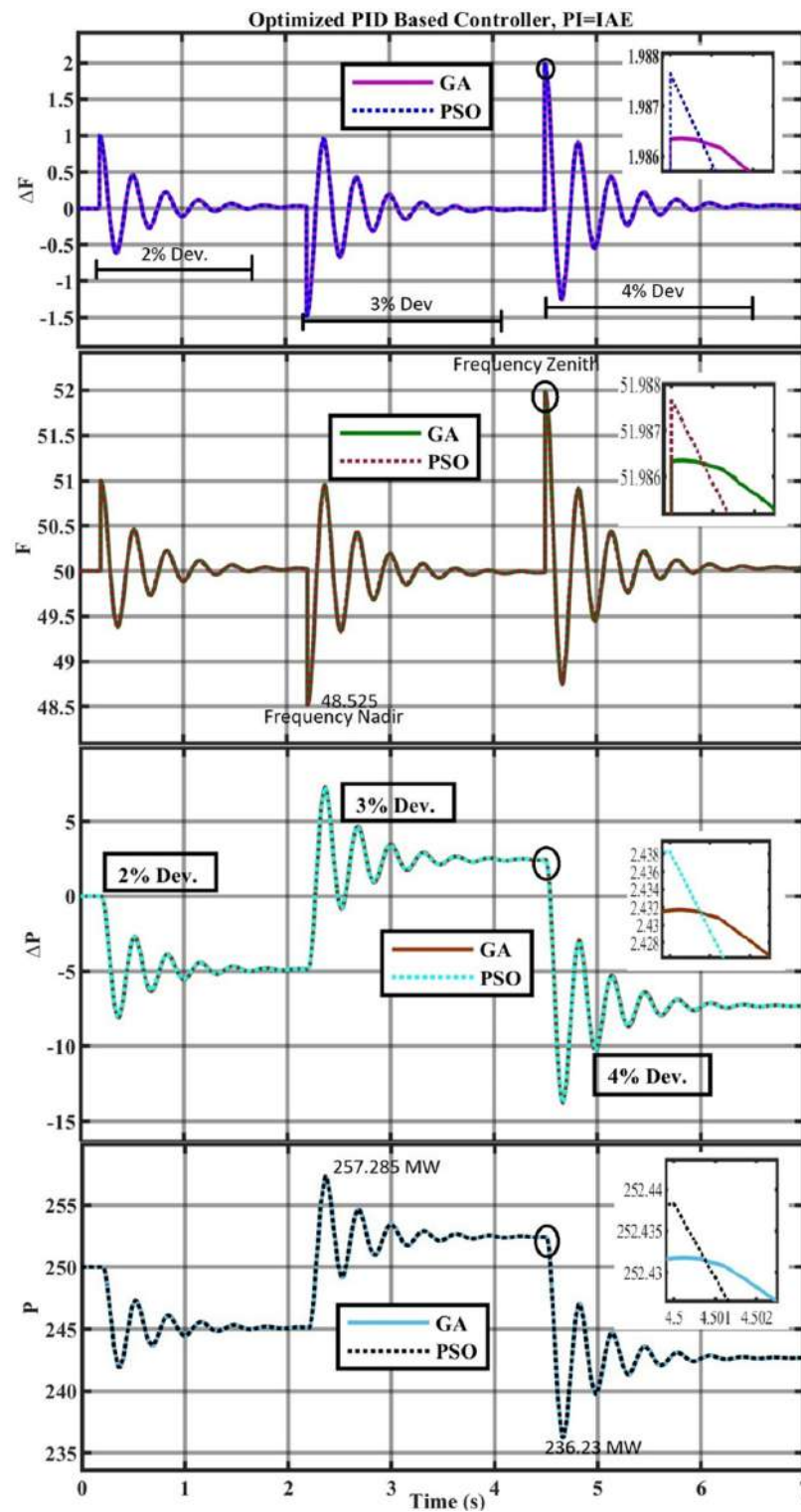
FIGURE 2.14: PSO & GA PID based, Performance Index=IAE
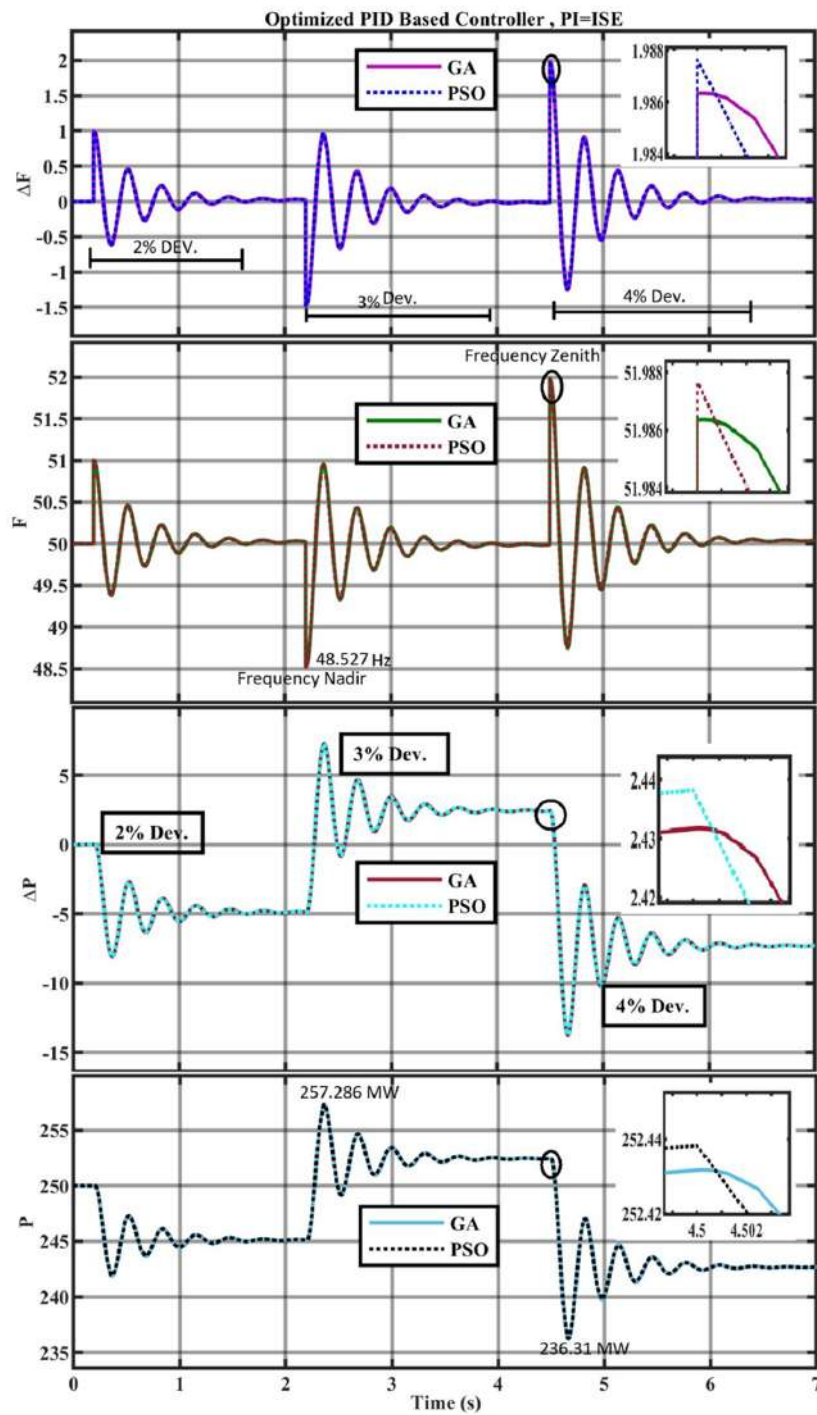
FIGURE 2.15: PSO & GA PID based, Performance Index=ISE

Chapter 2. Introduction to Virtual Synchronous Machine Concept and Its Control
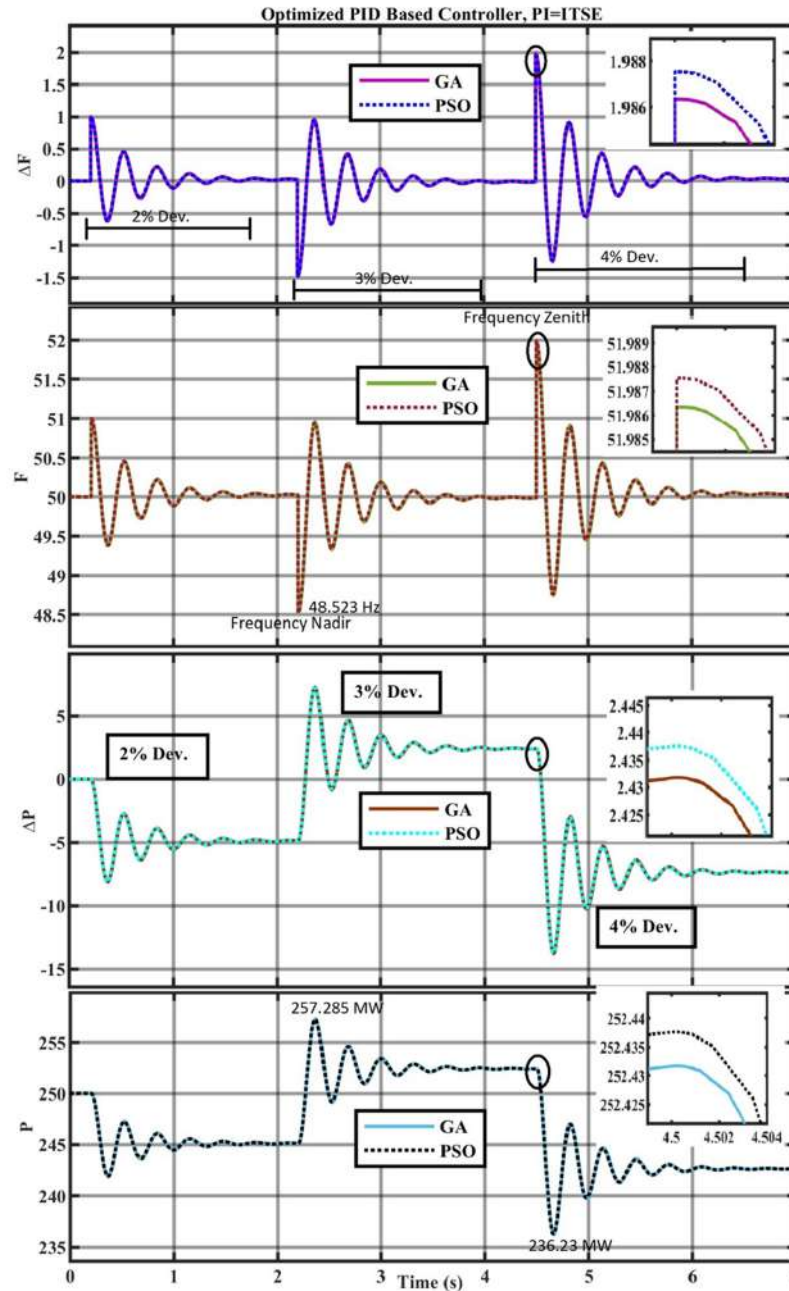
FIGURE 2.16: PSO & GA PID based, Performance Index=ITSE

2.4. Simulation Results and Discussion 39

TABLE 2.5: Statistical analysis of frequency deviation (ΔF) for PSO-PID and GA-PID controllers.

P.I.	Type of Controller	Max	Min	Undershoot (%)	Overshoot (%)	Peak to Peak	Mean	RMS
ITAE	PSO-PID	1.988	-1.477	-50.890	50.890	3.465	0.1721	0.8790
	GA-PID	1.983	-1.471	-50.967	50.967	3.454	0.1225	0.7492
IAE	PSO-PID	1.988	-1.478	-96.884	106.123	3.466	0.04730	0.5145
	GA-PID	1.985	-1.475	-50.953	50.953	3.460	0.1683	0.8919
ISE	PSO-PID	1.988	-1.478	-96.848	106.655	3.465	0.04846	0.4821
	GA-PID	1.983	-1.473	-50.980	50.980	3.456	0.1399	0.8155
ITSE	PSO-PID	1.988	-1.477	-50.890	50.890	3.465	0.1728	0.8888
	GA-PID	1.987	-1.477	-50.898	50.898	3.464	0.1804	0.9006

In Table 2.5, it is statistical analysis of the changes in frequency which is captured in Figures 2.13, 2.14, 2.15, 2.16.

Chapter 2. Introduction to Virtual Synchronous Machine Concept and Its Control

TABLE 2.6: Statistical analysis of Power Change (ΔP) for PSO and GA controllers.

P.I.	Technique	Max (MW)	Min (MW)	R Time (ms)	F Time (ms)	Undershoot (%)	Overshoot (%)	P to P	Mean	RMS
ITAE	PSO	7.188	-13.66	57.047	48.156	10.062	64.286	20.85	-2.505	4.915
	GA	7.260	-13.72	57.881	48.663	6.212	64.286	20.98	-2.536	4.988
IAE	PSO	7.198	-13.66	56.941	47.898	10.029	64.286	20.85	-2.475	4.898
	GA	7.285	-13.77	57.595	47.331	-2.243	69.118	21.06	-2.570	5.008
ISE	PSO	7.286	-13.69	58.979	47.216	12.148	67.143	20.98	-2.450	4.882
	GA	7.199	-13.63	60.128	49.269	6.928	62.500	20.82	-2.502	4.971
ITSE	PSO	7.198	-13.66	56.941	47.898	10.029	64.286	20.85	-2.475	4.898
	GA	7.285	-13.77	57.595	47.331	-2.243	69.118	21.06	-2.570	5.008

In Table 2.6 power change analysis is done; it gives in-depth understanding of how this controller is very effective.
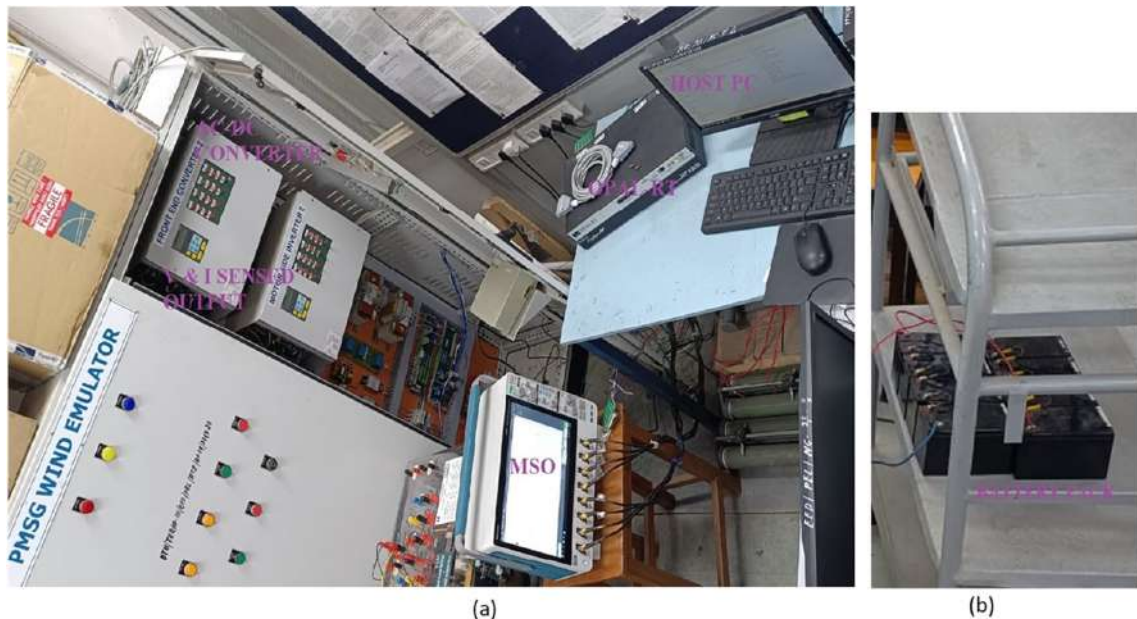
FIGURE 2.17: Experimental Hardware (a) setup (b) Battery

As observed in Table 2.5, the improvised PSO-PID controller has the highest overshoot among all the four performance indices, though it is restricted to the threshold of 3%. However, in all cases, it took the shortest time to settle down. On the other hand, the GA-PID controller has a smaller overshoot but a longer settling time.

2.5 Experimental Results and Discussion

Simulation was done on MATLAB/Simulink environment as discussed and results were shown. Furthermore, a real time hardware prototype was designed based on OPAL-RT (OP-4510) as shown in Figure 2.17 . This further illustrate the efficacy of the research concept in this chapter.

It is seen that the proposed dynamic controller has a quick dynamic response, as it takes less than two seconds to arrest any deviation, despite the intensity of the change. From the experiment, 2%, 3%, and 4% disturbances were used, and the response time in all three cases was found to be fast.

MATLAB simulation results and experimental results from real-time OPAL-RT are in agreement, giving a clear indication that the tuned optimal

(a)

(b)
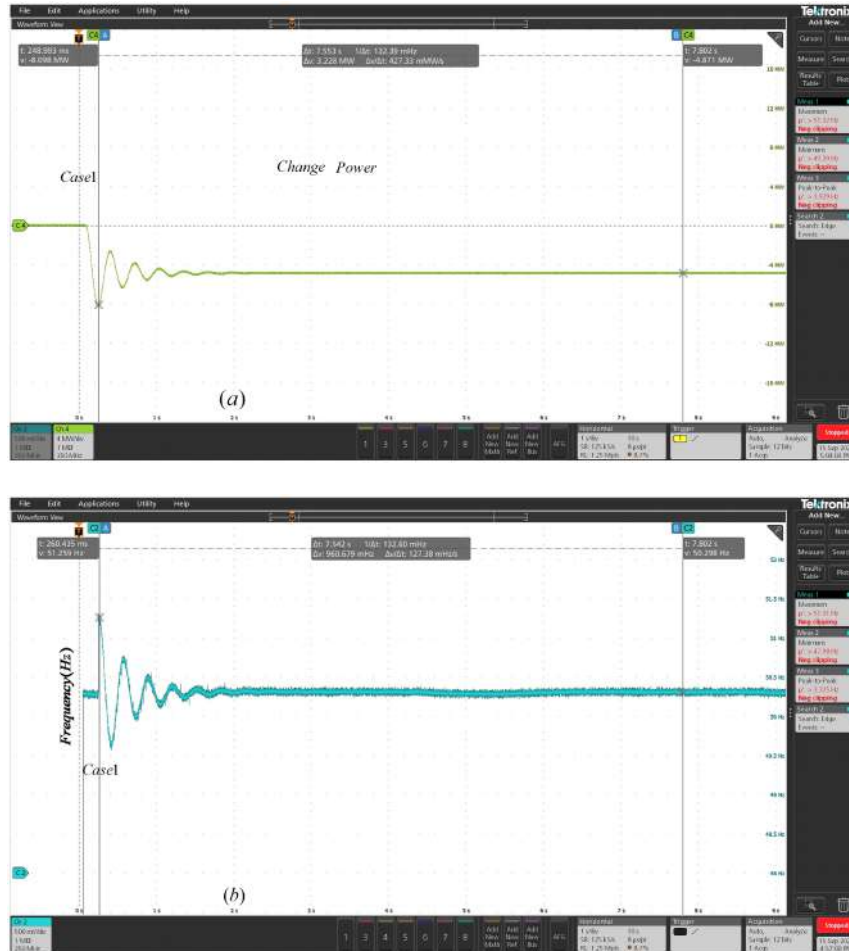
values of the PID controller can be used in an offline system. The outcome of both approaches is more or less similar. In Figure 2.18, the frequency nadir is 1.967 Hz, and in MATLAB simulations, as seen in Table 2.5, the average for all four performance indices is 1.985 Hz. This validates the proposed control approach, where the simulation results are almost emulated using hardware in the loop.

2.5. Experimental Results and Discussion

43

(c)

(d)

(e)

Chapter 2. Introduction to Virtual Synchronous Machine Concept and Its Control

(f)

(g)

(h)
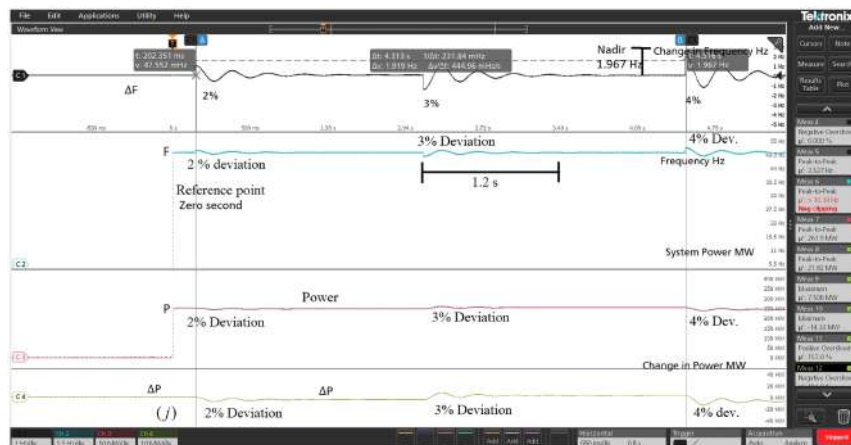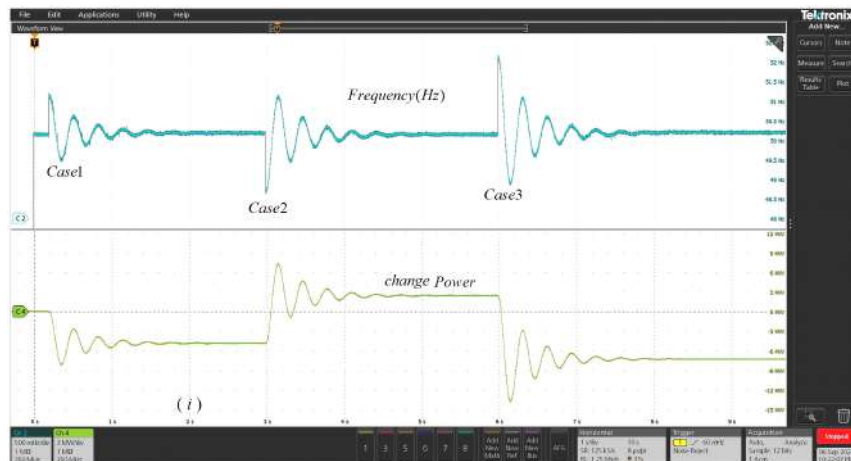
FIGURE 2.18: (a, b, c, d, e, f, g, h, i, j) Experimental results for frequency deviation, frequency, power and power change in Mixed Signal Oscilloscope (MSO)

Chapter 2. Introduction to Virtual Synchronous Machine Concept and Its Control

46

TABLE 2.7: Comparison of Different Control Strategies

Reference	Type of control	Merits	Demerits
[68]	Droop control and VSG is proposed	It is easy to implement with low cost	Complexity in tuning parameters
[69]	Derivative control-based virtual inertia	It reduces overshoot response	Complex tuning due to trial-and-error method
[70]	Adaptive dynamics programming	Faster frequency response and reduced overshoot in d-axis	It ignores the q-axis making it incomplete due to reactive component
[71]	PID controller based (GWO)	Frequency control in multi-source single area	It did not include multiple areas and may not be applicable in microgrid
[?]	BFOA tuned LQR-based VSG	Suppress frequency fluctuations	Damping oscillations and ROCOF is not considered
Proposed	MPSO based - Adaptive Virtual Inertia Control	Faster frequency response with reduced overshoot, settling time and simple parameters tuning	

Finally, comparisons were made between this proposed technique and some existing techniques as shown in Table 2.7 to ensure its effectiveness.

2.6 Conclusion

The designed test system based on two optimization techniques have been successfully implemented in MATLAB Simulink. The gains obtained through these optimization methods have been further utilized for the tuning of PID regulator which further exhibits the emulation of virtual inertia control. The three different uncertainty level caused by either intermittent RES or fluctuating load have been demonstrated to show the effectiveness of the proposed control approach. The problem of high RoCoF, high overshoot, and high undershoot, and long rise-time have been significantly eliminated. The proposed techniques are suitable for regulating both RoCoF and frequency control. The above analysis confirmed that the inclusion of optimization techniques in the micro-grid would act as a game-changer to elusive Inertia and damping. With the continuous penetration of RES/DG into our power system network, this technique will enable system control engineers to achieve steady state operation of overall system. As it already discussed in results section, the proposed controller's performance is tested and validated through the MATLAB simulation and hardware prototype, the controller responds fast to the given changes. From the experimental validation, the proposed controller with excellent outcome, it can be used in microgrid with nonlinear loads and power supply. This adaptive virtual inertia method using optimization techniques improves frequency response and thus, confirms the effectiveness of this controller.

2.7 The Chapter Summary

In the recent years, a sharp increase in integration of renewable energy sources (RES) in power system network has been observed. High penetration of RES interfaced with power electronics converters-inverters with reduced or no inherent inertia compromises modern power system overall stability. Due to low inertia, voltage and frequency deviations far off the allowable threshold occurs. To overcome this challenge, an adaptive inertia control strategy based on optimization technique is proposed. The improved particle swarm optimization (PSO) and Generic algorithms (GA) optimization techniques based PID controller has been used to generate the appropriate virtual inertia coefficient for
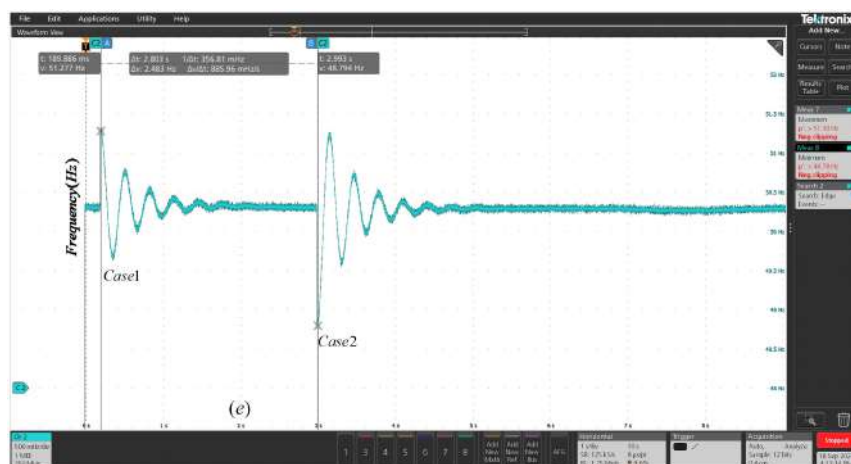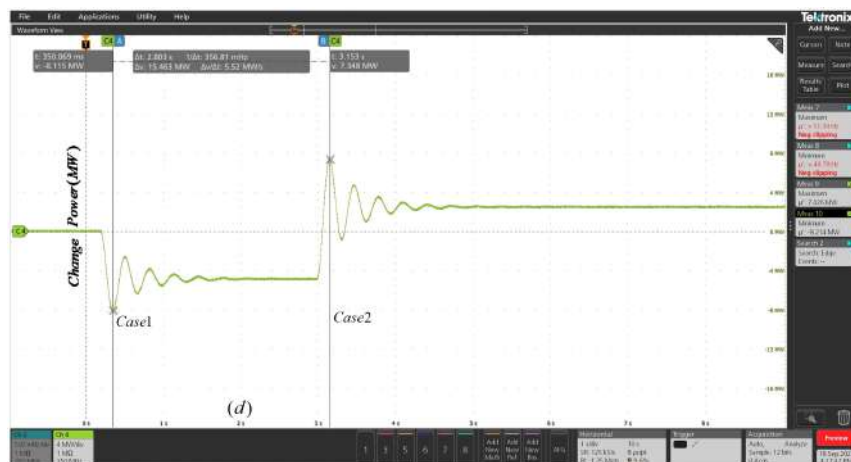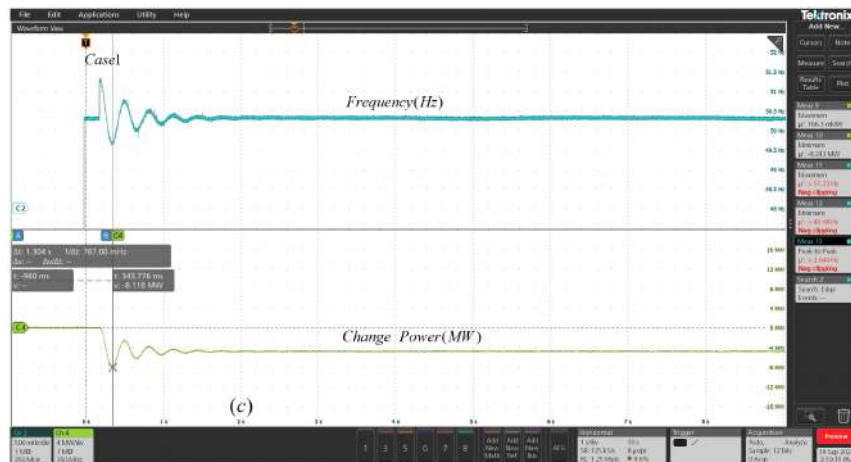
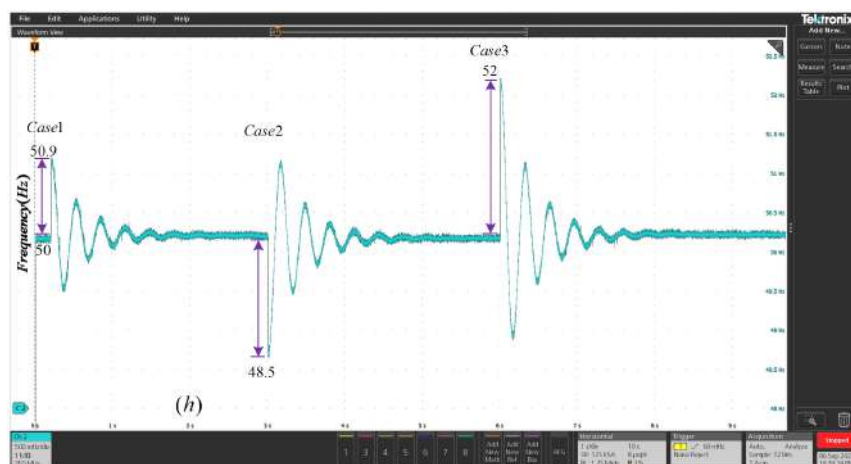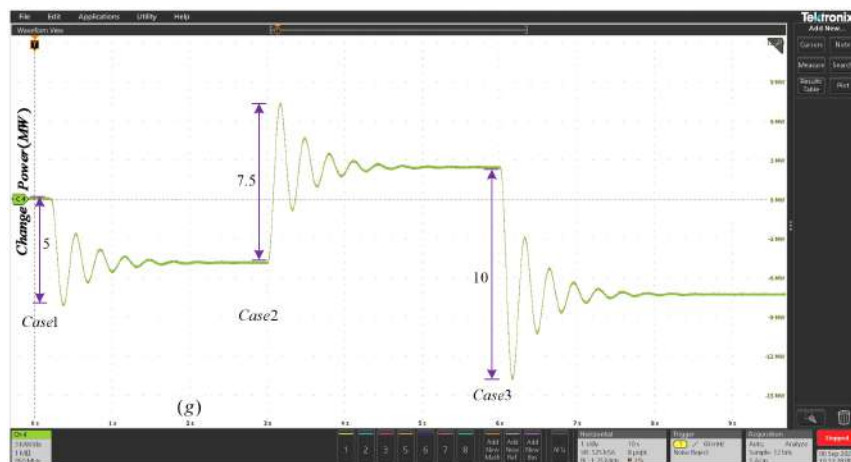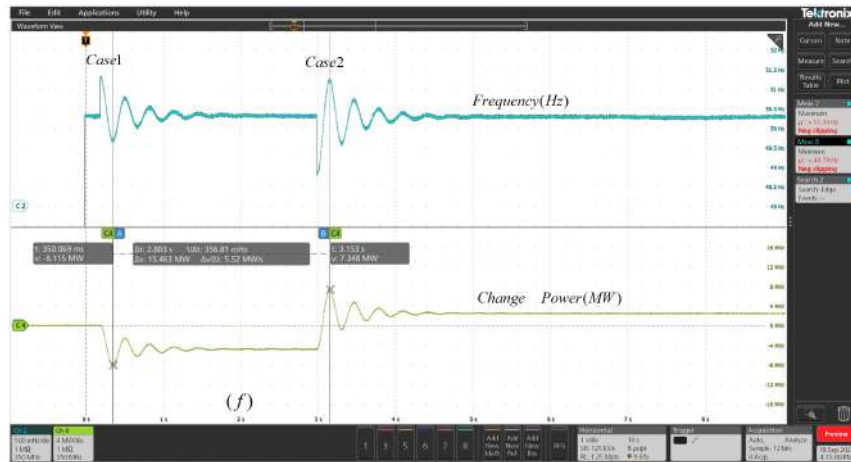*Chapter 2. Introduction to Virtual Synchronous Machine Concept and Its Control*

effective emulation of inertia in the presence of energy storage system. The conventional PSO suffers local optima stagnation, resulting into premature convergence during searching process in order to achieve global and local position. To address this issue, the velocity update equation was modified on inertia weight (w) using an additional exponential term with linear decreasing inertia weight PSO (LDIW-PSO). In this paper exponential power is taken strategically instead of squaring it in order to reduce the number of iterations for faster convergence. Finally, a microgrid based on wind and solar energy is simulated using MATLAB/Simulink where three cases; 2% disturbance, 3% disturbance and 4% disturbance have been considered. Here, the evaluation of proposed system is carried out based on four main performance indices (ITAE, IAE, ISE and ITSE). Furthermore, validation of was done through hardware prototype to get experimental results in real time. The results from MATLAB simulation and experimental setup are in sync.

49

Chapter 3

Hybrid Energy Storage Systems for Inertial Response in Micro-grid

3.1 Preamble

In modern times, the energy industry has seen significant growth. Several countries around the world are facing the challenge of ever-increasing energy demand. The conventional methods of power generation are already at their peak and going to be exhausted in near future. Additionally, the traditional methods of power generation are environmentally hazardous. Fossil fuels generate greenhouse gases, which contaminate the environment and pose a threat to the living organisms inhabiting the region. In order to address these issues, renewable energy sources (RES) are being rapidly implemented in contemporary power system networks. Nevertheless, the growing integration of power electronics interfaced RES results in to reduced inertia and hence, poses a significant challenge for the grid stability [3]. The reduced inertia triggers frequency instability (high rate of change of frequency (RoCoF), frequency nadir and zenith). Further, this problem is very much exaggerated in power system network confined to small geographical locations termed as micro-grid.

The inertia issue in micro-grid operation and control is of lot of concern and several schemes primarily based on rotational mass have been proposed. Synchronous generators operating without any load, commonly referred as synchronous condensers (SC) have been widely used to compensate the loss of inertia [72]. However, the use of dedicated synchronous condenser is bulky, inefficient and costly affair without any significant improvement in performance.

50Chapter 3. Hybrid Energy Storage Systems for Inertial Response in Micro-grid
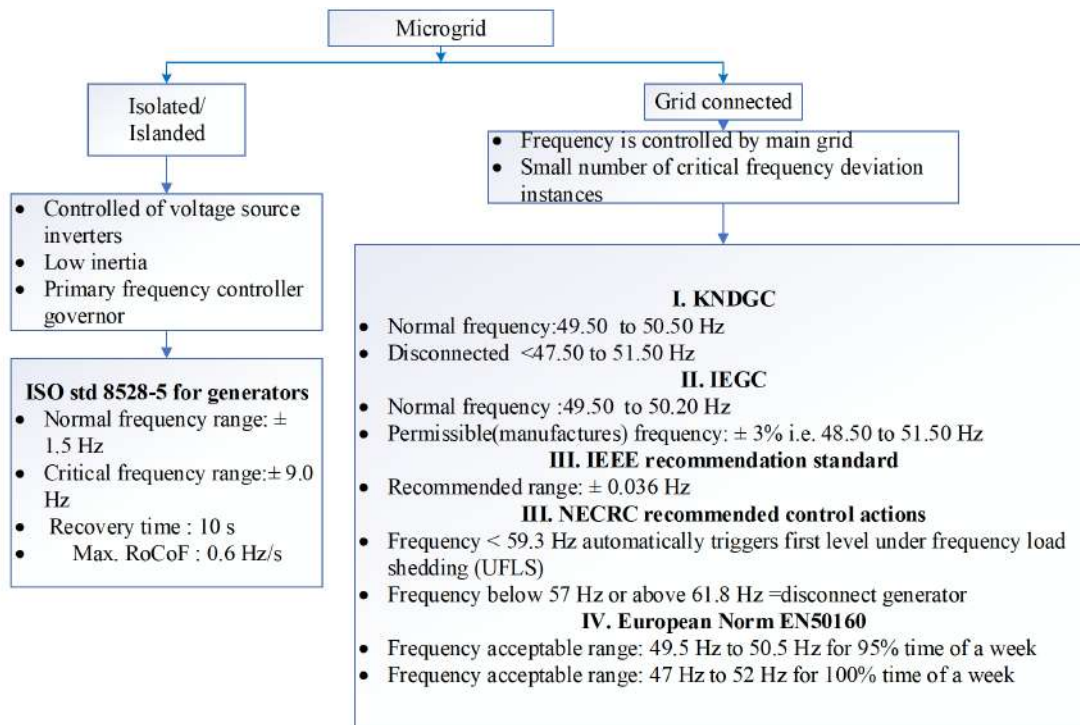
FIGURE 3.1: Frequency standards of Microgrid [1, 2]

To reduce the additional burden of machine, recently few schemes have been proposed where the inertia of rotating wind turbines is utilised as SC [37]. While this kind of technology seems very promising, but under variable speed operation of wind turbines, it becomes very difficult to extract the characteristics of typical SC and hence, not suitable for inertial control. The energy stored inside DC-link capacitors is also found to be very useful to overcome small transient load disturbances but have very limited capability heavily dependent on the size of capacitor. Further, this kind of approach is suitable only where slight variation in DC-link voltage is allowed and not applicable to rigid DC-links comprising batteries having almost fixed voltages. Sometimes, the generating facilities in a micro-grid are operated under partial-loading to keep a cushion for further increase in load. However, running a micro-grid under reduced loading is extremely inefficient and increases the per unit cost of generating electricity.

Figure. 1 shows frequency codes for restoration in micro-grid operation prevalent in various organizations and countries.

Very recently, the energy storage systems (ESS) have been discussed widely

with the intention of solving the problem of frequency instability in distributed generation system (DG) [73]. The ESS is found to be most promising for virtual synchronous machine emulation in power electronics dominant RES based power generation. ESS having limited capacity in terms of both power and energy, can be categorized on the basis of their response; rapid response ESS like flywheel, ultra-capacitors and li-ion batteries are called short-term while chemical battery (lead acid), pumped hydro storage and compressed air are known as long term ESS. Most of the research work reported in the area of ESS power management is limited to theoretical analysis in control stability of droop, but silent about optimal sizing of ESS [74, 75]. Optimal sizing of Hybrid ESS is one of the essential ingredients not limited only to cost effectiveness but also to achieve enhanced performance out of it. Further, it is also necessary to maintain State of charge (SOC) within a given acceptable level and that's why it need to be included in feedback control loop [24, 29]. Chu Sun proposed feedback control with additional Proportional and Integral (PI) regulator for fast-acting and slow acting energy storage system (FAESS and SAESS) to emulate synchronous generator [4]. However, in this proposal the design of PI parameters is done through trial-and-error method. The challenge of optimal energy control was addressed by Spyridon Chapaloglou in [76] by controlling primary frequency through optimal methods. But, the sizing aspect of ESS is not considered in this particular article. In [77, 78], PV-BESS is proposed and optimized using linear programming, but did not explained effectiveness of hierarchical control nature of the systems [79, 80].

Recently, HESS based energy management techniques have been proposed to address the inertia issue. Through the hybridization of a battery and an ultra-capacitor, fast frequency response (FFR) is achieved [81]. Inertia and damping emulation are restored using the energy recovered from them. Ultra-capacitor has high specific power density hence, its response time is rapid, that's why it is also referred as rapid response energy storage system (RRESS). The battery has high energy density hence, the response is slow and termed as slow response energy storage system (SRESS). The idea of virtual synchronous generators (VSGs) replicated by power electronic converters is becoming increasingly popular [9]. However, problems with response time and parameter fluctuations make overall control more complex. Numerous studies have been

52*Chapter 3. Hybrid Energy Storage Systems for Inertial Response in Micro-grid*

examined to analyse the non-inertia generation effect on frequency dependability, resilience, and stability of bulk power networks [41]. In [82], the ESS has been regulated for emulating the characteristics of virtual synchronous generator (VSG) to maintain frequency stability in low inertia network. A typical VSG control approach incorporates the droop control loops to regulate its output active and reactive power for the better terminal voltage regulation and faster inertial response. However, sizing of HESS and determining the gains of control loops for different operating conditions is a very tedious and complex task.

A HESS based VSG is proposed in [83, 84] where inertia constant (H) and damping constant (D) are emulated and compared with conventional parameters. Here, conventional PSO is used for parameter optimization which suffers from several convergence challenges. Furthermore, a low pass filter-based approach is adopted for power sharing between battery and supercapacitor without considering frequency zenith which is caused by abrupt load shedding of power supply. In [85], NN-based VFOPID is proposed to address reduced inertia problem in isolated microgrid which is very computationally intensive considering online updating of parameters. Since, the ultracapacitor and battery have different characteristics, it is very important to analyze them independently in order to design a HESS pack. Sizing of both battery and ultra-capacitor must be optimized in such a way that it is able to handle maximum change in energy demand while keeping the voltage and frequency within permissible limits. Although, determining the size of ultracapacitor and battery forming a HESS is a typical off-line optimization problem, but optimal utilization of their capacity for a given disturbance is an online optimization issue. Therefore, the controller gains must be updated while considering the amplitude of disturbance. A typical online optimization technique has been proposed in [86] where power fluctuations are handled by updating VSG variables using backtracking search optimization approach. Here, the damping co-efficient D is updated while taking RoCoF in account whereas inertia constant H is updated depending on frequency deviation. This technique exhibits superior performance in comparison to constant variable approach but at higher computational cost. A similar approach based on self-adapting inertia and damping constant has been proposed in [87]. In [66], a fuzzy logic based VSG has been proposed where the parameters are updated using change in

power from RES and frequency deviation only while neglecting the RoCoF. Another fuzzy logic based inertia control approach has been proposed in [88] where both the RoCoF and the frequency deviation have been considered for inertia updation. Since, fuzzy logic-based approaches are expertise dependent, the effectiveness of such algorithm depends on accuracy of rule formulation. The methodology described in reference [10] employs a bang-bang technique based virtual inertia calculation while considering damping coefficient as constant. A PSO based methodology has been presented in [89] where low pass filter is used to determine the power sharing of HESS. However, LPF has inherent disadvantage of introducing delay which affects the control performance of the system. A PSO optimized fuzzy controller is proposed in [90, 91] which is found to be marginally better than pure fuzzy based approach. However, writing the rules for such a heavily fluctuating system is still a big issue.

Since, RES based microgrid is highly volatile system, the gains of its PID regulator need to be updated as per the operating conditions. Determining the inertia gain under different operating conditions is a typical optimization problem for which lot of PSO based methods have been reported as discussed previously. But the conventional PSO is having premature convergence issue which affects the control accuracy. Therefore, in the proposed work, an improvised version of PSO approach has been implemented for the optimum adjustment of a PID regulator gains. Here, the improved PSO is a modified version of conventional PSO by incorporating natural exponential weight updating of velocity equation to avoid it from premature convergence. Furthermore, the optimal sizing of constituent component of HESS and effective utilization of their capacity in power sharing based on their response time improves the reliability of system at significantly lesser cost. The integral squared error (ISE) of frequency deviation is taken as objective function for the tuning of PID regulator with the aim of enhancing rate of change of the frequency, zenith & nadir while minimizing the restoration time.

Here is a summary of this chapter's main contributions:

- Application of improved PSO-based PID controller on bidirectional DC-DC converter interfaced HESS to enhance frequency response in microgrid under severe disturbances to ensure system stability.
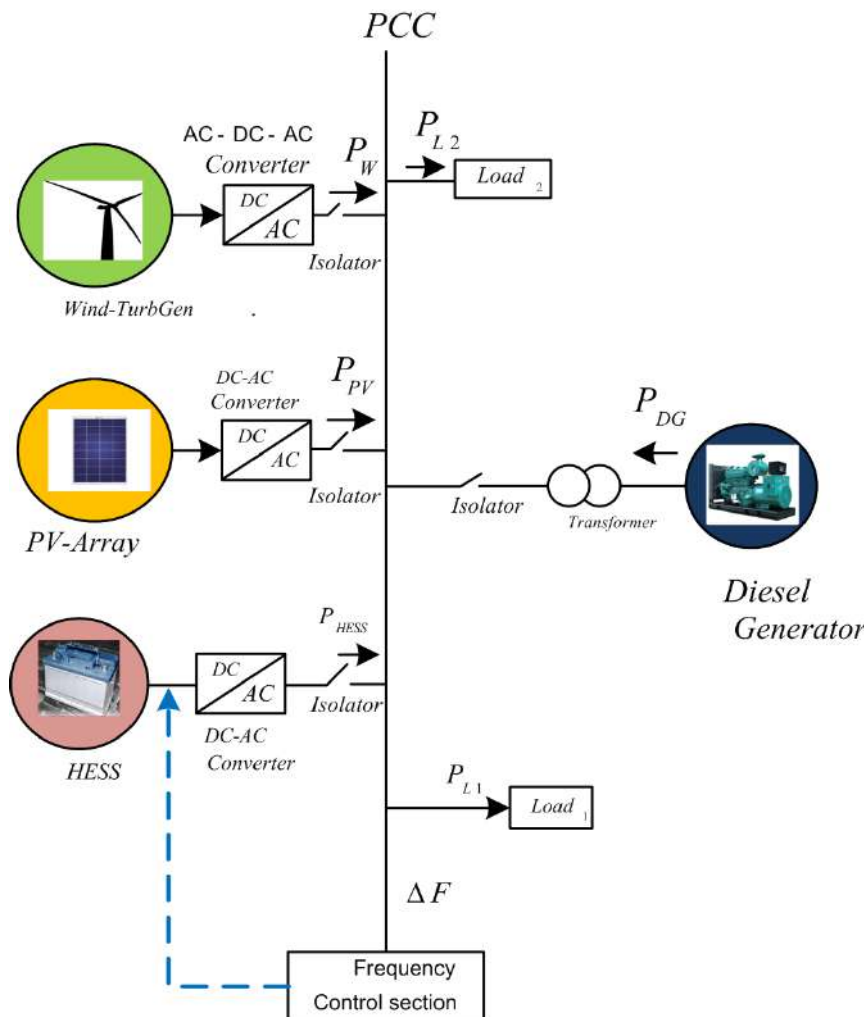
FIGURE 3.2: Diagram of typical Microgrid

- Automatically tuning of PID controller parameters based on both traditional PSO and improvised PSO in the novel adaptive virtual inertia control-based HESS.

- Enhancement of frequency nadir, restoration time, and RoCoF using improved PSO in comparison to conventional PSO tuned PID regulator.

- Optimal techniques applied to reduce the size of Ultracapacitor based HESS as a result of reduced restoration time, frequency nadir, and energy requirement.

3.2 System Configuration and control

Traditionally, synchronous generators are used to generate power and also to act as natural inertia and damping control. The turbine harnesses the stored kinetic energy to regulate the frequency. However, as renewable energy becomes more prevalent, the inherent inertia is diminishing. To accomplish this problem, the idea of virtual synchronous generators (VSG) has been implemented [92]]. In the proposed system as shown in Figure 3.2, a 15 MW PV generation unit (PVG), 200 MVA rated diesel generator unit (DG), wind power plant of 25 MW and battery/ultra-capacitor have been considered in the form of microgrid. Battery and ultracapacitor-based HESS has been considered to emulate the characteristics of VSG. HESS can offer active power regulation, energy management, and rapid and slow services in frequency control at a comparatively cheaper price [93]. The bidirectional DC-DC converter is used for coupling parallel combination of RRESS and SRESS to the DC-link of the grid interfacing inverter as seen in Figure 3.3 and Figure 3.4. The common inverter uses virtual governor control similar to a traditional SG along with inertia and damping emulation as integral part of its control objectives. However, the power reference of RRESS also includes an energy recovery control. The RRESS's stored energy can be expressed as a SoC-equivalent value, such as $\frac{CV_{dc}^2}{2}$ for ultracapacitor. The DC PTS connected to the RRESS is responsible for maintaining DC voltage on the shared DC bus. However, the DC PTS of the SRESS is designed to adjust its power output based on the power reference from droop and integrated control loop, similarly to the turbine and governor system. Consequently, the RRESS autonomously delivers rapidly changing elements by controlling virtual inertia constants and damping constants. If the SRESS is designated as the slack bus, integral control may be used to restore the frequency. Consequently, the RRESS efficiently delivers the rapidly changing elements by effectively controlling virtual inertia and damping. The SRESS monitors the slow-fluctuating components of the VSG while detecting any changes in frequency.

In this chapter, the parameters used were obtained from [59], and listed in Table 3.1

56Chapter 3. Hybrid Energy Storage Systems for Inertial Response in Micro-grid
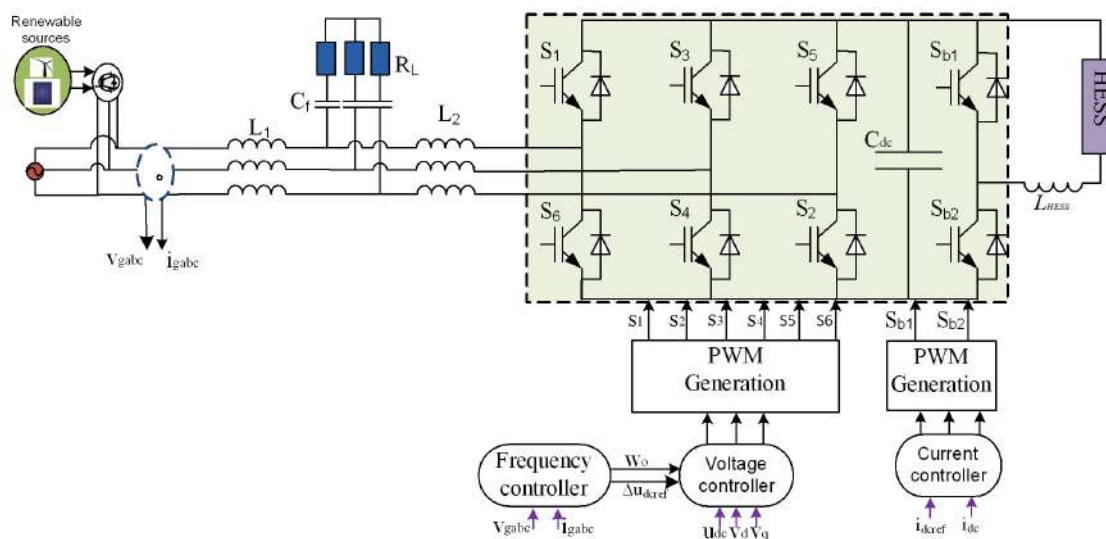
FIGURE 3.3: Schematic diagram of power converter in microgrid
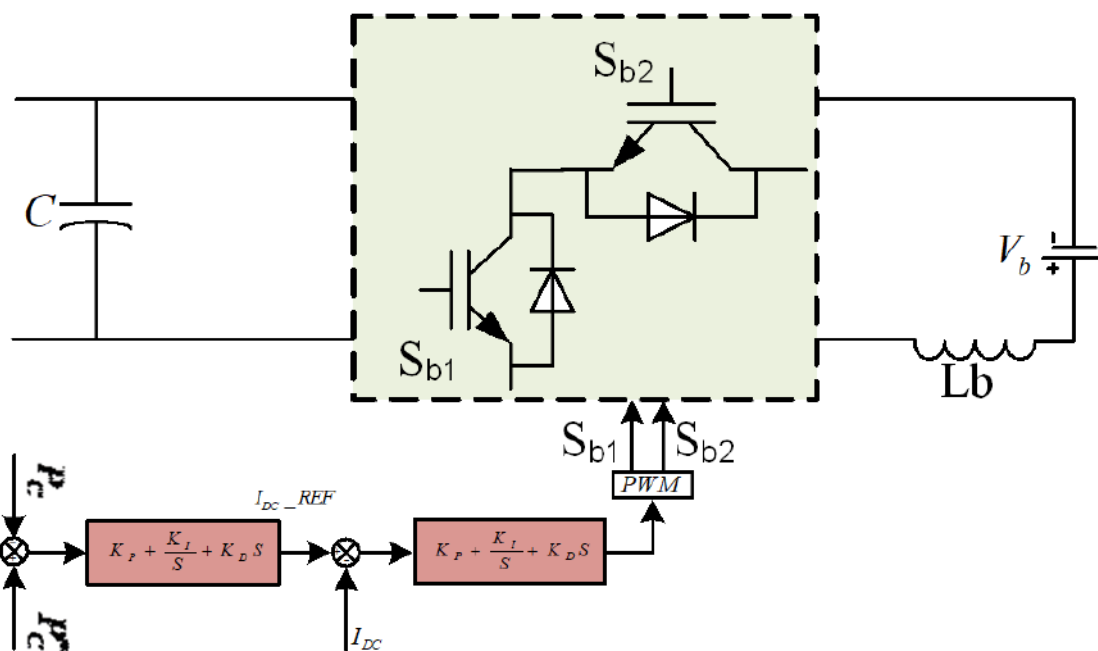
FIGURE 3.4: DC-DC bidirectional converter interface HESS diagram

TABLE 3.1: System Parameters

Features	Value
Battery voltage	350 V
Grid voltage	415 V
DC inductance	5.6 mH
DC link capacitance	2.82 mF
DC-link voltage	600 V
Frequency	50 Hz
Turbine Time Coefficient	0.5 s
Governor Time Coefficient	0.2 s
Generator Inertia Coefficient	5 s
Governor Speed Regulation	0.05
Damping coefficient	0.8

3.2.1 Energy Variation and Sizing of HESS Due to Frequency Deviation

Sizing of ultra-capacitor is crucial task when designing virtual synchronous machine, it should be decided in such a way that maximum variation of energy during transient disturbance may be addressed. The greatest change in energy capacity is assessed by;

$$\Delta E_{\max} = \frac{(E_{\max} - E_{\min}) + (E_{\max} - E_{\min})}{2} = E_{\text{nom}} \left(\frac{E_{\max}}{E_{\text{nom}}} \right) \tag{3.1}$$

$$\Delta E = \frac{J_{uc}(w_{nom}^2 - w_{nadir}^2)}{2} \quad \text{and} \quad \left. \frac{J_{uc}(w_{zenith}^2 - w_{nom}^2)}{2} \right|_{\max}$$

$$\left. J_{uc} w_{nom} \Delta w \left(\frac{J_{uc} w_{nom}^2}{2} \cdot \frac{\Delta w_{\max}}{w_{nom}} \cdot \frac{w_{uc,\text{rated}}}{\Delta w_{\max}} \right) \right|_{\max} \tag{3.2}$$

58 Chapter 3. Hybrid Energy Storage Systems for Inertial Response in Micro-grid

$$E_{\text{nom}} = \frac{H_{uc} S_{\text{rated}} (\Delta w_{\text{max}})}{w_{\text{nom}}} \bigg/ \left(\frac{\Delta E_{\text{max}}}{E_{\text{nom}}} \right) \tag{3.3}$$

For ultra-capacitor, maximum energy change is determined by;

$$\Delta E_{\text{max}} = CV_{(\text{dc,nom})} \Delta V_{(\text{dc,nom})^2} \left(\frac{\Delta V_{(\text{dc,max})}}{V_{(\text{dc,nom})}} \right)_{(\text{dc,max})} \tag{3.4}$$

To determine the size of the capacitor, equations 3.3 and 3.4 are equated with a well-designed inertia constant H_{uc}:

$$CV_{(\text{dc,nom})}^2 \times \left(\frac{\Delta V_{(\text{dc,max})}}{V_{(\text{dc,nom})}} \right) \left(\frac{H_{\text{uc, rated}} \Delta w_{\text{max}}}{w_{\text{nom}}} \right)$$

$$H_{\text{uc}} = \frac{C_{\text{dc}} V_{\text{dc}}^2}{2 S_{\text{rated}}} \cdot \frac{\Delta V_{\text{nom, dc, max}}}{V_{\text{dc}} \Delta f_{\text{max}}} \tag{3.5}$$

$$H_{\text{uc}} = H_{\text{vi}} \cdot \frac{\Delta V_{\text{nom, dc, max}}}{V_{\text{dc}} \Delta f_{\text{max}}} \tag{3.6}$$

$$H_{\text{vi}} = \frac{C_{\text{dc}} V_{\text{dc}}^2}{2 S_{\text{rated}}}$$

As seen in equation 3.6, the factors to consider for the virtual inertia constant H_{uc} are: given dc-link voltage V_{dc}, maximum ratio of voltage variation $\frac{\Delta V_{\text{dc, max}}}{V_{\text{dc}}}$, minimum ratio of frequency variation $\frac{f_{\text{nom}}}{\Delta f_{\text{max}}}$, and the rated dc-link capacitance C_{dc}.

Virtual inertia can be generated by designing a proportional controller as follows:

$$K_{\text{vi}} = \frac{\Delta V_{\text{dc, max}}}{V_{\text{dc}} \cdot \frac{f_{\text{nom}}}{\Delta f_{\text{max}}}} \tag{3.7}$$

A proportional controller for allowable deviation of both frequency and voltage is indicated by the MATLAB graph as shown in Figure 5 (a), (b). The coding in MATLAB is done with the following values: the frequency change $\Delta f_{\text{max}} = 0.2$, $w_{\text{nom}} = 50$ Hz, the power rated was scaled down $S_{\text{rated}} = 1000$ VA, $\frac{\Delta V_{\text{dc,max}}}{V_{\text{dc,nom}}} = 0.15$, and $C = 2.82$ mF [21].
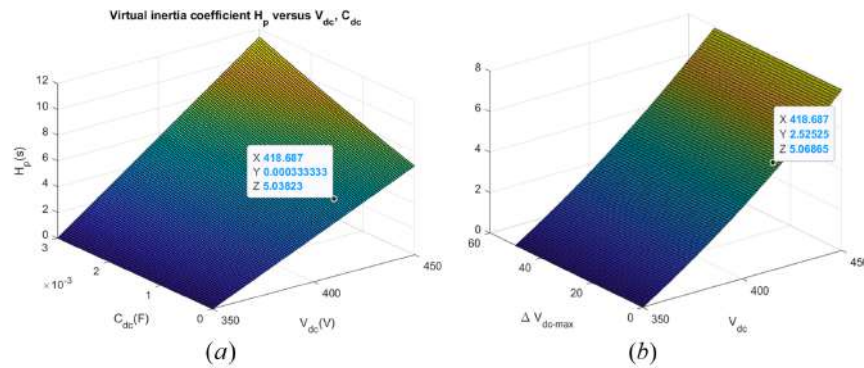
FIGURE 3.5: Virtual inertia coefficient

As seen in Figure 5 (a), for an inertia of 5.03823 and a voltage within the acceptable threshold of 400 ± 36 V (in this case 418.687 V), the capacitance needed is 333.333 μF. The available capacitors can be found in market stores. In Figure 5 (b), the change in voltage is restricted to 2.52525 V, which is 5.3031%, and is within the acceptable limits.

3.2.2 Diesel Generator

The governor of the SG controls the real power. The governor's main objective is to regulate the output power of diesel engine by adjusting the mechanical power of the synchronous generator to match the difference between mechanical and electrical power. The swing equation is as follow in equation 3.8

$$\Delta P_m(t) - \Delta P_L(t) = \frac{2Hd\Delta f(t)}{dt} + D\Delta f(t) \tag{3.8}$$

Where:

- ΔP_m : Power production varies depending on the turbine

- ΔP_L : Change in power demand

- Δf : Frequency deviation

- H : Inertia constant

- D : Damping constant

$$\frac{1}{2HS + D}$$
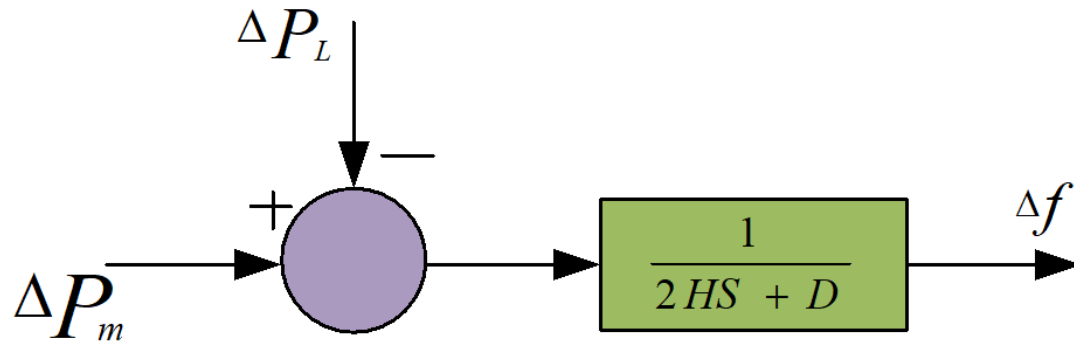
FIGURE 3.6: Frequency deviation model
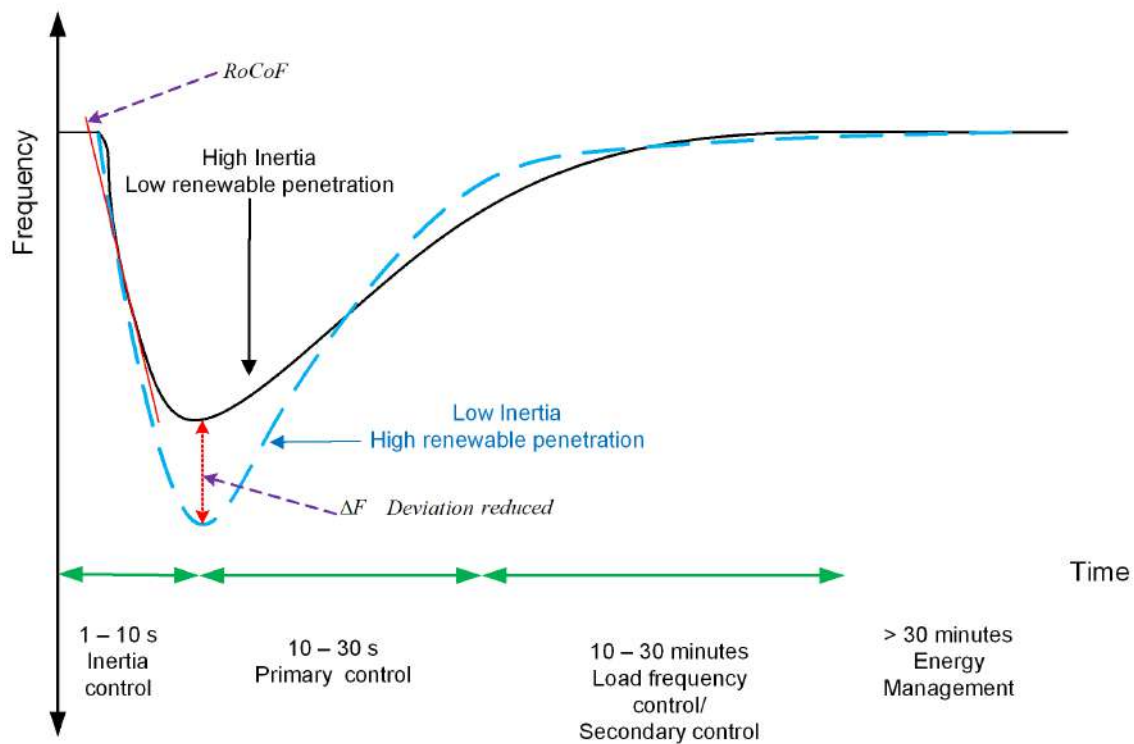
FIGURE 3.7: Main frequency deviation curve

The equation 3.8 is represented in Figure 3.6.

The Figure 3.7 shows the profile of how system frequency is controlled. In any network grid frequency is among the most crucial performance indicator. Frequency degradation of the system is due to abrupt disturbance caused by generation tripping or load shedding. Frequency is regulated to prevent large (RoCoF) and high frequency deviation beyond allowable maximum.

3.3 Proposed Virtual Inertia Control Concept for Frequency Regulation

3.3.1 Particle Swarm Optimization (PSO) Implementation for PID Controller Parameters Tuning

Control of HESS is essential to enhancing system stability. In this part, we will discuss how to regulate virtual inertia by determining ΔV_{dc} and Δf. This is done by utilising a PID controller to acquire the actual power reference. Here, an optimisation technique is applied to automatically tune the PID regulator. The improved PSO is a modified version of conventional PSO by incorporating natural exponential weight updating of the velocity equation to avoid premature convergence. PSO was first introduced in 1995 by James Kennedy and Russel C. Eberhart [60]. It explains the social nature shown by animals, such as a group of birds or fish. This technique is powerful, easy to implement, has low computational burden, and is an efficient tool. It is suitable for online optimization. The following formulas determine the position and speed of each particle: local position p_i and best global position g_i of the particles as follows:

$$u_i^{(t+1)} = wu_i^t + c_1r_1(p_i^t - d_i^t) + c_2r_2(g_i^t - d_i^t) \tag{3.9}$$

$$d_i^{(t+1)} = d_i^t + u_i^{(t+1)} \tag{3.10}$$

Where r_1 and r_2 are random constants ranging from 0 to 1, c_1 and c_2 are the cognitive coefficient and social coefficient, respectively, ω is the inertia weighting function.

Chapter 3. Hybrid Energy Storage Systems for Inertial Response in Micro-grid

- ωu_i^t: inertia

- $c_1 r_1 (p_i^t - d_i^t)$: cognitive unit

- $c_2 r_2 (g_i^t - d_i^t)$: social unit

The inertia weight ω is essential during exploitation and exploration in the search space. A well-optimized value reduces the convergence period. To modify the inertia weight and update it dynamically, a highly successful method based on linearly decreasing inertia weight PSO was provided in reference [56], as given in equation 3.11

$$w = (w_{\text{start}} - w_{\text{end}}) \times \left(\frac{T_{\text{max}}}{T_{\text{max}}} \right) + w_{\text{end}} \qquad (3.11)$$

Where,

- ω_{start}: starting inertia weight

- ω_{end}: end value of inertia

- T_{max}: maximum iterations

During the searching procedure, the Linear Dynamic Inertia Weight-Particle Swarm Optimization (LDIW-PSO) encountered difficulty settling into a local optimum. Furthermore, excessively small or high values of the inertia constant may lead to an increase in the number of iterations and the time it takes for convergence, thus negatively affecting the performance of the optimization engine.

In order to address this problem, we multiply the natural exponential with ω_{end} to improve the equation for updating velocity, which was already introduced in our earlier publication [94]. Similarly, [57] incorporated an exponential square, resulting in an additional rise in computational burden. To reduce computational burden while maintaining speed, a weight update matrix now includes an exponential component with an optimal value of T_{max} [95]. Consequently, the total time it takes for convergence lowers as the number of iterations is reduced. The adjusted equation 3.12 has been modified as follows:

$$w = (w_{\text{start}} - w_{\text{end}}) \times \left(\frac{T_{\text{max}}}{T_{\text{max}}} + w_{\text{end}} \times e^{-\frac{t}{(T_{\text{max}}/10)}} \right) \qquad (3.12)$$

Where $w_{\text{start}} = 0.9$ and $w_{\text{end}} = 0.2$.

This optimization technique is applied to maintain frequency stability in the microgrid. It is vital to maintain frequency stability following disturbances by minimizing the frequency nadir, zenith, and the rate of change in frequency (RoCoF) after the disturbance. Furthermore, there is a need for quicker restoration of the steady-state frequency. The magnitudes of the highest observed lowest point and rate of change of frequency (RoCoF) of the point of common coupling (PCC) frequency after the disturbance may be represented as:

$$\text{Obje1}(K_p, K_i, K_d) = \max |f_{\text{PCC}} - f_{\text{nom}}| \tag{3.13}$$

$$\text{Obje2}(K_p, K_i, K_d) = \max \left| \frac{df_{\text{PCC}}}{dt} \right| \tag{3.14}$$

Where f_{nom} is the normal or rated power in the microgrid and f_{PCC} is the measured frequency at the point of common coupling (PCC). The value of RoCoF is also obtained during the disturbance. The Integral Squared Error (ISE) performance index is utilized to optimize the values of K_p, K_i, and K_d in the system.

Flowchart in Figure 3.8 is an algorithm for MPSO, modified inertia weight as inserted in equations **??**.

It is worth mentioning that the power required to maintain the frequency stability of the system may be determined by analysing the discrepancy between the voltage and normalized frequency. For adjustment and better frequency stability support, PID controller is applied for correction in the differences [96], as stated in Equation(15), which is an extension of equation 3.7, illustrates the achievement of reference active power.

$$P_{\text{ref}} = \left(\frac{\Delta f}{f_{\text{nom}}} - \frac{\Delta V}{V_{\text{nom}}} \right) \cdot \left(K_{P1} + \frac{K_{I1}}{S} + K_{D1}S \right) \tag{3.15}$$

In this proposed control strategy, power flows out from the ESS when there is increase in load or when a supply shuts down. When RES source is added, the power flows to the ESS. The converter act as bidirectional virtual support. Virtual inertia control is critical for frequency stability as it reduces RoCoF and frequency zenith and nadir.

64Chapter 3. Hybrid Energy Storage Systems for Inertial Response in Micro-grid
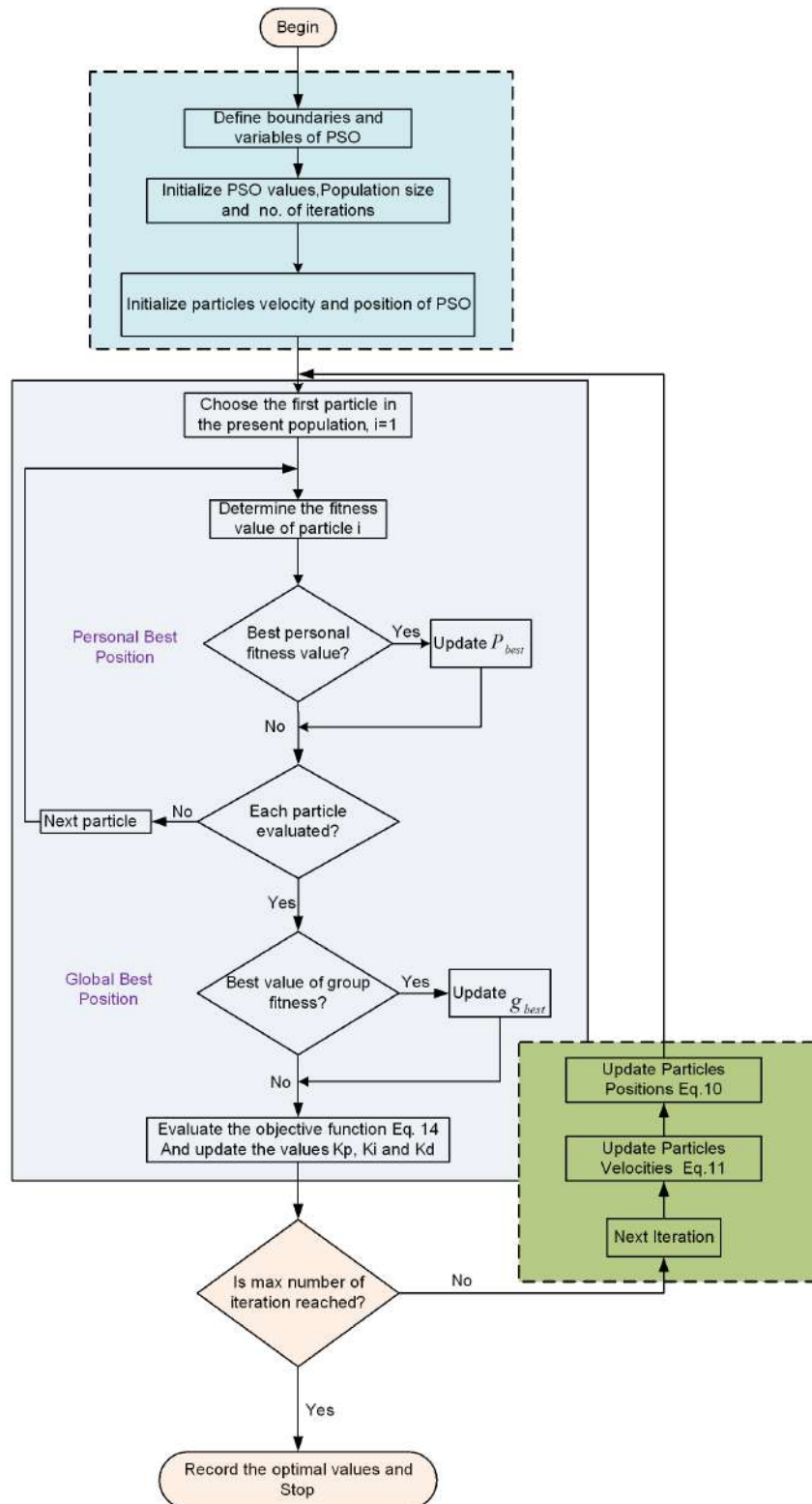
FIGURE 3.8:   Improved Particle swarm optimization (MPSO)
flowchart
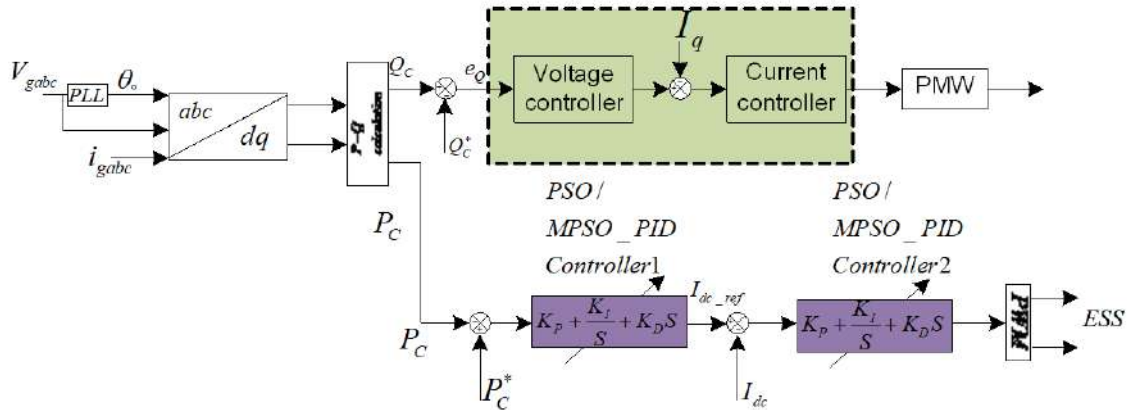
FIGURE 3.9: Block diagrams of control frame for switching signals
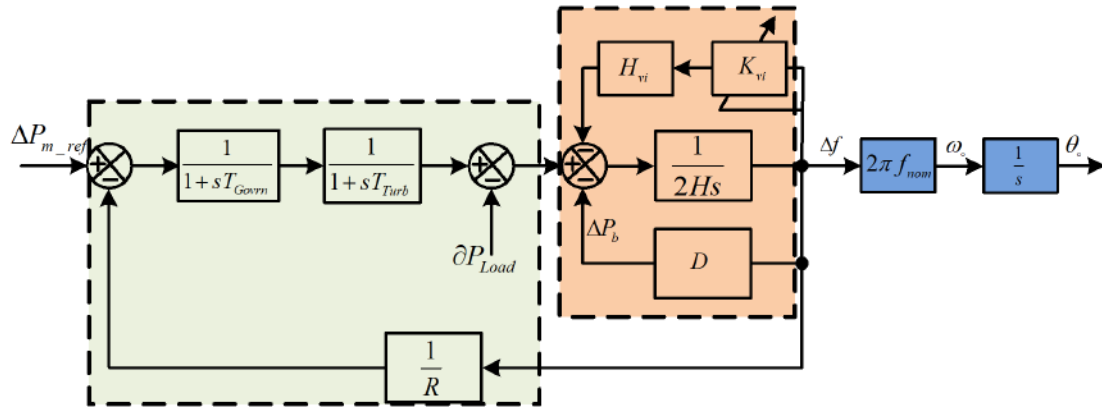
FIGURE 3.10: Block diagram of Inertia control structure of frequency regulation

3.3.2 Modelling of block diagrams of frequency control

The frequency control block is shown in the diagram. The frequency Q_g, f_g, and P_g are the measured grid reactive power, frequency, and real power, respectively. The outcomes of the frequency control are the displacement angle θ_0, output frequency f_0, and angular frequency ω_0. The controller operates in a similar manner to the standard frequency controller of synchronous generators [97]. The switching signals that control the gates are shown in Figure 3.9. The frequency control diagram is shown in Figure 3.10.

66Chapter 3. Hybrid Energy Storage Systems for Inertial Response in Micro-grid

3.4 Analysis of Simulation and Experimental Findings and Discussion

3.4.1 Simulation findings and Discussion

The effectiveness of the proposed technique was evaluated by simulating the frequency of the microgrid using Matlab/Simulink. The ultracapacitor is designed to improve frequency responsiveness. Parameter tuning is done by the use of optimisation techniques. As shown, frequency deviation Δf is the optimal objective function;

$$\text{ISE} = \int_0^{T_{\text{Sim}}} \left| \Delta f^2 \right| dt \tag{3.16}$$

Where:

- ISE - Integral Squared Error

- T_{Sim} - simulation time range

The objective function in equation 3.16 is applied using both optimization techniques, and the outcomes are recorded in Table 2. In the performance index ISE, the error is squared; therefore, it handles both positive and negative errors.

TABLE 3.2: Optimal values

Parameters	PSO	Improved PSO
K_P	1000	1000
K_I	39.0995	0.6893
K_D	0	0

The cases considered in the analysis of this proposed controller in the MG's frequency response are as follows:

CASE 1: Increased Power generation of 5 MW from PV Figure 3.11, illustrates the frequency response of microgrid due sudden increase in PV generated power at 0.2 s by virtue of increased radiations. The frequency rose abruptly post disturbance attributed to power generated by PV unit as seen in Figure 3.12.
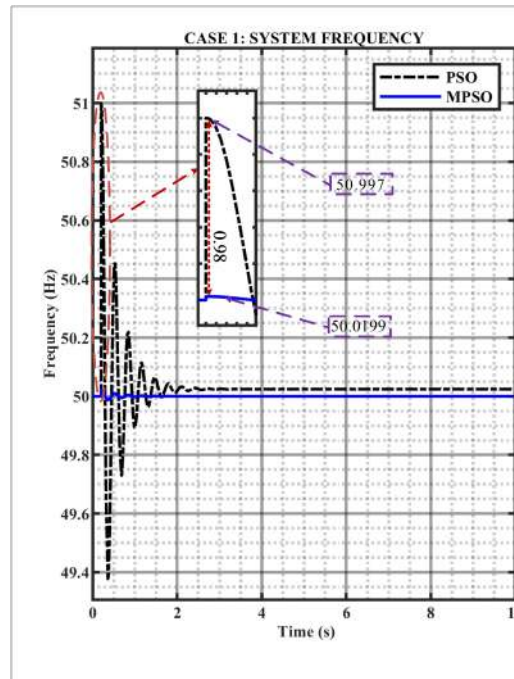
FIGURE 3.11: Frequency response for case 1

Both the convectional PSO and Improved PSO have been implemented for parameters tuning in such a way that the deviation in frequency is contained within the permissible threshold.   However, Improved PSO has smaller frequency deviation compared with conventional PSO; that is, 50. 0199 Hz and 50.997 respectively. The difference in frequencies is used to calculate the capacity of ultracapacitor energy saved by applying equation 3.3.   The difference in frequencies using both the methods is found to be 0.98 Hz which is equivalent to additional amount of energy storage of 490 kW.s. needed to curtail the frequency deviation. In other words, the improvised PSO helps in reducing the additional storage capacity in comparison to conventional PSO.

CASE 2: Increase in load demand of 7.5 MW In this scenario, a sudden surge in load demand of 7.5 MW is considered at 3 s.   Due to this disturbance, frequency drop is seen in Figure 3.13. just after the increase in load as depicted in Figure 3.14. In this scenario, the lowest point is 48.52 Hz using conventional PSO, though it is within allowable frequency deviation but it requires large ultracapacitor to accommodate the fluctuation of such magnitude. For improved PSO, the frequency deviation is found to be 49.97 Hz. The different between the

68Chapter 3.   Hybrid Energy Storage Systems for Inertial Response in Micro-grid
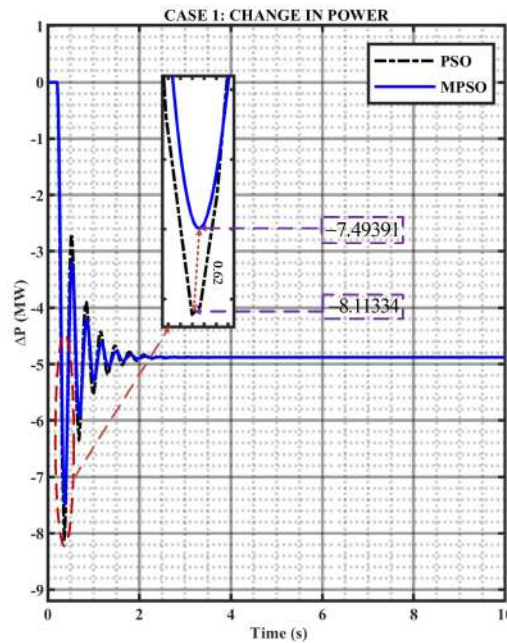
FIGURE 3.12: 5MW Increased Power generation of 5 MW from PV

two strategies in terms of frequency is 1.45 Hz. Thus, by applying equation 3.3, the additional storage capacity of 1.0875 MW. s is saved using proposed Improvised PSO. For convenience of comparison, the disturbance for scenario 1 was kept constant throughout the simulation at 0.2 of 5MW second. Furthermore, the fact that this technique can handle both circumstances at once is proof that it is better.

CASE 3: Increase in wind generated power of 10 MW In this scenario, a sudden enhanced wind power of 10 MW is considered at 6 s due to sudden increase in wind velocity. Due to this sudden increase evidence in Figure 3.16, imbalance between demand and supply arises which results in frequency shoot up as shown in Figure 3.15. The highest point is 51.9886Hz based on PSO and 50.0398 Hz based on Improved PSO. It is to be noticed that the differences in frequency using both the strategies is 1.95 Hz. The energy calculated for this much frequency difference is of 1.95 MW.s. This shows that the cost of installing larger Ultracapacitor is reduced with Improved PSO. To make comparisons simple, disturbances for Case 1 at 0.2 seconds of 5MW and Case 2 at 3 seconds of 7.5 MW were included during simulation. Given that it can manage all three eventualities at once, this technique

3.4. Analysis of Simulation and Experimental Findings and Discussion 69
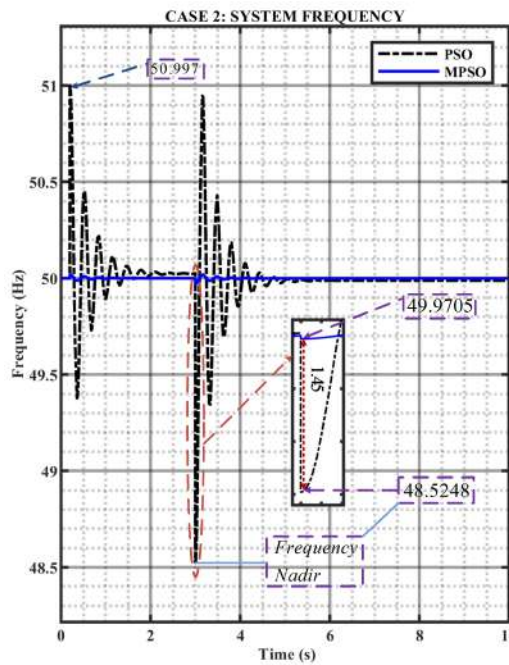
FIGURE 3.13: Frequency response for case 2
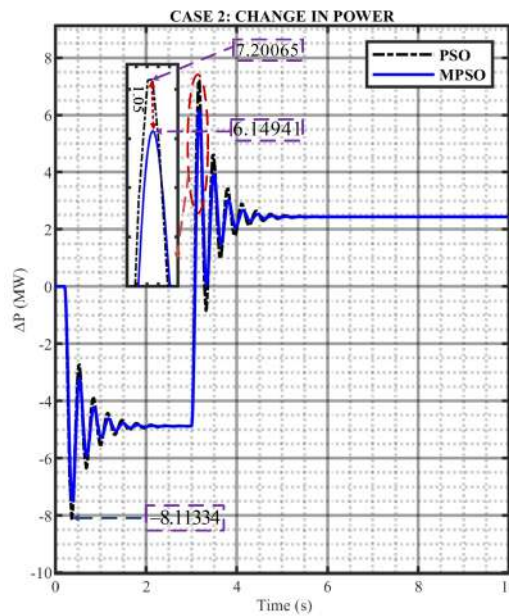
FIGURE 3.14: Increase in load demand of 7.5 MW

Chapter 3. Hybrid Energy Storage Systems for Inertial Response in Micro-grid
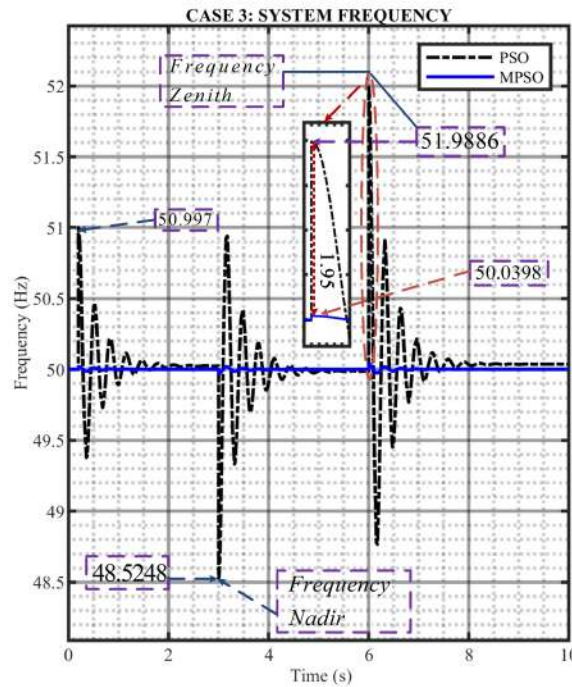
FIGURE 3.15: Frequency response for case 3

provides further proof of its superiority. The results of the simulations show that frequency is restored in every instance.

TABLE 3.3: Microgrid Frequency Deviations

CASE	Conventional PSO	Improved PSO
1	0.997	0.0199
2	1.4752	0.0295
3	1.9886	0.0398

From Table 3.3, the tabulated results of the simulation of the microgrid frequency deviation are presented. This was conducted under all test conditions. The findings clearly demonstrate that the proposed controller outperformed the conventional method. The proposed method ensures frequency stabilization and economical use of ultracapacitors.

It can be observed that for a minimum disturbance of 5 MW, the change in frequency is 0.997 (1.994%), while with Improved PSO, the frequency change is

3.4. Analysis of Simulation and Experimental Findings and Discussion 71
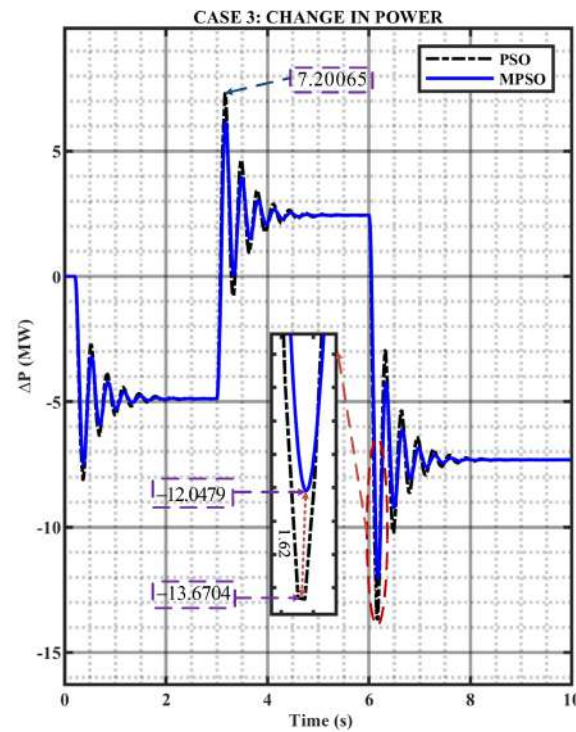
FIGURE 3.16: Increase in wind generated power of 10 MW
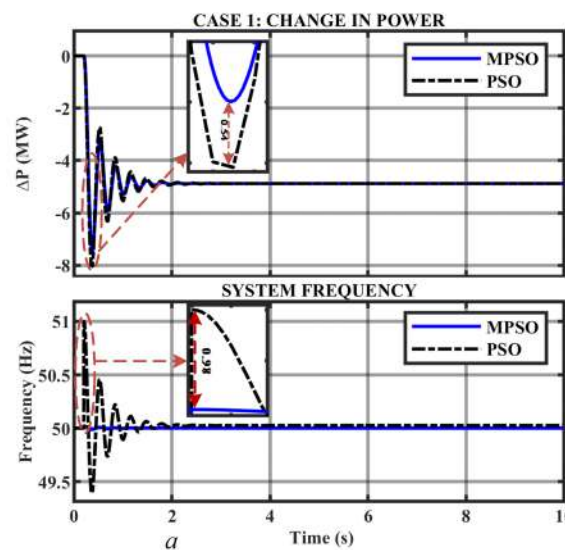
FIGURE 3.17: Combination of frequency deviation and power variation in case 1

72Chapter 3. Hybrid Energy Storage Systems for Inertial Response in Micro-grid
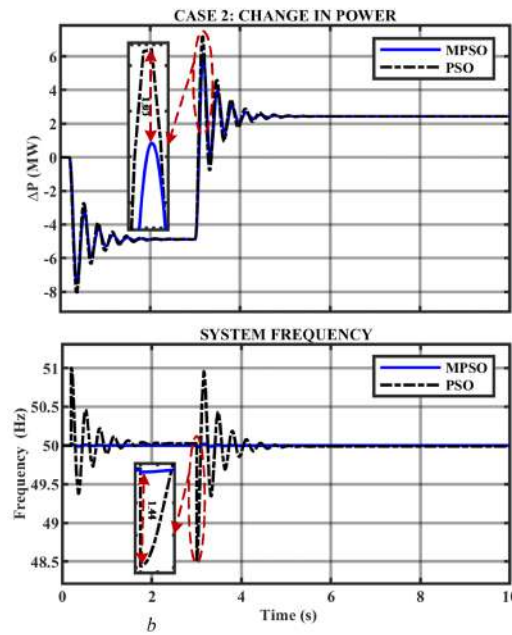
FIGURE 3.18: Combination of frequency deviation and power variation in case 2
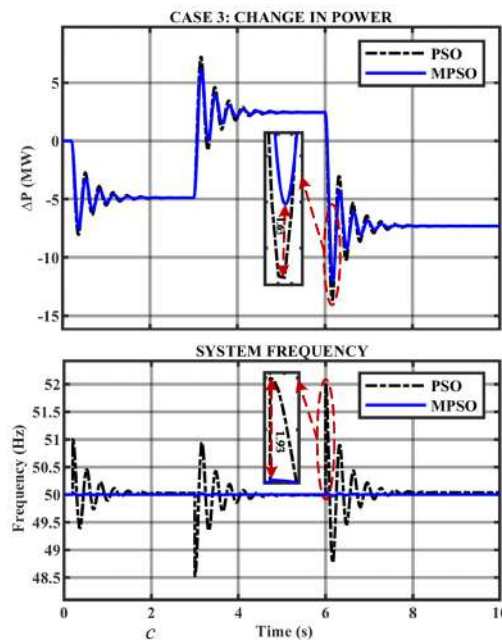
FIGURE 3.19: Combination of frequency deviation and power variation in case 3

0.0199 (0.0398%). Similarly, with a maximum disturbance of 10 MW, the change in frequency is 1.9886 (3.977%), while Improved PSO yields a frequency change of 0.0398 (0.0796%). Thus, it is evident from the two extreme cases that with Improved PSO, the change in frequency is very small. For brevity, Table 3.4 summarizes the frequency response in a microgrid under different disturbance scenarios.

TABLE 3.4: Disturbance and Frequency Response

Disturbance	Frequency Response	Response Type
Load Fluctuation	Load Increasing	Decrease (nadir)
	Load Shedding (decreasing)	Increase (zenith)
Wind Speed Variation	Speed Increment	Increase (zenith)
	Speed Decrement	Decrease (nadir)
Solar Irradiation Variation	Radiations Increment	Increase (zenith)
	Radiations Decrement	Decrease (nadir)
Contingency	RES Disconnecting	Decrease (nadir)
	RES Connecting	Increase (zenith)

3.4.2 Experimental Results and Discussion

The simulation study carried out in the MATLAB/Simulink environment is validated in real time using (OP-4510) OPAL-RT as demonstrated in Figure 3.20. This offers as further evidence of the effectiveness of the proposed study concept in real-time setting.

The fast dynamic response of the proposed dynamic controller is apparent it is capable of quickly reducing the frequency deviation in under two seconds, regardless of the degree of the disturbance. In the experimental study, disturbances of 2%, 3%, and 4% were introduced and it can be observed that the response times in all three situations is found to be very quick. The results from the real-time OPAL-RT (OP-4510) and MATLAB simulations are consistent, indicating that offline systems may employ the adjusted optimum PID controller
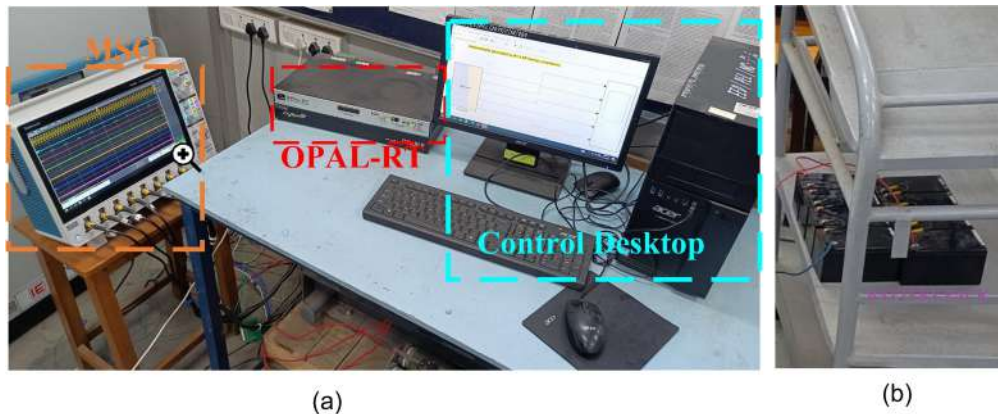
FIGURE 3.20: Photo of Experimental setting (a) setup (b) Battery pack

parameters.   This is done to support the suggested control strategy, which virtually emulates simulation results with hardware in loop.

As seen in Figure 3.21(a)-(f), the same three cases have been implemented using HIL. It is worthwhile to note that with disturbance in load operating conditions, the disturbance in frequency is restored as per grid code requirements. Moreover, the restoration period using proposed method is found to be very much smaller in comparison to conventional methods which further results in enhanced stability. Finally, a brief comparison and distinction with existing state-of-the-art methods of control in grid-connected ESSs have been provided in Table 3.5.

3.5   Conclusion

In this chapter, frequency stabilization of renewable energy sources based low inertia microgrid has been achieved with HESS. The optimal sizing of HESS is done in such a way that it utilizes the response characteristics of Ultracapacitor and battery in order to have enhanced performance with reduced cost. Ultracapacitor is used to mimic inertia for high frequency power deviation as seen during simulation whereas battery is applied for long term power variation in microgrid. A modified form of particle swarm optimization was used to optimize the PID factors. The efficiency of the proposed control strategy has been proved by examining three distinct levels of uncertainty generated by either

3.5. Conclusion

75
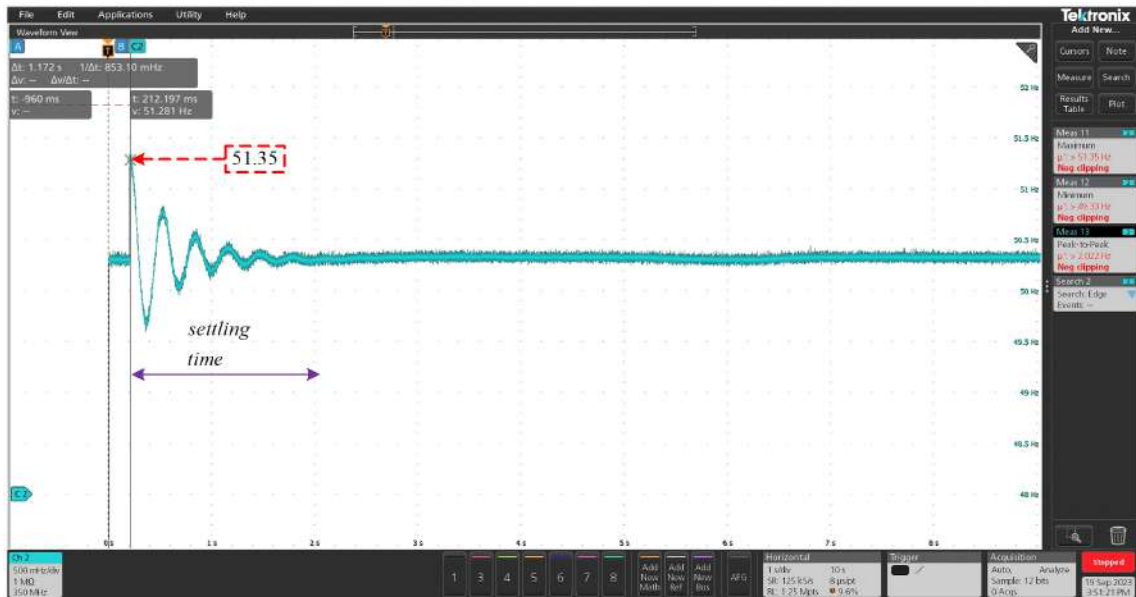
(a)

(b)

76Chapter 3. Hybrid Energy Storage Systems for Inertial Response in Micro-grid
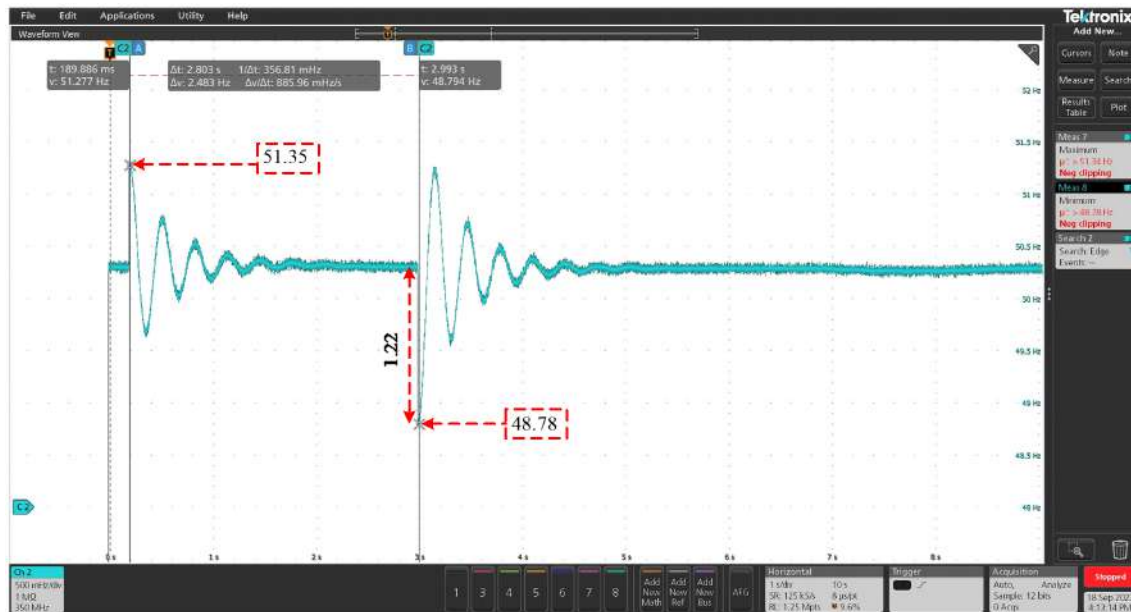
(c)

(d)

3.5. Conclusion

77
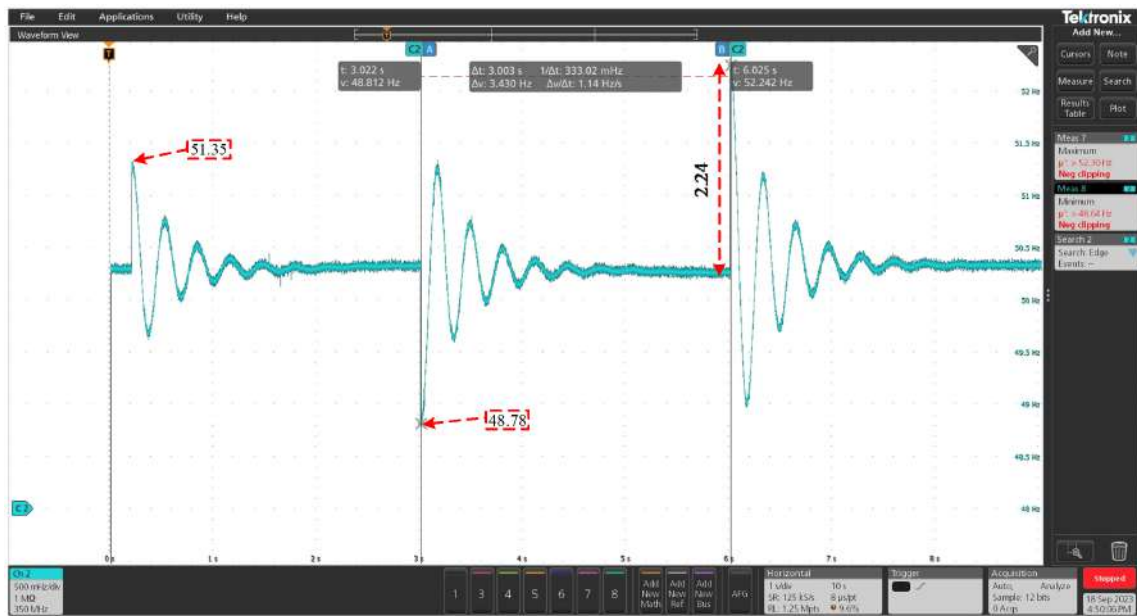
(e)

(f)

FIGURE 3.21: Frequency deviation (a) 5MW, (c) 7.5MW, (e) 10MW.
Power change (b) 5MW, (d) 7.5MW, (f) 10 MW

78Chapter 3. Hybrid Energy Storage Systems for Inertial Response in Micro-grid

intermittent renewable energy sources or changing load. There has been a considerable decrease in the problems related to the rate of change of frequency, overshoot, undershoot, and rising time. As a result, the required size of ultracapacitors has been reduced. In turn, the cost of the entire system is reduced. The effectiveness of modified particle swarm optimization is evident when comparing it to traditional particle swarm optimization. It is worthy to note that there is significant amount of energy saving capacity of 1. 95MW.s for a disturbance of 10 MW. Moreover, the conventional particle swarm optimization technique yielded a frequency deviation of 1.9886 Hz, but the proposed Improved particle swarm optimization technique successfully decreased it to 0.0398 Hz. Therefore, the suggested method enhances the overall efficiency of the microgrid across various operational scenarios. The simulation findings, together with the experimental findings, confirm the efficacy of the proposed strategy in terms of determining the appropriate size of the Hybrid Energy Storage System (HESS) and enhancing the control performance of the Microgrid. The future investigation should consider seamless power sharing in HESS and the ratios based on online optimization.

3.6 The Chapter Summary

Modern power system networks are under statutory obligations to integrate renewable energy sources. The primary reason is to meet ever increasing energy demand and also to curtail environmental pollution by greenhouse gases. However, the higher penetration of renewable energy sources has the tendency of reducing inertia of overall power system network. Consequently, frequency stability is affected and deviates beyond allowable permissible limits leading to power blackouts, load shedding and even total system failure. To address the issues associated with reduced inertia, an optimal control of hybrid energy storage system (HESS) has been proposed. HESS is basically a combination of battery and ultracapacitor, where ultracapacitor addresses rapidly varying power component by mimicking inertia while the battery compensates long term power variations. Thus, the HESS is effectively controlled to compensate the loss of inertia by regulating its energy flow. For the purpose of improved efficiency

3.6. The Chapter Summary 79

and better power management of the HESS, an improvised particle swarm optimization (MPSO) based virtual inertia control design have been proposed. The proposed MPSO is utilised to tune the gains of bidirectional dc-dc converter in such a way that improves frequency nadir with faster response to transient disturbances. This proposed method is simulated in MATLAB and its merits are validated in real time using hardware in loop. On analysing of the results, it can be observed that frequency nadir is improved by 48.96% with significant reduction in rate of change of frequency in comparison to conventional PSO.

Chapter 3. Hybrid Energy Storage Systems for Inertial Response in Micro-grid

TABLE 3.5: Comparison of Controllers and Contributions

Reference	Type of Controller	Contribution
[98]	Hybrid ESS based on heuristics methods	Tuning PID controller parameters using GA and PSO but suffers from local optima.
[89]	Optimal virtual synchronous generator control of HESS	Designing optimal VSG using PSO but suffers from local optima and frequency oscillations take a long time to settle.
[99]	PID controller based on the Grey Wolf Optimization (GWO) algorithm	Frequency regulation in the microgrid designed for a multi-source single area system, however, it does not take into account multiple areas or the impact of RES.
[100]	BFOA tuned LQR-based VSG	Suppress frequency variations using robust design strategies but suffers from convergence challenges.
Proposed	HESS based on improved PSO	Optimizing PID controller settings using an enhanced version of PSO and traditional PSO. The Improved PSO algorithm is an online optimization technique that successfully addressed the difficulties of local optima and lengthened iterations.

Chapter 4

Performance analysis of Various Control Strategies for Micro-grid

4.1 Preamble

There is environmental concern attributed to high emission of greenhouse gases from automobiles, industries and unsustainable agricultural practices [101]. To address this phenomenon, several countries have come up with various solutions. Most have invested in renewable sources of energy and encourage electric vehicles, which are less polluting [102]. The system integrates renewable energy sources to power electronic devices [3].

Research on electric vehicles, the interaction between the grid - vehicle bidirectionally, vehicle - load, and vehicle to home , has been extensive [103, 104]. The bidirectional concept (G2V, V2G) allows power exchange between the grid, homes, loads and electric vehicles (EVs), allowing EVs to function as an ESS. Most research demonstrate that the vehicle-to-grid approach can enhance the grid's functionality in terms of efficiency, stability and reliability. The battery charging concept is fundamentally very important in electric vehicles. Designing of EV chargers is vital and it is considered in this chapter along the operation of EVs. Places of battery charging normally called charge station virtually behave like a grid connected microgrid. In addition to reducing greenhouse gases emission significantly by reducing consumption of fossil fuel it also offers supplementary services such as frequency regulation or voltage stabilization. The charging stations often participate in frequency control. The objective of modelling the charging station (CS) is to organize collaborative exchange of

power between battery-powered EVs and the microgrids.

The main purpose of this section the control of batteries during charging and discharging. The functionally of EVs is considered as they utilize the batteries. In the future, the growing penetration of electric vehicles (EVs) in the market will enable them to support the microgrid. EVs that draw power from battery can serve as both a power source and a load for the MG. When parked in a lot, EVs can supply power to the charging station. The system frequency is regulated through this mutual dependent between the CS and MG [104]. EVs parked at the charging station can generate or draw energy to support the microgrid. However, a single EV cannot provide sufficient support to the MG on its own; it requires the collective contribution of a group of EVs to effectively assist the MG with renewable energy sources (RES). The large number of EVs at the CS can function as an energy storage devices for the MG. They are utilizing to simulate virtual inertia through the virtual synchronous machine mechanism. EV batteries can serve as source of energy within the VSM control framework. In general, EVs can be used both for transportation and for supplying power to the MG via charging stations. Through the VSG mechanism, EVs can function as an ESS by utilizing a parking lot equipped with a CS. EVs parked in this lot can charge or discharge the necessary energy to and from the CS, depending on the MG's frequency regulation needs. Maintaining a continuous power supply to the microgrid (MG) loads can be difficult due to the inconsistent availability of RES.

An essential part of this chapter focuses on EV chargers, power electronics devices are utilized for the purpose of power exchange and control. Gate switches made of low resistance and minimal capacitance. High switching frequencies of hundreds of kHZs range and high voltages are comfortably handle by MOSFET [105]. Silicon (Si) made devices are getting boost in semiconductors devices as they have high power transfer efficiency. Power electronics converters are utilized to regulation of EV batteries charging and discharging and power exchange with the grid.

Electric vehicle batteries have traditionally been managed by proportional integral (PI) controllers. The PI controller has been in used for several decades as it is simple, reliable, durable, and easy to configure. However, it is not immune to challenges like undershoot, overshoot, taking long time to settle and their performance is also influenced by the set point. Additionally, they are not
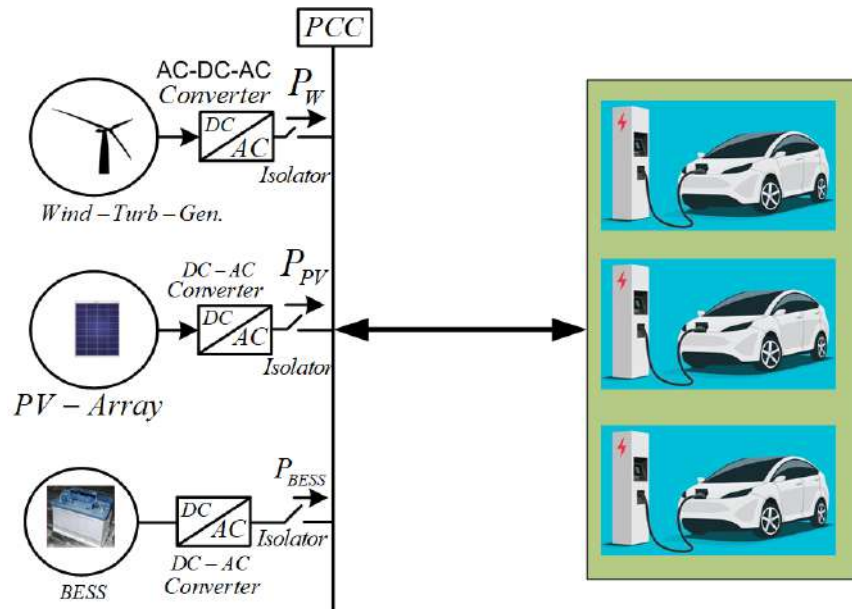
FIGURE 4.1: Schematic Diagram of Microgrid for Charging Station

well-suited for non-linear, complex systems. In consideration of the above mentioned challenges, the PI controllers is not best suited to be utilize in battery changing and discharging [106, 107]. The power exchange in (V2G and G2V) scenario put more consideration on power quality. The harmonics, power factor, PQ effect, voltage regulation and frequency control along with topological complexity take centre stage during modelling 16. The plugs comprises of the essential features of the EV battery charger [108, 109]. Furthermore, in this chapter proposed Adaptive Neuro-Fuzzy Inference System (ANFIS) to address the former controller weaknesses as it known for it superior features. The technique is reliable as it exhibits no undershoot or overshoot. It takes a short period of time for oscillation to settle. The controller is based on paired data, input/output. Tts prowess comes from the combination of both neural network and fuzzy logic while performing adaptive self-tuning and systematic adjustment [94, 110]. At the end of this chapter, comparison is made.
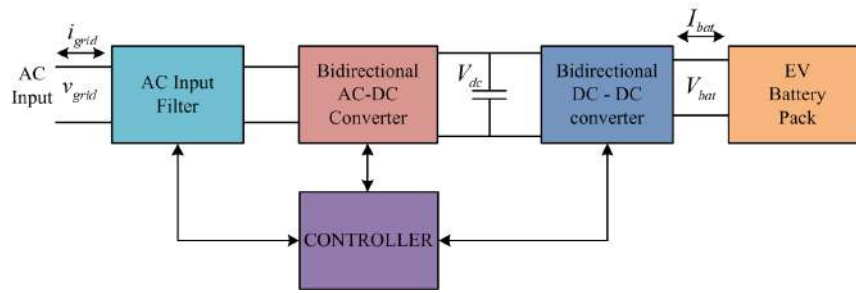
FIGURE 4.2: Diagram schematic EV charger
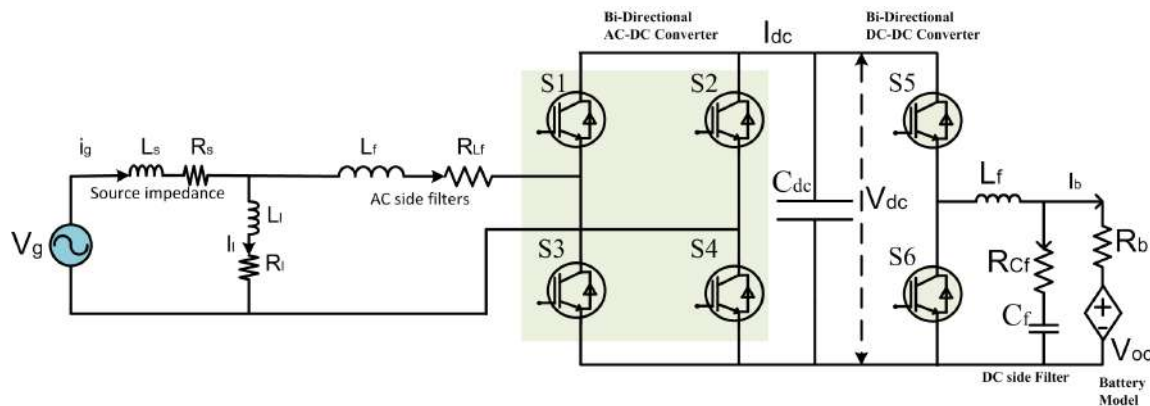
FIGURE 4.3: EV charger schematic circuit

4.2 System Designing and Configuration

AC harmonic filters were connected on the grid side; an AC-DC power converter; a Buck-boost bi-directional power converter; and a controller that regulates signals for both the converter and inverter are all integrated into the single-phase charger design described in this thesis, as illustrated in Figure 4.2.

In Figure 4.3, the schematic diagram of an EV battery charger is illustrated. This is the proposed topology to be considered in this chapter. It shows 4.1 the grid voltage V_g, grid current i_g, grid inductance L_s, grid side filter inductance L_f, shunt resistance R_l and inductance L_l for the loads, and the AC-DC power inverter. The switches S_1, S_2, S_3, S_4 operate in a bi-directional manner and are primarily used for the regulation of the V_{DC} voltage.

The DC-DC converters are known as Buck-Boost converters, as shown in Figure 4. The main function of the Buck-Boost converter is to regulate the unregulated DC link voltage. It operates in two modes: Boost mode (S_6) to

4.2. System Designing and Configuration   85

TABLE 4.1: System Parameters

Description	Symbol	Value
Grid voltage	v_{grid}	240V rms
Frequency	f	50 Hz
Source inductance	L_S	1 micro-Henry
AC side filter inductance	L_{f_ac}	5 mH
Impedance	$R_1 + L_1$	5 Ω + 10 mH
Battery voltage (Li-Ion)	V_{bat}	240V
State of charge	SoC	50%
IGBT Switches	R_{on}	1 mΩ
Source resistance	R_S	10^5 Ω
DC link capacitance	C_{dc}	2200 micro-Henry
Initial voltage	V_{initial}	260V
DC side filter inductance	L_{f_dc}	4 mH
DC side filter impedance	$R_{f\_dc} + L_{f\_dc}$	0.1 mΩ + 200 micro-Henry

discharge batteries while boosting the grid, and Buck mode (S_5) for charging, as it drains current from the grid. Output voltage regulation is determined by the on-off duration of the cycle, called the duty cycle, as shown in the following equation:

$$V_{\mathrm{output}} = -\frac{D}{1-D}V_{\mathrm{input}} \qquad (4.1)$$

D is the duty cycle, ranging from 0 to 1.

Modeling and designing the Buck-Boost converter is a careful exercise done through strategic selection of the inductor L and capacitor C. In addition, the stability of the Buck-Boost converter is determined through state space analysis. The turning on and off of switches S_5 and S_6 are logically coordinated to ensure that the system is stable, efficient, and reliable. The control strategies in the following section are designed to regulate the Buck-Boost converter.

86 *Chapter 4. Performance analysis of Various Control Strategies for Micro-grid*
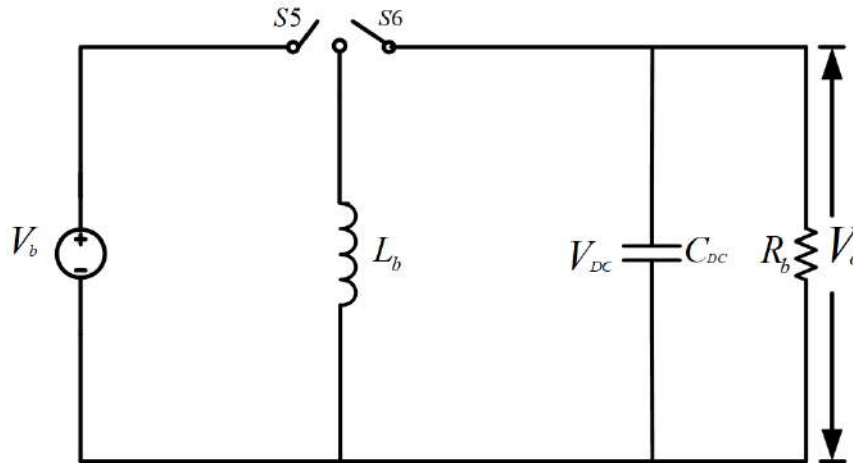
FIGURE 4.4: Circuit Diagram Buck-Boost Converter

4.3 Control Strategies

Several methods have been proposed in executing the G2V and V2G modes by various researchers. In this chapter, two modes operation was considered to regulate pulses as follows: PI, FOPID, and ANFIS respectively.

4.3.1 Proportional and Integral (PI) controller

Reductions in the water level are considered feedback, and the necessary level is considered the desired input. Therefore, a computation will be made to determine the discrepancy between the anticipated and actual values. It also helps to achieve the intended outcomes when this error is reduced to zero. The PI sends a control signal after acknowledging the error in this procedure. The acronym for integral and proportionate is PI. Yet, the derivative term is absent from PI controllers as they are only utilised in processes similar to the liquid level that this study looks at. Generally, a P-controller provides a reliable response, but it also introduces some steady-state inaccuracy. The time it takes for the current response to increase to the desired level is shortened. The PI-controller address the steady-state inaccuracy that the P controller produces. Nevertheless, it also reduces the stability of the system and slows down its response time. The following equation provides the PI controller's output
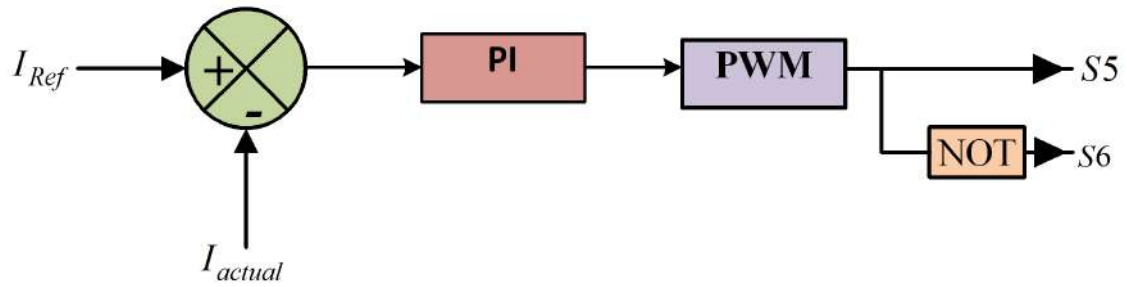
FIGURE 4.5: PI Control diagram

a
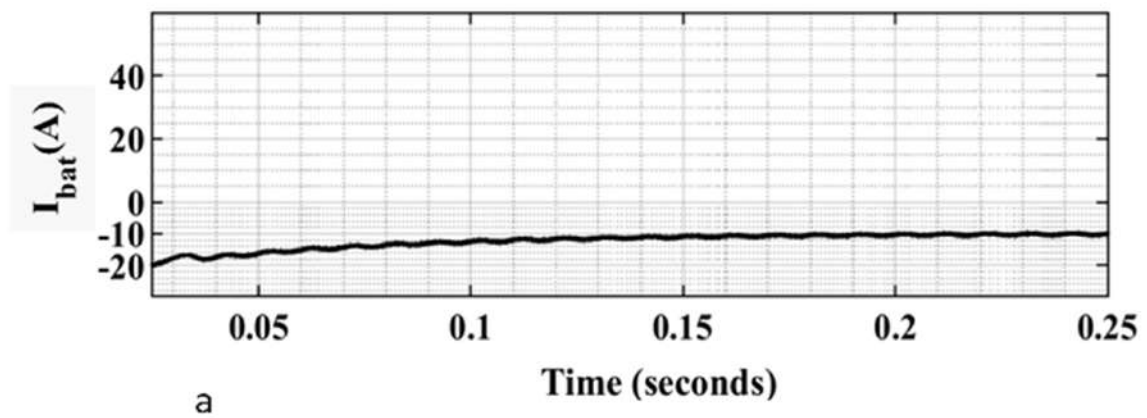
$$G_{\text{con}}(s) = K_p + \frac{K_i}{s} \tag{4.2}$$

Gate Signals Generation

This is the standard procedure for producing pulses while utilising PI. Figure 4.5 illustrates how the error signal passes through the PI after being compared to the reference value and battery current. In this control strategy, the G2V and V2G modes are high and low respectively.

Figure 4.5(a)–(b) illustrate both charging and discharging modes respectively. Buck-Boost act as bi-directional converter. In the Boost mode, inversion occurs, resulting in discharging, while in the BUCK mode, current flows to the battery, resulting in charging.
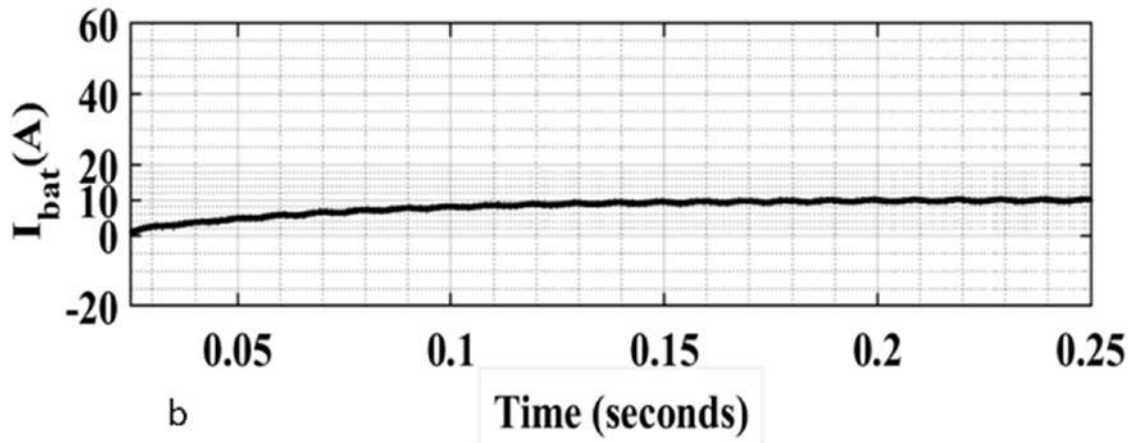
FIGURE 4.6: PI controller battery current (a) G2V, (b) V2G

4.3.2 Fractional, Order, Proportional, Integral and Derivative (FOPID) controller

The concepts of integration and differentiation are extended from integer orders to fractional orders in a branch of mathematics called fractional calculus (FC). Fractional order was first introduced in 1695. However, computational difficulties have only recently made real-time control implementations of fractional-order systems possible.

Normal PID controllers are commonly used in industries because of their simplicity. The FOPID (Fractional Order PID) is considered an extension of the integer-order PID controller and is typically referred to as $PI^\lambda D^\mu$. The equation 4.3 represents the transfer function of the FOPID controller.

$$C(s) = \frac{D(s)}{U(s)} = k_p + \frac{k_i}{s^\lambda} + k_d s^\mu \tag{4.3}$$

where the integration order is represented by λ, and the differentiation order is represented by μ, which are real positive non-integer numbers. As stated in equation 4.3, the fractional-order integration or differentiation is defined by αD_{tim}^p, one of the several integration operators discussed in the literature.
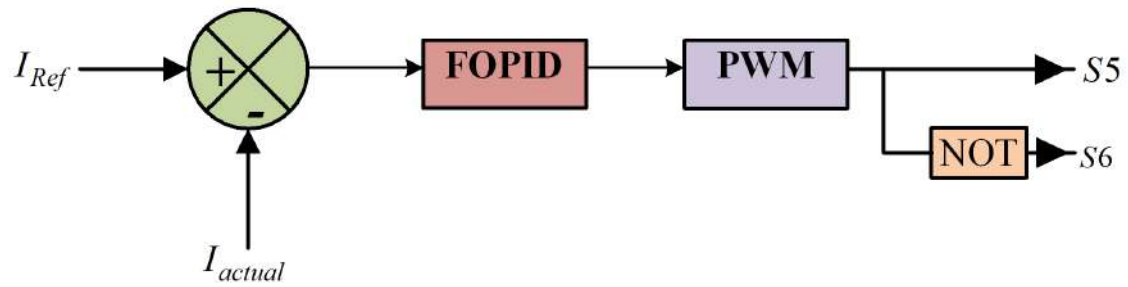
FIGURE 4.7: Control framework for Fractional Order PID

$$\alpha D_{\text{tim}}^{p} = \begin{cases} \frac{d^p}{dt^p}, & p > 0 \\ 1, & p = 0 \\ \int_{\alpha}^{\text{tim}} d\tau^{-p}, & p < 0 \end{cases} \qquad (4.4)$$

The facility's operating frequencies must be incorporated within the selected frequency range. The frequency range in this thesi ranges from 0.001 to 1000 Hz. The computed controller parameters are presented in Table 4.2.

TABLE 4.2: FOPID variables and their values

	Variables	FOPID
1	K_P	1.7089
2	K_i	1.2000
3	K_d	1.2050
4	λ	0.4156
5	μ	0.1532

Gate Signals Generation

As seen in Figure 4.7, the comparison between the I_{bat} and the given value generates a deviation (error signal). The error signal is transmitted to the FOPID controller. The output is fed to the PWM generator, which generates the pulses.
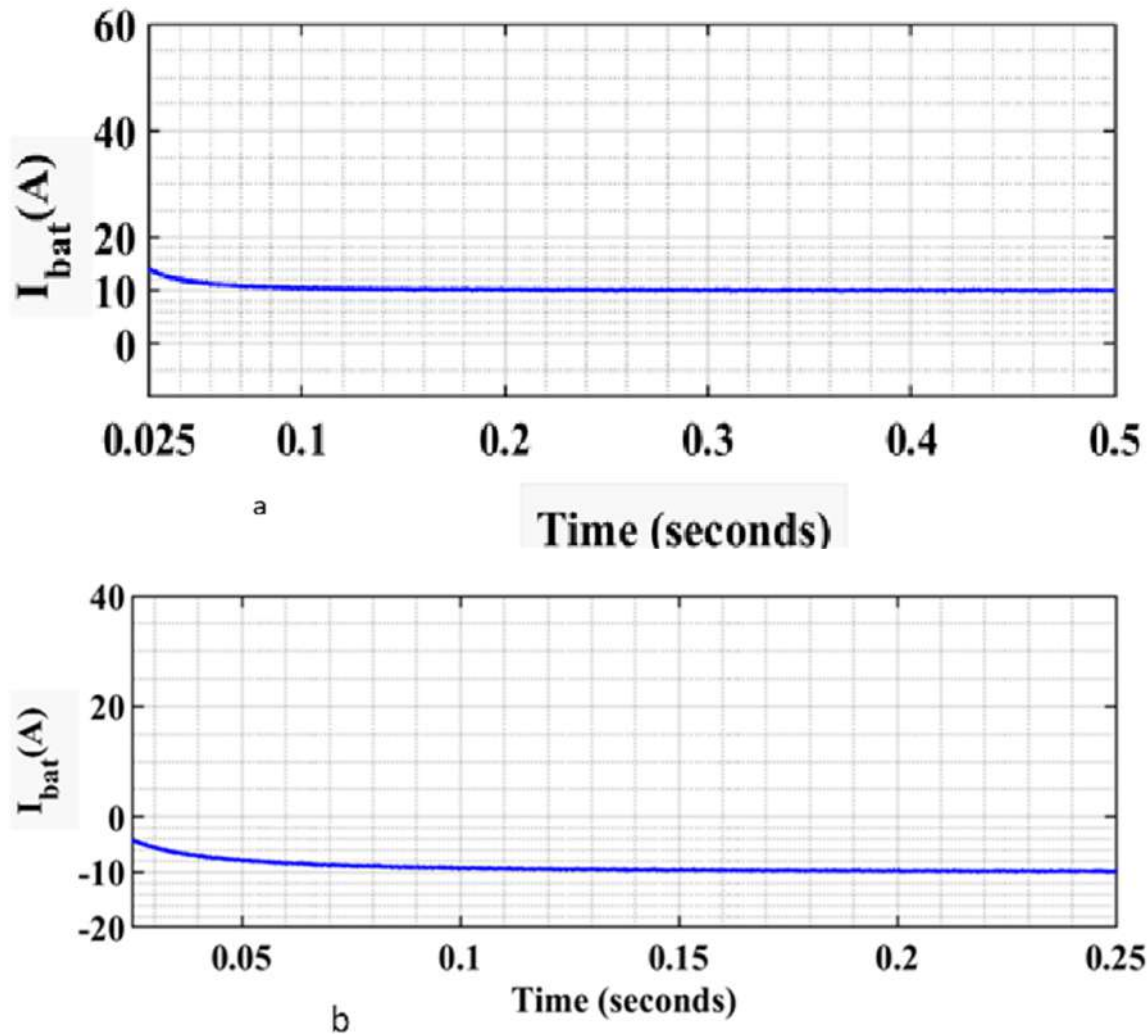
FIGURE 4.8: (a) V2G and (b) G2V mode, I_{bat} nature based on FOPID

It is evidence in Figure 4.8 (a)–(b) that the battery current followed the given reference values 10A and -10A. The graph illustrates discharging that is G2V and charging V2G modes respectively.

4.3.3 Adaptive Neuro-Fuzzy Inference System (ANFIS) controller

The ANFIS controller utilizes a Takagi-Kang-Sugeno fuzzy model with a robust 1:3:3: 3:1 architecture. Drawing on design elements from our earlier publication, this structure achieves a cohesive and consistent visual style. This chapter
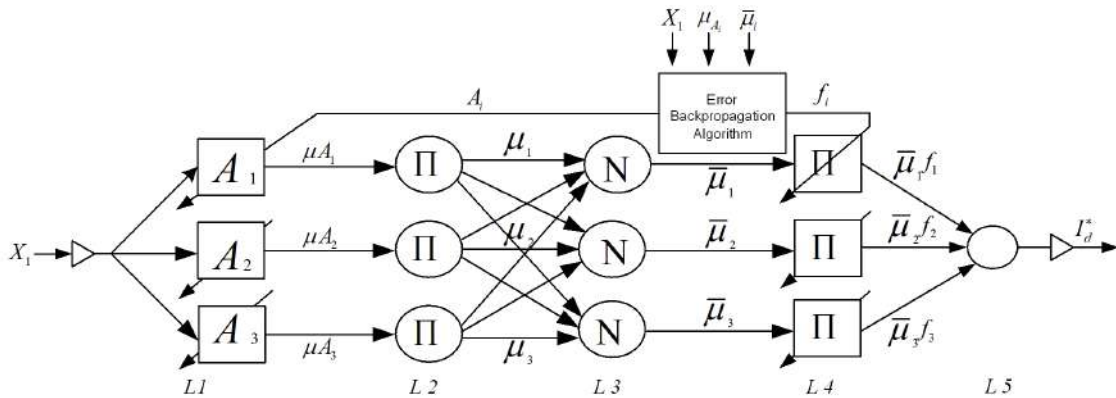
FIGURE 4.9: ANFIS controller

unveiled novel technique ANFIS controller that is comprised of 5 layers, the 1st layer is known as fuzzification layer. It is a logic layer. The 3 membership functions modify the incoming negative sequence voltage. The parameters of the trapezoidal function and triangular function are adjusted in response to input variations. The trapezoidal functions, from a mathematical standpoint, Gradient descent-based error backpropagation algorithms are applied to continuously update both the precondition parameters and the consequent parameters equations [111, 112]. There are 5 layers of ANFIS controller, they are explained as follows: L1: it is fuzzification layer, it is in square shape. In each input, 3 membership functions are allocated. The constant coefficients of the equations describing the trapezoidal function and triangular function are continually employed and updated with the change in input. Computation challenges are reduced by trapezoidal and triangular membership functions. As illustrated in Figure 4.9 ,it can also be shown mathematically as follows:

$$\mu_{A_1}(X_1) = \mu_{B_1}(X_2) = \begin{cases} 1, & X \leq b_1 \\ \frac{X-a_1}{b_1-a_1}, & b_1 < X < a_1 \\ 0, & X \geq a_1 \end{cases} \tag{4.5}$$

$$\mu_{A_2}(X_1) = \mu_{B_2}(X_2) = \begin{cases} 1 - \frac{X-a_2}{0.5b_2}, & |X - a_2| \leq 0.5b_2 \\ 0, & |X - a_2| \geq 0.5b_2 \end{cases} \tag{4.6}$$
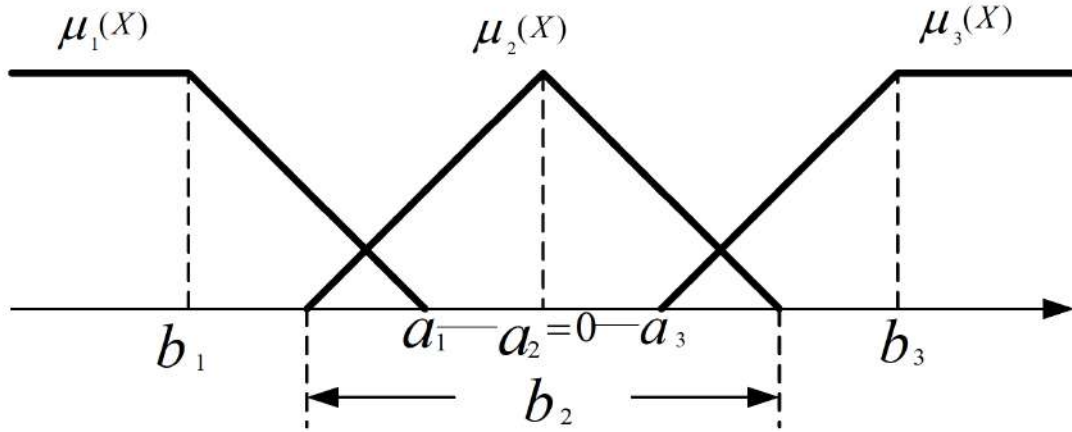
FIGURE 4.10: Fuzzy membership functions

$$\mu_{A_3}(X_1) = \mu_{B_3}(X_2) = \begin{cases} 0, & X \leq a_3 \\ \frac{X-a_3}{b_3-a_3}, & a_3 < X < b_3 \\ 1, & X \geq b_3 \end{cases} \qquad (4.7)$$

With the gradual change of the error signal, the values of (a_1, b_1) are updated. The error is the difference in frequency. These parameters are known as precondition or premise parameters, hence the layer's name.

L2: In this layer, the node is represented by a circle labelled as . Each one of these has two inputs. The inputs are multiplied and transmitted to the third layer. This second layer is normally called the multiplication layer.

$$\mu_i = \mu_{A_i}(X_1) \cdot \mu_{B_i}(X_2) \quad \text{for } i = 1, 2, 3. \qquad (4.8)$$

where μ_i is the output layer which denotes the firing strength of the given rule.

L3: In this 3rd layer, the nodes are denoted by circles. The layer normalizes the firing strength of ea

$$\bar{\mu}_i = \frac{\mu_i}{\mu_1 + \mu_2 + \mu_3} \quad \text{where } i = 1, 2, 3. \qquad (4.9)$$

L4: In this 4th layer, the nodes are denoted by square node with the following function
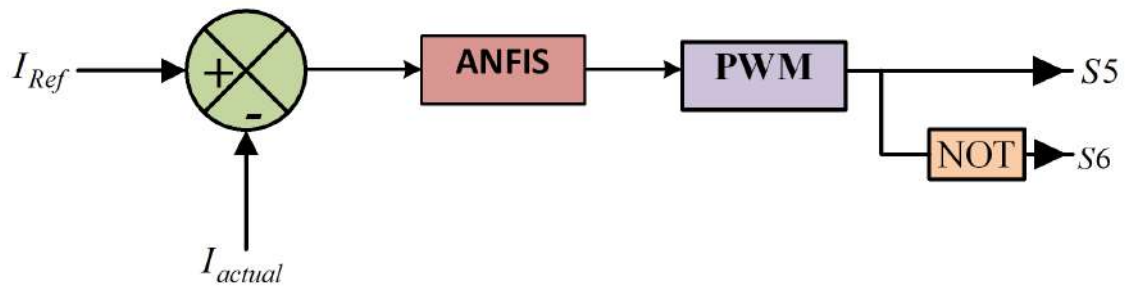
FIGURE 4.11: ANFIS Control diagram

$$o_i = \bar{\mu}_i \cdot f_i^n = \bar{\mu}_i(a_0^i + a_1^i \cdot X_n) \quad \text{where } i = 1, 2, 3 \quad \text{and } n = 1, 2. \tag{4.10}$$

The parameters $\{a_0^i, a_1^i\}$ are tuned to act as a function of the input. These parameters are also known as consequent parameters.

L5: It is the output layer. It is expressed as follows:

$$Y_1 = \bar{\mu}_1 f_1^X + \bar{\mu}_2 f_2^X + \bar{\mu}_3 f_3^X. \tag{4.11}$$

Gate Signals Generation

The DC-DC power converter's control diagram utilising ANFIS is illustrated in Figure 4.11. An error is sent to ANFIS based on the comparing battery current with the given value. The signals from the ANFIS are fed to PWM generator to generate pulses.

The received signals reveal that the converter operates in Buck-Boost modes. Figure (a)–(b) illustrates the functioning buck converter during changing mode which is high and low during discharging mode.

4.4 Simulation Results and Discussion

Figure 4.13 shows the closed-loop control of Buck-Boost converter close loop control model representing Buck-Boost converters. Both V2G and G2V modes of the model are built and analyzed. During the simulation, a single-phase 240V RMS voltage rectifier is connected via IGBT switches (S_1, S_2, S_3, S_4). A fixed
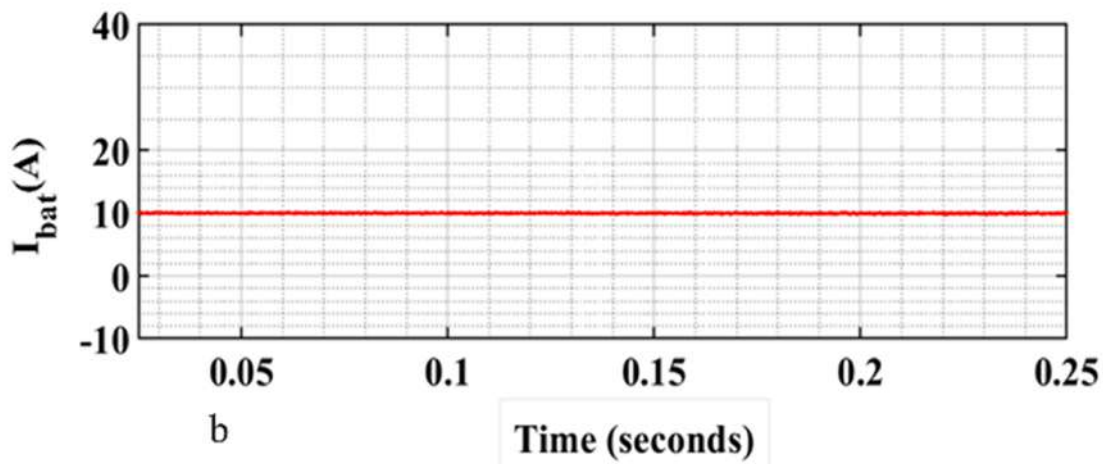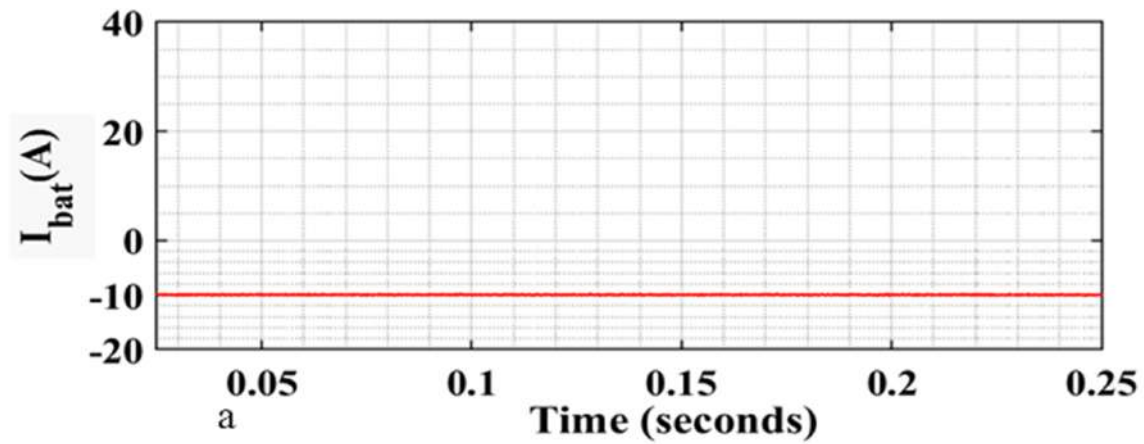
FIGURE 4.12: (a) G2V and (b) V2G mode, ANFIS-based I_{bat} nature
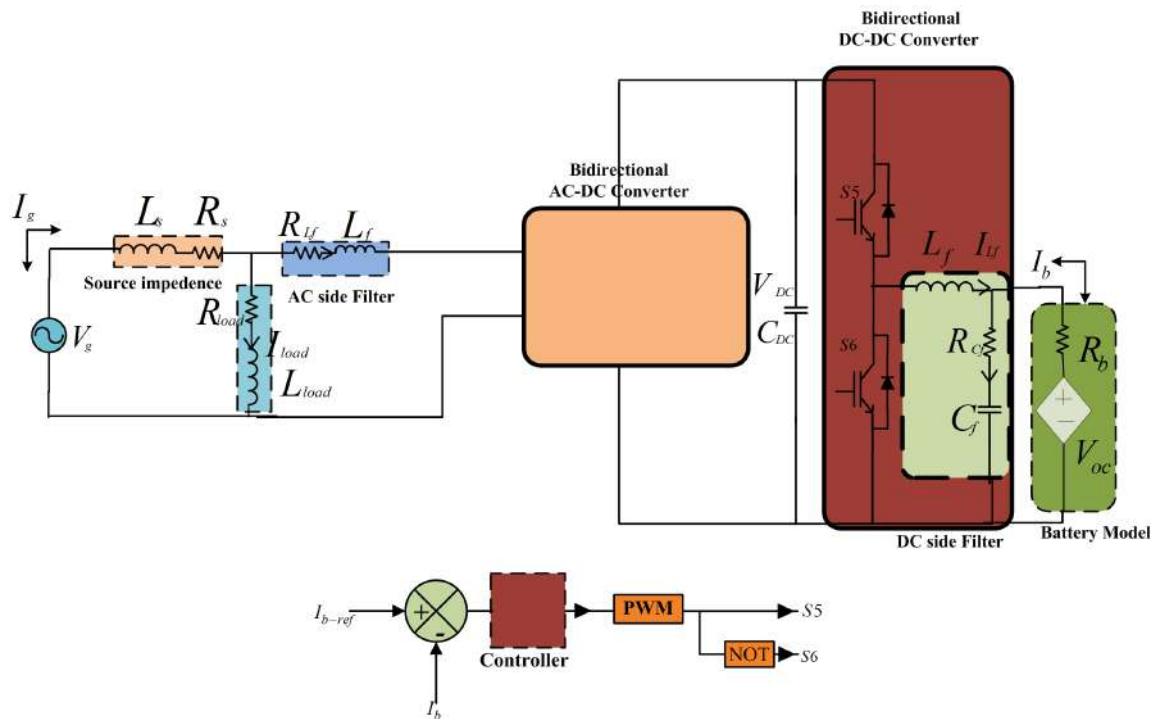
FIGURE 4.13: Buck-Boost converter close loop control

voltage, or one that is controlled by converter control, is necessary for the effective transfer of electricity. Notably, a Bi-Directional Buck-Boost converter that handles V2G (discharging) and G2V (charging) functions is attached.

The waveform shown in Figure 4.14 represents v_g and i_g, the in-phase voltage and current during the charging process, while they are out of phase during the discharging mode, respectively. The process maintains unity power factor. It reflects the power quality with minimal effects on PQ and harmonics.

When the three controllers were used in the battery charging and discharging exercise, Figure 4.15 showed the supply current response. Each controller was implemented, and their replies were documented. The ANFIS demonstrates minimal transients, but the PI shows considerable transients.

Figure 4.16 provides a clear representation of the Vdc voltage in relation to the DC link voltage. The graph shows that the ANFIS controller is the most reliable, maintaining the DC voltage at 400 volts. This further supports the conclusion that the ANFIS controller is superior, offering stability and consistency.

A 260V Li-Ion battery was connected to the charger, and the three controllers

96 *Chapter 4. Performance analysis of Various Control Strategies for Micro-grid*
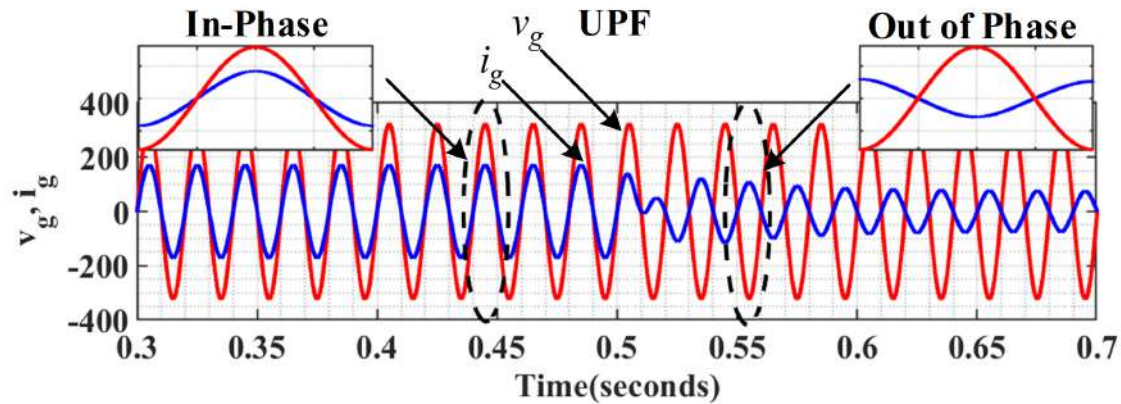
FIGURE 4.14: grid voltage v_g
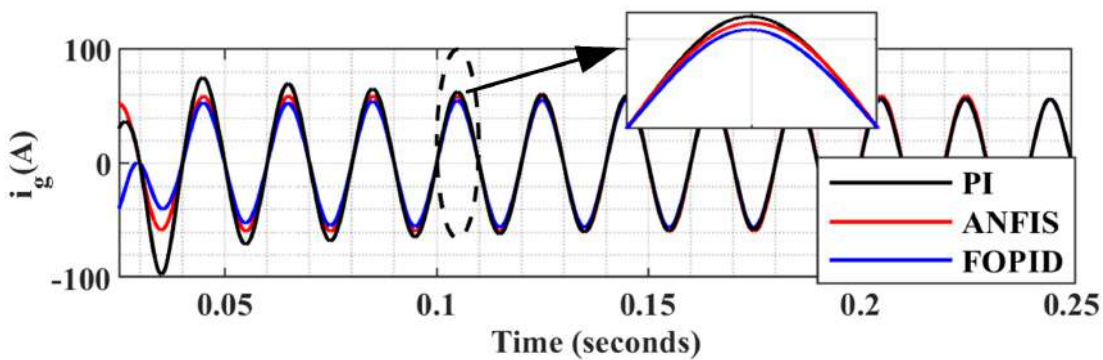
FIGURE 4.15: Grid current i_g
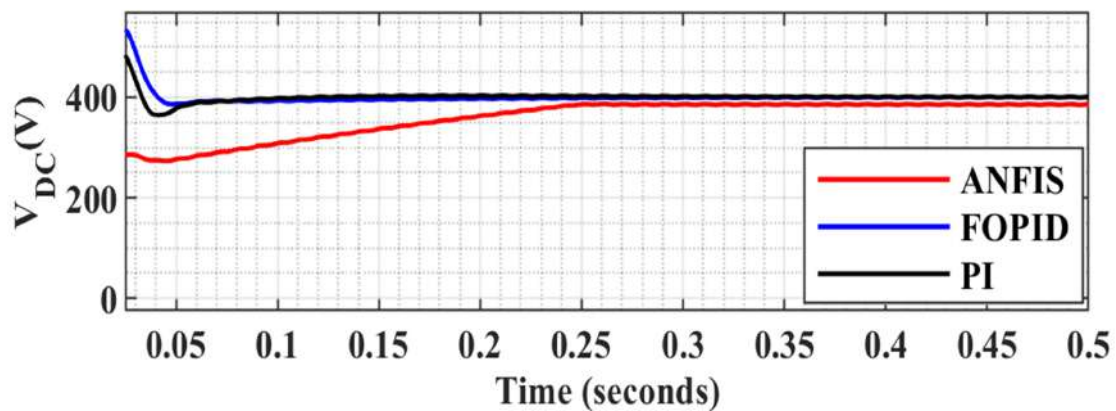
FIGURE 4.16: Vdc voltage
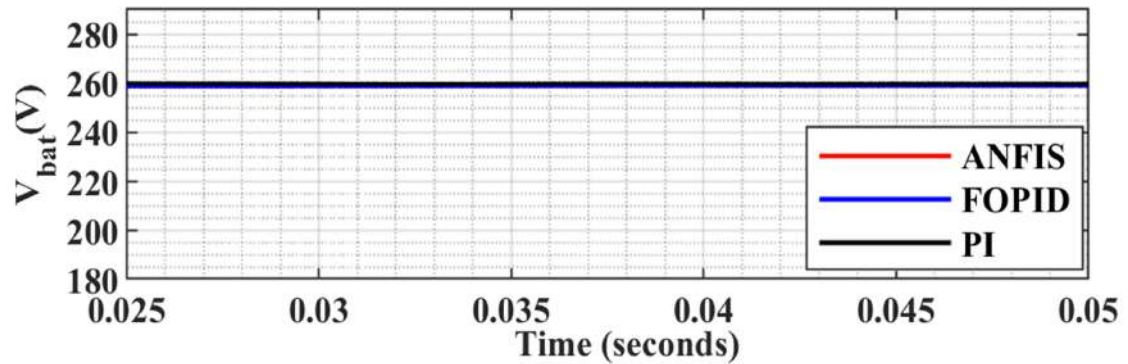
FIGURE 4.17: battery voltage
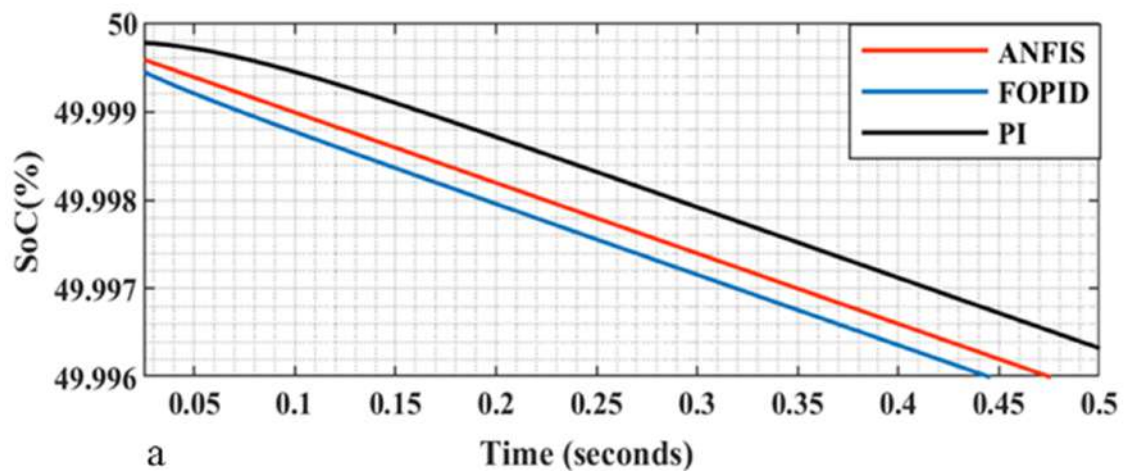
were deployed as illustrated in Figure 4.17. At the conclusion of the simulation, a comparison was conducted among the controllers. Once more, ANFIS demonstrates its efficacy by exhibiting fewer spikes, whereas the other two have been adversely affected by harmonics.

4.4.1 Vihecle to grid Mode

This discharge mode, power is transmitted from the battery to the grid. Figure 4.18(a) depicts the behavior of the State of Charge (SoC) during the discharging mode. The discharge process in the ANFIS controller is seen to be seamless. It is also stable. The PI controller exhibited leading characteristics, but the FOPID controller demonstrated lagging ones.

b
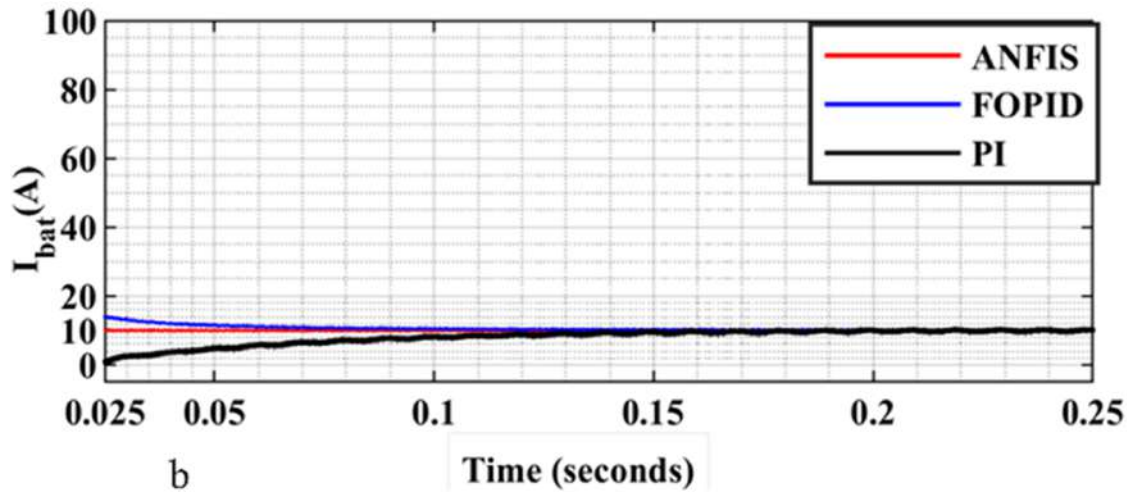
FIGURE 4.18: (a) SoC in discharging mode (b) I_{bat} discharging mode
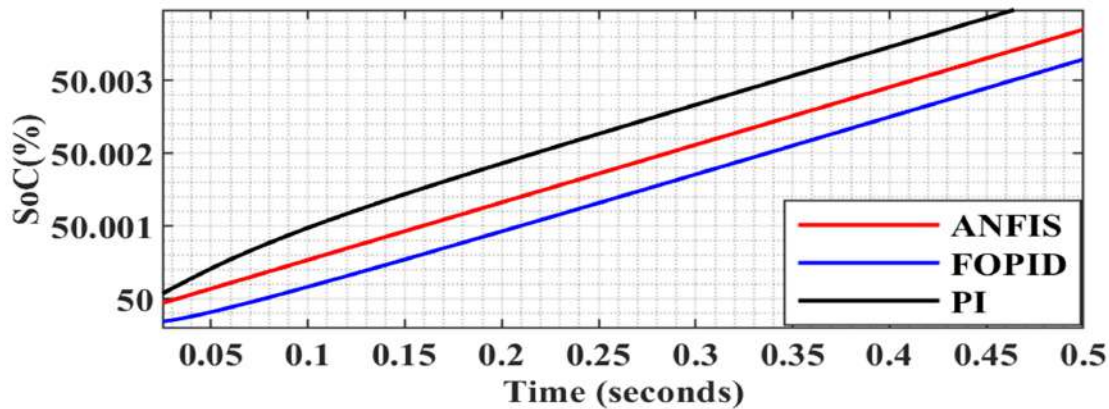
FIGURE 4.19: Battery charging

It is notable in Figure 4.18(b) illustrated battery current I_{bat} in dischange mode. It worth noting that, the performance of the ANFIS better than the both PI and FOPID, and the current of positive 10A value indicates a discharge state.

4.4.2   Grid to vihecle Mode

Figure 4.19 illustrates the State of Charge (SoC) during the charging mode. Similar to the discharge mode, ANFIS demonstrates a smooth charging rate without fluctuations, FOPID reveals a gradual but slow charging process, while PI exhibits a more rapid process with fluctuation.
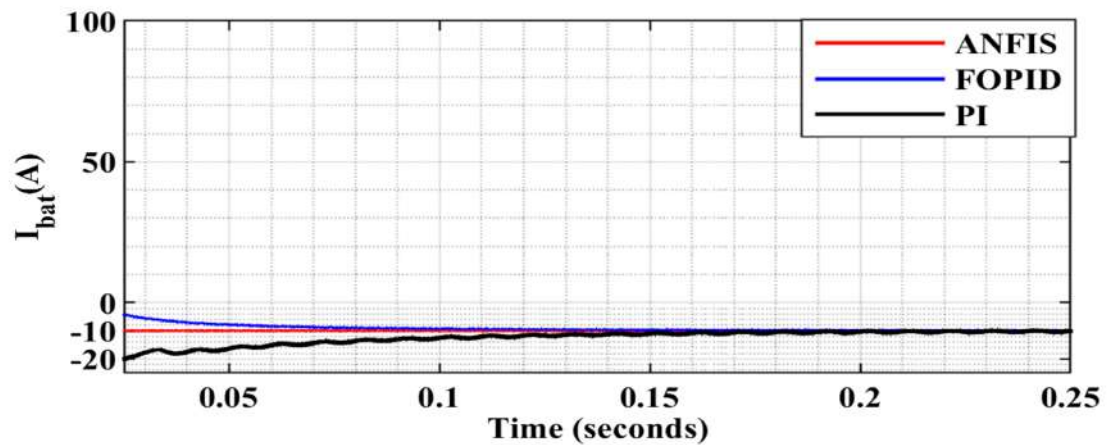
FIGURE 4.20: Charging state of current

Figure 4.20 illustrates the flow of battery current during the charging process. Simulation study was conducted on all three controllers. The ANFIS controller demonstrated superior performance relative to both the PI and FOPID controllers. Negative current (-10A) signifies the charging state.

4.5 Conclusion

V2G and G2V discharging and changing respectively are proposed in this work in form of EV battery charging system. The bidirectional power flow between the charging and discharging, and the microgrid (MG) is managed by the VSG control mechanism. It has also been confirmed that the charging and discharging, responds more quickly to load changes or fluctuations in the system compared to a diesel generator. The power imbalance between power generation and demand during charging and discharging help to support frequency stability. The ANFIS, FOPID, and PI controllers are compared with respect to battery current and state of charge in both charging and discharging scenarios. The MATLAB simulation in the findings showed the superiority of ANFIS controller over both PI controller and FOPID controller. From this work, the performances of source voltage, battery voltage, V_{dc}, and source current were evaluated under the ANFIS and FOPID controllers. Future research in this field can focus on harmonics.

4.6   The Chapter Summary

Plug-in electric vehicles (PEVs) effectively interact with the AC microgrid through the bidirectional nature of vehicle-to-grid (V2G) and grid-to-vehicle (G2V) operations.   The two-way power flow between the charging and discharging, and the microgrid (MG) is managed by the VSG control mechanism. It has also been confirmed that the charging and discharging, responds more quickly to load changes or fluctuations in the system compared to a diesel generator. Power imbalance between power generation and demand during charging and discharging help to support frequency stability. This chapter presents the integration of a buck-boost converter in a non-isolated bi-directional system, along with adaptive control based on reference values, as an effective method for managing EV battery charging and discharging. We conducted a comparison analysis of PI, FOPID, and ANFIS during this chapter. The PI, FOPID, and ANFIS controllers were simulated in a single-phase network with an on-board EV charger in MATLAB/Simulink.   The comparison study unequivocally shows that ANFIS-based controllers are more effective than FOPID and PI controllers.

Chapter 5

Performance Enhancement using GA Based Model Predictive Control for VSM

5.1   Preamble

In the last few decades, the energy sector has undergone tremendous change. The concern of rising global energy consumption is a challenge confronted by several countries. Furthermore, conventional power producing techniques are harmful to the environment.   Greenhouse gas emissions from fossil fuels contaminate the environment and endanger local life.   Consequently, recent research have proposed power converters that supply voltage with controlled source Pulse width modulation (PWM) approach have been largely applied in grid-interfaced power network systems, such as renewable energy sources (RES) [113, 114]. Regrettably, instability, unpredictability, and randomness characterise the energy supply of the majority of renewable sources Sustainable and stable operation is unattainable for microgrids with loads and RES. As such, various control strategies have been suggested for PWM converters switching control for fixed dc-link voltage, UPF and pure sinusoidal wave [115].   Schemes like proportional-resonant,   voltage-oriented   control   (VOC),   hysteresis   and proportional integral (PI) have been extensively researched on [116, 117]. Phase-lock-phase (PLL) technique provide rotational frame coordinate from the grid interfaced.   VOC technique is applied in PWM to regulate real and imaginary powers to tack the given references [118]. However, it is not immune

Chapter 5. Performance Enhancement using GA Based Model Predictive Control for VSM

to power ripples and harmonics. conventional linear PI controller has been widely adopted in PWM converters but has a drawback of complex computational burden while tuning PI parameters. The sliding mode controller is proposed by [119] as a solution to the drawbacks of conventional linear PI control. The parameters are chosen. In the sliding mode control (SMC), which is not immune to system disturbances and parameter adjustment. Nevertheless, there are sluggish dynamic response faults, hysteresis, and communication delays. As a result, high-frequency chattering is introduced, which limits the system's ability to increase frequency.

Conversely, due to its straightforward design, model predictive control (MPC) is also extensively employed [120]. To determine the ideal switching state, optimise the value function of the ESS converter. MPC strengthens the system's resilience while lowering interferences and disturbances. References [120, 121] highlight how MPC performs better and is more resilient in closed loops when compared to the conventional PI control technique. In order to reduce the cost function and have the real current track the reference current, [121] offer the model predictive current control (MPCC) technique. Nevertheless, the control of the bus voltage is not taken into account. A model predictive voltage and power method is proposed by [122] to regulate the bidirectional dc-dc converter of the BESS. Ac/dc interlinking converter control is obtained from power technique.

The MPC method allows for efficient tracking of both active and reactive power. In the traditional MPC approach, a PI controller is used to derive the grid active power reference from the DC-link voltage reference, as the DC-link voltage is closely linked to active power [123].The acquired active power reference, together with the established reactive power reference, is subsequently input into the cost function to ascertain the ideal switching state for the forthcoming sampling period. Nonetheless, due to the discrete-time switching characteristics of the converter, tuning the PI coefficients through trial-and-error can be challenging. When system operating conditions change, the selected P and I coefficients may no longer be appropriate for the updated system parameters [124]. To address this issue, techniques like adaptive genetic algorithm PI control and dynamic reference voltage have been proposed. This thesis presents a novel model predictive control (Enhanced MPC) approach based on MPC and adaptive GA based PI control is put forth. The DC microgrid

FIGURE 5.1: Configuration of a single-phase AC/DC converter

framework is first created, and models of the energy storage converters are created. The adaptive GA technique provides the PI parameters. After that, the enhanced MPC control strategy is developed using a systematic prediction model. This paper research on single phase PWM converters. The proposed scheme is multi-objective; DC voltage control and reactive powers when load is varied. Lastly, the validity of the enhanced MPC is confirmed by simulation and experimental data.

5.2 System Configuration and Modelling of AC/DC Single Phase Converter

It shows the power flow circuit of a single-phase AC/DC converter, which is composed of four insulated gate bipolar transistors (IGBT) switches, S_1, S_2, S_3, and S_4. Harmonic series filters, consisting of inductor L and resistance R, are connected on the grid side, while capacitor C is integrated with the DC side.

The mathematical expression for the single-phase model is as follow;

$$\begin{bmatrix} L_g \frac{di_g}{dt} \\ C_{dc} \frac{dV_{dc}}{dt} \end{bmatrix} = \begin{bmatrix} -R_g & 0 \\ S_g & -1 \end{bmatrix} \begin{bmatrix} i_g \\ I_L \end{bmatrix} + \begin{bmatrix} V_g - V_{AB} \\ 0 \end{bmatrix} \tag{5.1}$$

Where V_g represents the grid voltage, i_g denotes the grid current, V_{AB} signifies the input voltage of the converter, I_L indicates the output current, V_{dc} refers the

Chapter 5. Performance Enhancement using GA Based Model Predictive Control for VSM

load voltage, and S_g represents the switching states which determine the gate signals.

$$\begin{cases} 1, & \text{Upper gate switches } S_1 \text{ and } S_2 \text{ are ON} \\ 0, & \text{Lower gate switches } S_3 \text{ and } S_3 \text{ are OFF} \end{cases} \quad (5.2)$$

S_g is alternating, hence ON and OFF states alternate between the upper and lower gate switches. Both reactive power Q and real power P drawn from the grid can be calculated as follows:

$$\begin{cases} P = \frac{V_p I_p \cos\phi}{2} \\ Q = \frac{V_p I_p \sin\phi}{2} \end{cases} \quad (5.3)$$

Where V_p is peak voltage and I_p is peak current, while ϕ is the displacement angle.

In three-phase converters, Park and Clarke transformations are used to achieve stationary α and β or d-q coordinates in a rotating orthogonal system. In single-phase systems, a virtual two-phase system is created by applying the Helbert transformation equation [125]. The main components of the virtual transformation two-axis (α and β) are as follows:

$$\begin{cases} V_{g\alpha} = V_g = V_p \cos(\omega t) \\ V_{g\beta} = V_p \sin(\omega t) \end{cases} \quad (5.4)$$

$$\begin{cases} i_{g\alpha} = I_g = I_p \cos(\omega t - \phi) \\ i_{g\beta} = I_p \sin(\omega t - \phi) \end{cases} \quad (5.5)$$

From these fundamentals, active and reactive power can be expressed as shown in the α and β form:

$$\begin{cases} P = \frac{V_p I_p \cos\phi}{2} = \frac{V_{g\alpha} I_{g\alpha} + V_{g\beta} I_{g\beta}}{2} \\ Q = \frac{V_p I_p \sin\phi}{2} = \frac{V_{g\beta} I_{g\alpha} - V_{g\alpha} I_{g\beta}}{2} \end{cases} \quad (5.6)$$

The active power and reactive power of equation 5.6 are computed, and the differential of i_g in equation one is substituted in orthogonal form.

$$\begin{cases} \frac{dP}{dt} = \frac{1}{2L}\left[V_P^2 - (V_{g\alpha}V_{AB\alpha} + V_{g\beta}V_{AB\beta}) - 2RP\right] - \omega Q \\ \frac{dQ}{dt} = -\frac{1}{2L}\left[(V_{g\beta}V_{AB\alpha} - V_{g\alpha}V_{AB\beta}) - 2RQ\right] + \omega P \end{cases} \tag{5.7}$$

The equation 5.7 is very instrumental when implementing the MPC controller. Equation 5.7 can be sampled at intervals $(K + 1, 2, 3, \ldots, t)$ and resistance can be ignored since it is small and hence ineffective.

$$\begin{cases} P(K+1) = P(K) - \omega T Q(K) + \frac{T}{2L}\left[V_P^2 - V_{g\alpha}(K)V_{AB\alpha} - V_{g\beta}(K)V_{AB\beta}(K)\right] \\ Q(K+1) = Q(K) + \omega T P - \frac{T}{2L}\left[V_{g\beta}(K)V_{AB\alpha}(K) - V_{g\alpha}(K)V_{AB\beta}(K)\right] \end{cases} \tag{5.8}$$

The cost function employed for module optimization is in this system is shown in equation (9)(12).

$$J = \sqrt{(P - P_{\text{actual}})^2 + (Q - Q_{\text{actual}})^2} \tag{5.9}$$

Where P_{actual} and Q_{actual} are the given desired active power and reactive power, respectively.

5.3 Control Strategies

5.3.1 Dynamic reference analysis using convectional PI Design

It is notable from Figure 5.4 that the primary purpose of this controller is to regulate both active and reactive power within the system in response to fluctuations. The MCP is permitted the requisite power to flow. Conversely, the PI Controller modulates the DC-link voltage to adhere to the specified trajectory. MCP is very susceptible to model discrepancies and potentially determinations of inaccurate model parameters equation 5.13. To achieve expected dc-link voltage, the deviation error between the actual voltage and measured is given by;

$$\Delta V = V_{dc} - V_{\text{dc, actual}} \tag{5.10}$$

The optimized PI controller is used to reduce the error to zero

Chapter 5. Performance Enhancement using GA Based Model Predictive Control for VSM

FIGURE 5.2:   Illustration of the enhanced MCP scheme with convectional PI

$$G_{\Delta V} = K_P + \frac{K_I}{s} \tag{5.11}$$

The dynamics reference design for DC bus voltage:

$$\frac{C}{2} \frac{dV_{dc}(t)^2}{dt} = P_s - P_{\text{load}} \tag{5.12}$$

$$P_{\text{load}} = \frac{V_{dc}(t)^2}{R_{\text{load}}}, \quad P_S = \frac{V_{sd}(t) I_{sd}(t)}{2} \tag{5.13}$$

$$\frac{C}{2} \frac{dV_{dc}(t)^2}{dt} + \frac{V_{dc}(t)^2}{R_{\text{load}}} = \frac{V_{sd}(t) I_{sd}(t)}{2} \tag{5.14}$$

The equation shown above utilizes I_q to regulate the voltage of the DC bus. Owing to the non-linear nature of the system with V_{dc}^2, it is easiest to regulate V_{dc}^2 in order to linearize the system under this control of V_{dc}.

$$\frac{C}{2} \frac{dV_{dc}(t)^2}{dt} + \frac{V_{dc}(t)^2}{R_{\text{load}}} = P_S(t) \Leftrightarrow \frac{V_{dc}(s)^2}{P_S(s)} = \frac{R_{\text{load}}}{\left(\frac{R_{\text{load}}C}{2} s + 1 \right)} \tag{5.15}$$

5.3. Control Strategies

FIGURE 5.3: DC link-voltage

The analysis reveals that the dynamics of the current loop are much faster than those of the voltage loop.

$$\frac{I_d(s)}{I_{d,\,actual}(s)} \approx 1 \tag{5.16}$$

The voltage loop gain is

$$G_{\text{loop}}(s) = \left(\frac{V_{dc}(s)^2}{P_s(s)}\right)\left(\frac{K_p s + K_i}{s}\right) = \frac{2K_p}{Cs} \cdot \frac{s + \frac{K_i}{K_p}}{s + \frac{2}{R_{\text{load}}C}} \tag{5.17}$$

$$V_{dc}(s)^2 = V_{\text{dc, actual}}(s)^2 \cdot \frac{G_{\text{loop}}(s)}{1 + G_{\text{loop}}(s)} \tag{5.18}$$

$$\frac{V_{dc}(s)^2}{V_{\text{dc, actual}}(s)^2} = \frac{1}{1 + \left(\frac{C}{2K_p}s\right)} \tag{5.19}$$

$$\frac{V_{dc}(s)^2}{V_{\text{dc, actual}}(s)^2} = \frac{1}{1 + (\tau_v s)} \tag{5.20}$$

$$s + \frac{K_i}{K_p} = s + \frac{2}{R_{\text{load}}C} \tag{5.21}$$

$$s + \frac{K_i}{K_p} = s + \frac{2}{R_{\text{load}}C} \tag{5.22}$$

The illustration is shown in Figure 5.3 The underlying assumption is that the voltage time constant τ_v must be at least ten times greater than the current time constant τ_i in the current dynamics loop. Additionally, τ_i is equal to 20 times the period of the switching frequency.

$$k_p = \frac{C}{2\tau_v}, \quad k_i = \frac{1}{\tau_v R_{\text{load}}} \tag{5.23}$$

The dynamic method is based on trial and errors.

5.3.2 Adaptive Generic Algorithm (GA) for tuning PI

To avoid time consuming and complex trial and error method, the use of Genetic Algorithms (GA) has facilitated the efficient and effective generation of optimal values by refining the PI parameters. In repeated cycles, the chromosome population is iterated, with each cycle representing a generation. Genetic operators—selection, crossover, and mutation—are applied to produce a new group [64]. Each generation is tied to an objective function, following Charles Darwin's principles of natural selection, fitness, and survival of the fittest [65]. The probability equation is,

$$p(\eta, t) = \frac{M \cdot p(\eta, t-1) f(\eta)}{\sum f(H)} \tag{5.24}$$

Here, p represents probability, η denotes a gene, t indicates time, M signifies the population, and $f(\eta)$ refers to the fitness value of a gene, with the fitness values $\sum f(H)$ summed across all populations. Genetic Algorithms (GA) are employed to determine the boundary values for PI controller gains K_p and K_i, which are obtained through an optimization process. The adaptive GA has been used to efficiently and quickly obtain optimal PI parameters. Genetic algorithms are a highly effective method for solving complex computational problems.

It is notable from Figure 5.4 that main objective of this controller is to regulate active and reactive power in the system to response to any fluctuation. The MCP in this thesis allowed the desired power to flows. On the other hand, GA based PI regulate dc-link voltage to follow the given track. MCP is very susceptible to model discrepancies and potentially determinations of inaccurate model parameters 5.13.

The limits are listed in Table 5.1.

Where the boundaries size, iterations and Population size taken are provided in Table 5.2 and Table 5.3.

The flowchart of adaptive GA adopted is in Figure 5.5.
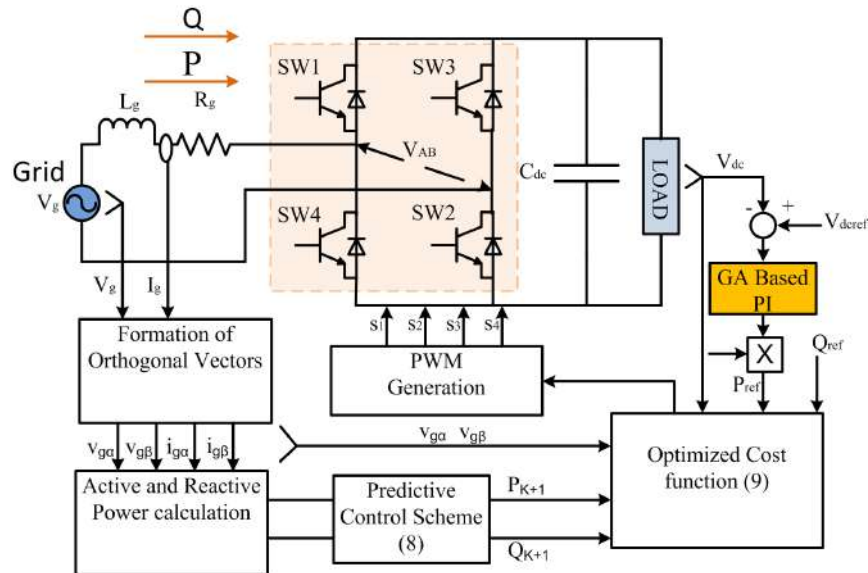
FIGURE 5.4: Illustration of the enhanced MCP scheme with optimized PI

TABLE 5.1: GA limits

Description	Data
Pop size	50
Maxiter	20

5.4 Simulations and Results Discussion

5.4.1 Dynamic reference analysis using convectional PI Results Discussion

This section presents the simulation results produced from the Model Predictive Control (MPC) and the PI schemes. The simulations were conducted using the MATLAB/Simulink software, using a thorough ac/dc converter arrangement as shown in Figure 5.1. Table 5.1 displays the operational simulation and electrical parameters of the converter. It is important to mention that the intended voltage across the dc-link is 400 V. It should be noted that, in the simulation, the PI values were derived from cascaded dynamic voltage loop, taking into account the overshoot and restoration time. Voltage sags and swell were considered. It

Chapter 5. Performance Enhancement using GA Based Model Predictive Control for VSM
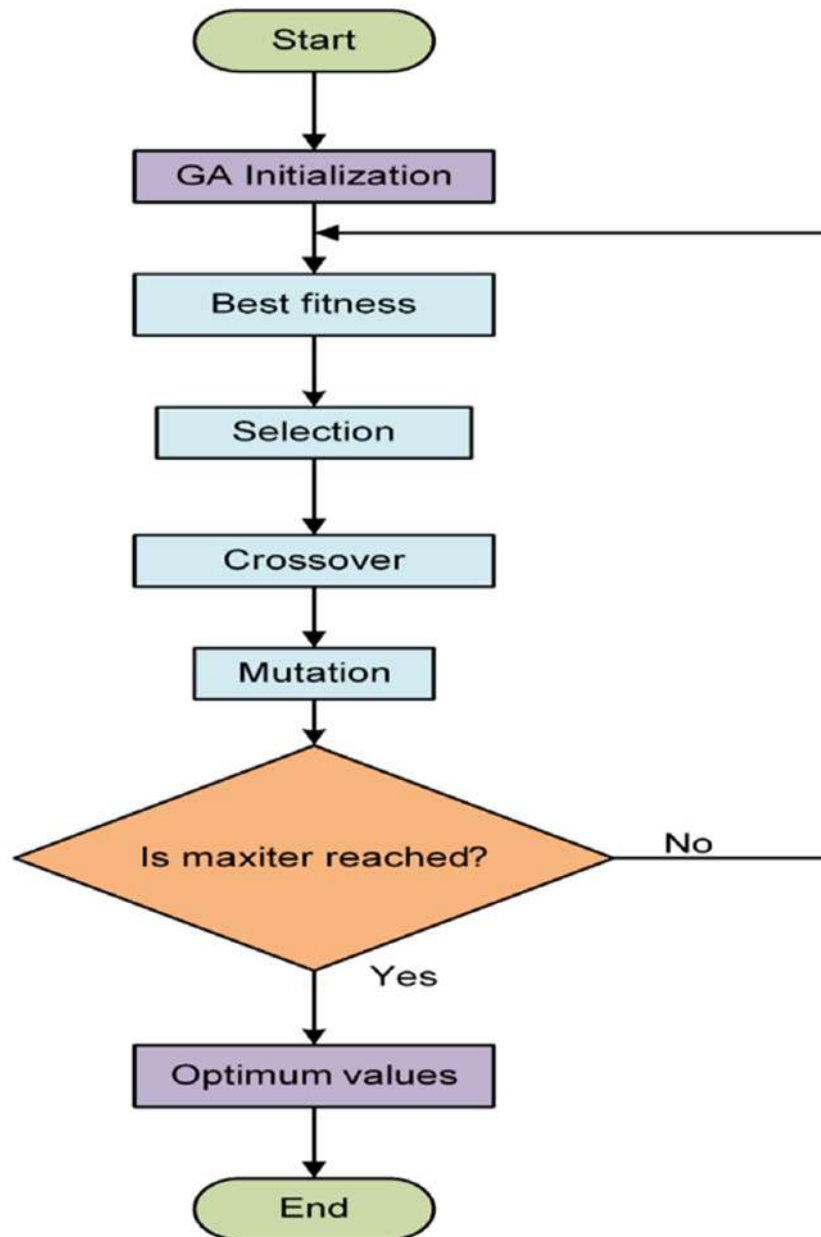
FIGURE 5.5: Adaptive GA flowchart

TABLE 5.2: GA Elements

Elements	Data
Population size	100
Maximum iteration	50

TABLE 5.3: GA boundary condition

Parameters	Lower Boundary	Upper Boundary
K_P	0	1000
K_I	0	1000

was simulated with This chapter presents enhanced MCP controller for active and reactive power regulation. Constant switching frequency is obtained through optimization of PWM. DC voltage regulation is achieved through an adaptive GA-based PI controller. The effectiveness of this optimization technique is validated using the MATLAB/Simulink environment. This validation demonstrates its sturdy performance and reliability, hence confirming its practical appropriateness for real-world application. The control scheme is a multi-objective; active as well as reactive power from enhanced MCP controller precisely regulated to the required levels, resulting in little deviation and shorten restoration time. In addition, dc voltage was regulated independently. and $K_i = 0.25$.

5.4.2 Adaptive Generic Algorithm (GA) for tuning PI Results Discussion

This section covers the simulation results obtained using the Model Predictive Control (MPC) and Adaptive Genetic Algorithm (GA) techniques. The simulations were performed using MATLAB/Simulink software with a detailed ac/dc converter setup as shown in Figure 5.1. The operational and electrical parameters of the converter are outlined in Table 5.1. The dc-link voltage was set to 200 V. Three scenarios were simulated: the first maintained the actual reactive power, Q_{actual}, set at 0 var to achieve unity power factor, while the other two

Chapter 5. Performance Enhancement using GA Based Model Predictive Control for VSM
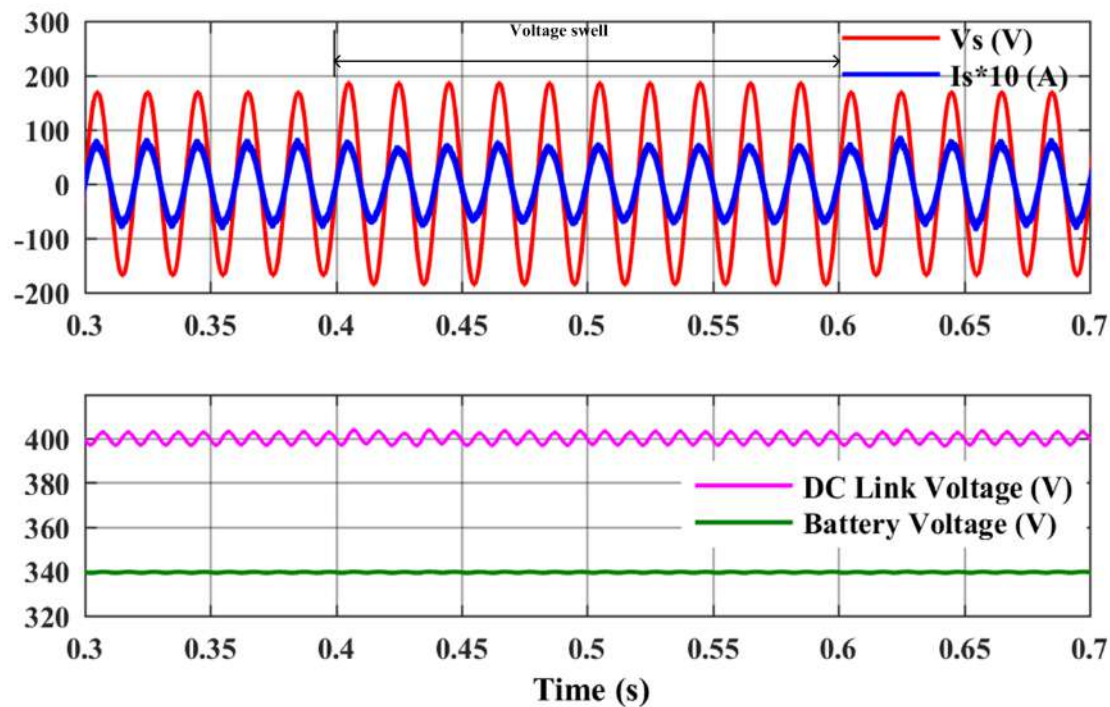
FIGURE 5.6: voltage swell due to untuned PI

scenarios examined both leading and lagging power factors. The PI values in the simulations were optimized using the adaptive GA, taking into account overshoot and recovery time.

Operation under increased active power consumed

Figure 5.8 depicts the simulation results of active power tracking with unity power factor. At 0.5 s, abrupt load demand increases from 1.75kW to 2.5 kW. At this juncture, it is notable dc-link voltage maintained at 200V thanks to GA based PI. Reactive power Q remained 0 VAR before and after disturbances. In addition, PWM modulations enlarge to accommodate more active power. When connected, the source current I_S is in phase with the corresponding source voltage V_S simply because there is no reactive power transmitted. Figure 5.8 depicts the representation of active power, reactive power, supply voltage and current, and PWM modulations. The performance of the suggested MCP controller was found to be exceptional.
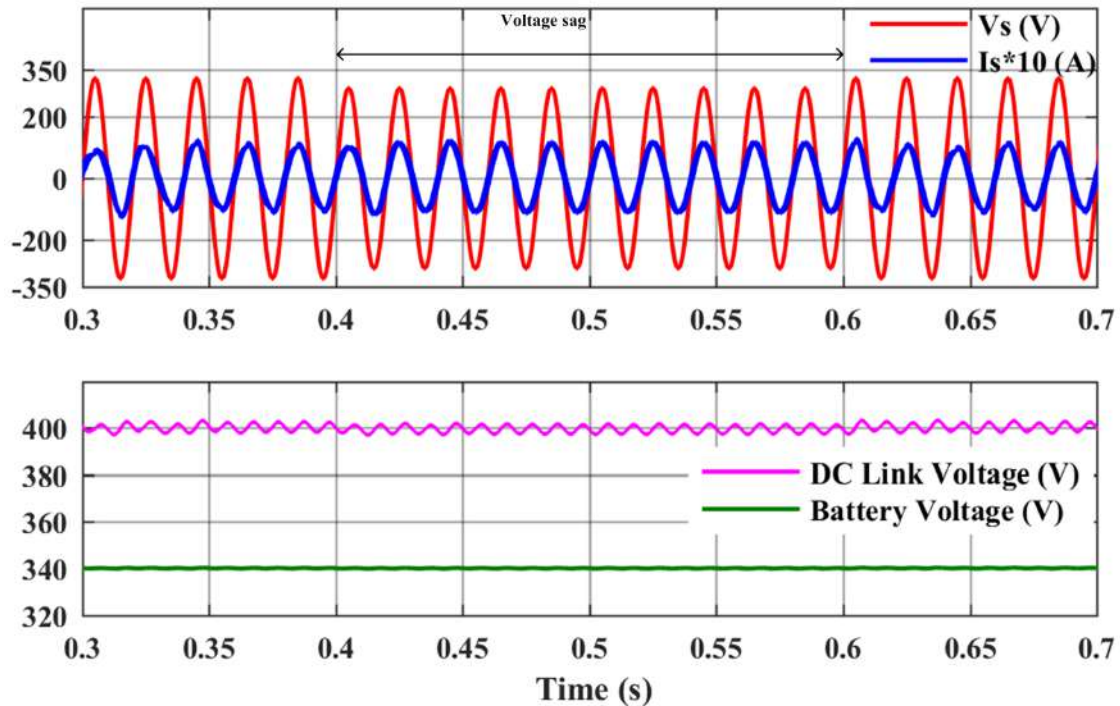
FIGURE 5.7: voltage sag due to untuned PI

Operation under step down of reactive power from 0 to 0.4 kVAR

It is observed in Figure 5.9 that, active power is supplying a constant power of 1.2 kW. At 0.5 s, the source current, I_S, leads its phase voltage showing leading power factor waveform. The controller achieved its objective by maintaining dc link voltage and settling reactive power in 75 mS.

Operation under step up of reactive power from 0 to 0.4 kVAR

In Figure 5.10, it is noted that the active power remains constant at 1.2 kW. At a time of 0.5 seconds, step up change in system reactive power. The presence of a MCP controller allows the system to stabilize within 100 milliseconds, with the output voltage being regulated at 200 volts using a proportional-integral (PI) controller. The voltage and current wave forms exhibit a lagging power factor.

Chapter 5. *Performance Enhancement using GA Based Model Predictive Control for VSM*
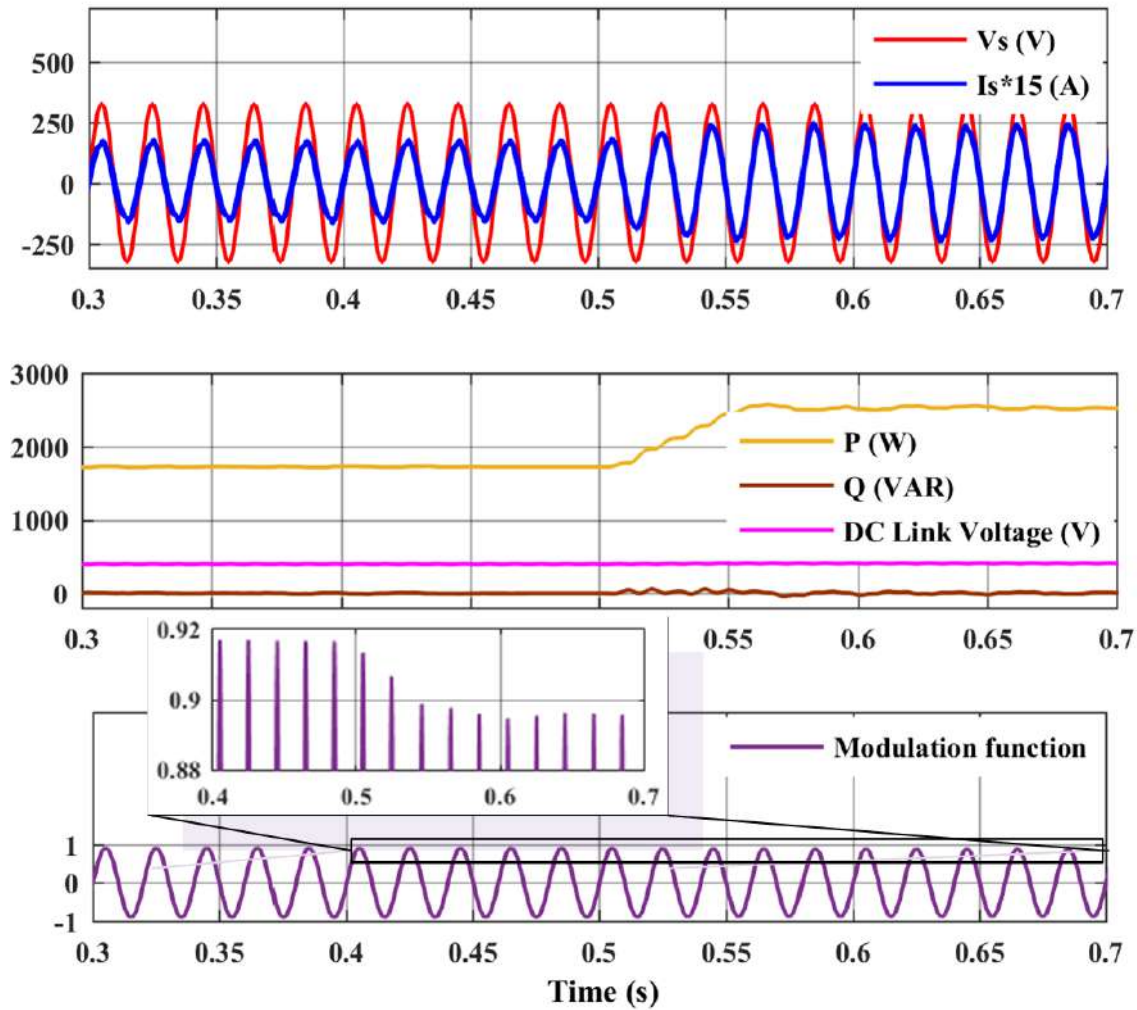
FIGURE 5.8: The response due to increase active power consumed

5.4. Simulations and Results Discussion

115
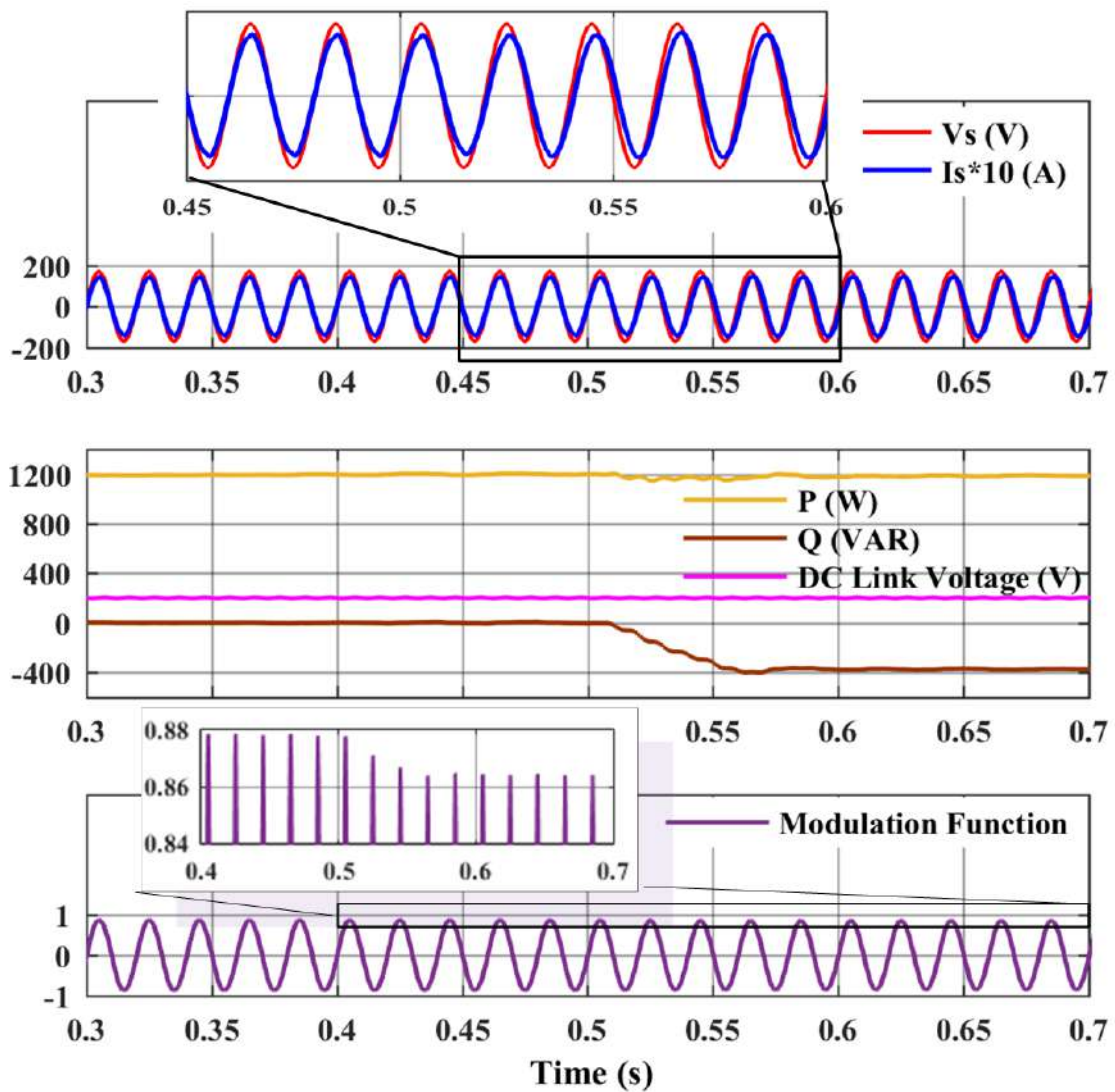
FIGURE 5.9: The response due to Capacitive compensation (VAR)

116

Chapter 5. Performance Enhancement using GA Based Model Predictive Control for VSM
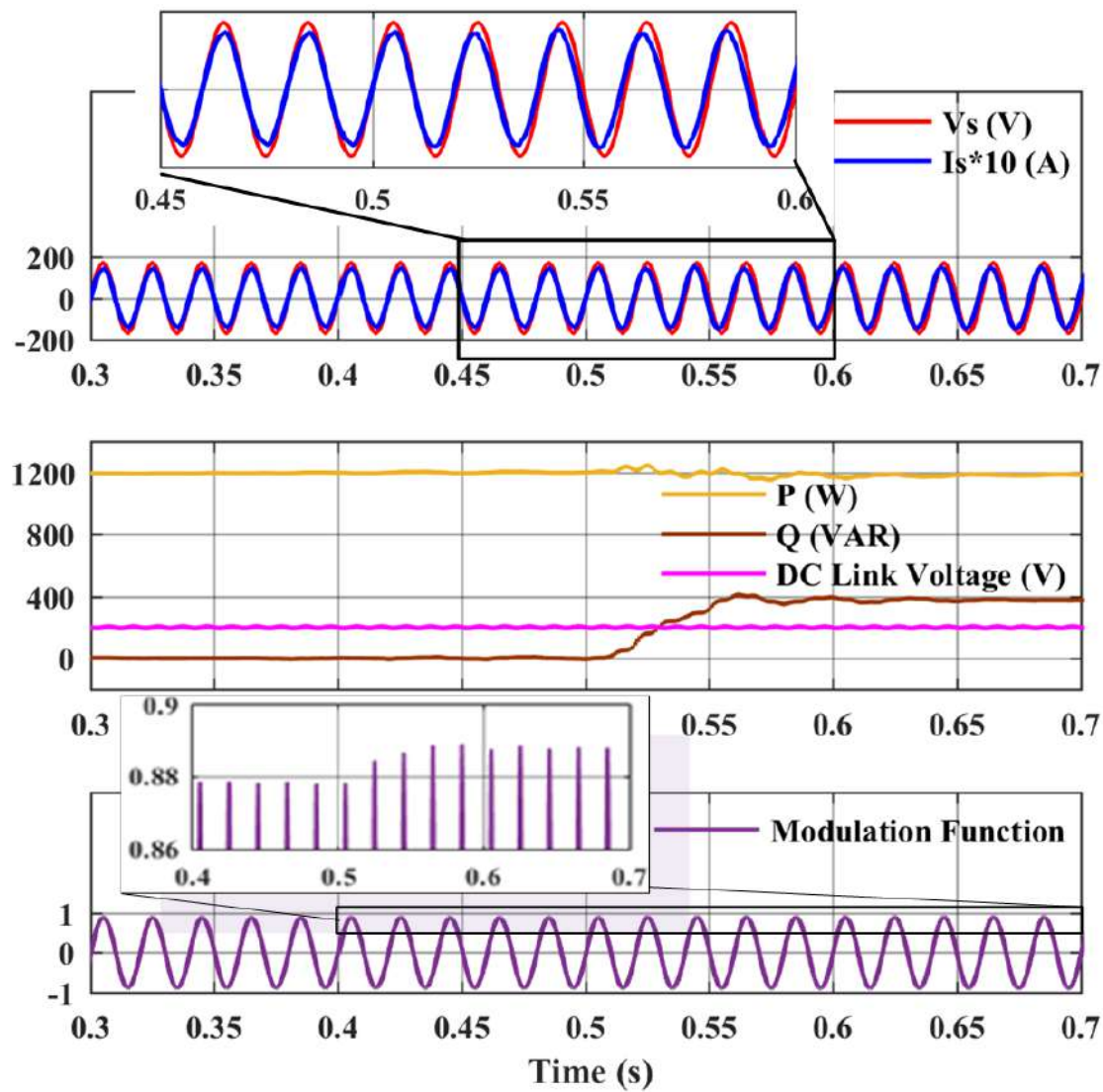
FIGURE 5.10: The response due to Inductive compensation (VAR)

5.5 Conclusion

In this chapter, it proposed MCP for active and reactive power control and Adaptive GA based PI controller for dc voltage control. Simulations were performed to ascertain their effectiveness. The performance of the controllers is exceptional. The intended objectives have been successfully achieved in all three situations, with rapid dynamic and consistent steady state performance. The suggested approach prevents any sag or swell of the DC voltage.It is feasible to independently regulate the DC voltage, active power, and reactive power. The proposed approach reduces the fluctuation in active power and minimizes distortion in the grid current. The use of an Adaptive Genetic Algorithm (GA) approach to fine-tune the PI parameters helps to avoid the demand of extensive computations.

5.6 The Chapter Summary

This chapter presents enhanced MCP controller for active and reactive power regulation. Constant switching frequency is obtained through optimization of PWM. DC voltage regulation is achieved through an adaptive GA-based PI controller. The effectiveness of this optimization technique is validated using the MATLAB/Simulink environment. This validation demonstrates its sturdy performance and reliability, hence confirming its practical appropriateness for real-world application. The control scheme is a multi-objective; active as well as reactive power from enhanced MCP controller precisely regulated to the required levels, resulting in little deviation and shorten restoration time. In addition, dc voltage was regulated independently.

118

Chapter 6

Conclusions and Future Scopes

This chapter summarizes the key outcomes of the research, presenting main conclusions and discussions on the findings, as well as recommendations for future research directions.

6.1 Conclusions

In this thesis, different kinds control strategies are presented to virtual synchronous machine in low inertia microgrid, both grid and off grid connected were conducted. The control techniques were conducted in MATLAB/Simulink and validated in real time OPAL RT 04510 in the laboratory. The exhaustive number of laboratory experiment were carried out to ensure conclusive results are obtained to validate the suggested control techniques in this thesis. The frequency of the microgrid often fluctuates due to sudden disturbance or variation in load and power generation. These frequency fluctuations can be reduced by adding inertia to the system. However, high penetration of RES reduced the necessary inertia in the network, creating a need for virtual inertia to maintain the MG's frequency. To address this, a Virtual Synchronous machine (VSM) control strategies mechanism is used. This mechanism supplies virtual inertia, which helps stabilize the MG frequency, and can be sourced from hybrid energy storage systems (HESS). This thesis proposes a solution to the degraded frequency stability microgrids caused by the high integration of RESs. The research objectives outlined have been successfully achieved, with the key findings summarized as follows:

6.2   Contributions

The following are the key findings from the study described in this thesis:

1. The first objective proposed is an adaptive inertia control strategy based on optimization technique. The improved particle swarm optimization (PSO) and Generic algorithms (GA) optimization techniques based PID controller has been used to generate the appropriate virtual inertia coefficient for effective emulation of inertia in the presence of energy storage system. The conventional PSO suffers local optima stagnation, resulting into premature convergence during searching process in order to achieve global and local position. To address this issue, the velocity update equation was modified on inertia weight (w) using an additional exponential term with linear decreasing inertia weight PSO (LDIW-PSO). In this objective exponential power is taken strategically instead of squaring it in order to reduce the number of iterations for faster convergence. This research identifies the fundamental causes of control stability issues in microgrids. These insights will aid researchers in designing virtual synchronous machine, as well as improving oscillation damping and inertia control mechanisms.

2. The second objective suggested an optimal control of hybrid energy storage system (HESS). HESS is basically a combination of battery and ultracapacitor, where ultracapacitor addresses rapidly varying power component by mimicking inertia while the battery compensates long term power variations. Thus, the HESS is effectively controlled to compensate the loss of inertia by regulating its energy flow. For the purpose of improved efficiency and better power management of the HESS, an improvised particle swarm optimization (MPSO) based virtual inertia control design have been proposed. The proposed MPSO is utilised to tune the gains of bidirectional dc-dc converter in such a way that improves frequency nadir with faster response to transient disturbances. In this control strategy, inertia is quantified to ensure the microgrid has sufficient recovery energy. An optimal inertia response, along with a primary frequency response, improves system stability and helps lower overall costs.

3. This chapter discusses the incorporation of a buck-boost converter in a non-isolated bi-directional system, alongside adaptive control based on reference values, as a practical approach for regulating EV battery charging and discharging. A comparative analysis of PI, FOPID, and ANFIS controllers was carried out. Simulations of the PI, FOPID, and ANFIS controllers were performed in a single-phase network with an onboard EV charger using MATLAB/Simulink. The main purpose was to investigate the stability of voltage in microgrid on EV system. The control strategies managed to maintained voltage, current and power within allowable threshold hence ensuring network health. The results clearly demonstrate that the ANFIS-based controller outperforms both the FOPID and PI controllers.

4. This chapter introduced an improved MCP controller for regulating active and reactive power. The optimization of PWM ensures a constant switching frequency, while the DC voltage is controlled through an adaptive GA-based PI controller. The adopted optimization method is validated in the MATLAB/Simulink environment, showcasing its strong performance and reliability, thereby affirming its suitability for real-world applications. The control scheme addresses multiple objectives, precisely regulating both active and reactive power from the enhanced MCP controller with minimal deviation and faster restoration times.

6.3 Future Scopes

This thesis presents essential concerns and potential avenues for future research and development.

1. In the future, hybrid energy storage systems will need to be controlled in real time, with the ability to quickly determine the amount of energy required during sudden disturbances, allowing fast energy storage systems to respond accordingly.

2. Sectoral, demand-side, and cluster microgrid system with adaptive strategic control can be leveraged to provide virtual inertia, thereby improving frequency stability.

3. A techno-economic analysis and comparison between synchronous condensers and energy storage systems should be conducted on a large scale to assess their reliability and cost-effectiveness and the system frequency stability.

4. The integration of a fleet of electric vehicles (EVs) into modern power networks causes fluctuations in grid parameters. To ensure frequency stability and improve control flexibility, adaptive bidirectional battery charging should be considered.

122

Bibliography

[1] *Reciprocating internal combustion engine driven alternating current generating sets — Part 5: Generating sets*, International Organization for Standardization (ISO) Std., 2013. [Online]. Available: https://cdn.standards.iteh.ai/samples/81844/3dd696ded80349f29547ba03decd6705/ISO-8528-5-2022.pdf

[2] "Frequency response initiative report," North American Electric Reliability Corporation (NERC), Tech. Rep., 2012. [Online]. Available: https://www.nerc.com/pa/Stand/Project200712FrequencyResponseDL/Bal-003-1-Background_Document-Clean-2013_FILING.pdf

[3] J. Fang, H. Li, Y. Tang, and F. Blaabjerg, "On the inertia of future more-electronics power systems," *IEEE Journal of Emerging and Selected Topics in Power Electronics*, vol. 7, no. 4, pp. 2130–2146, Dec 2019.

[4] C. Sun, S. Ali, G. Joos, and F. Bouffard, "Design of hybrid-storage-based virtual synchronous machine with energy recovery control considering energy consumed in inertial and damping support," *IEEE Transactions on Power Electronics*, vol. 37, no. 3, pp. 2648–2666, 2022.

[5] H. Zhao, Q. Wu, S. Hu, H. Xu, and C. N. Rasmussen, "Review of energy storage system for wind power integration support," *Applied Energy*, vol. 137, pp. 545–553, 2015. [Online]. Available: https://doi.org/10.1016/j.apenergy.2014.04.103

[6] A. Chatzivasileiadi, E. Ampatzi, and I. Knight, "Characteristics of electrical energy storage technologies and their applications in buildings," *Renewable and Sustainable Energy Reviews*, vol. 25, pp. 814–830, 2013. [Online]. Available: https://doi.org/10.1016/j.rser.2013.05.023

[7] I. Serban and C. Marinescu, "Control strategy of three-phase battery energy storage systems for frequency support in microgrids and with uninterrupted

supply of local loads," *IEEE Transactions on Power Electronics*, vol. 29, no. 9, pp. 5010–5020, September 2014.

[8] M. Rahimi and M. M. A. H. K., "Performance enhancement of parallel-operated inverter-based virtual synchronous generators supplying active load," *IET Electric Power Applications*, vol. 17, pp. 1–20, 2023.

[9] S. Maleki, J. Nikoukar, and M. H. Tousi, "Robust frequency control of microgrids: a mixed virtual inertia emulation," *International Transactions on Electrical Energy Systems*, vol. 2023, pp. 1–14, 2023.

[10] J. Alipoor, Y. Miura, and T. Ise, "Power system stabilization using virtual synchronous generator with alternating moment of inertia," *IEEE Journal of Emerging and Selected Topics in Power Electronics*, vol. 3, no. 2, pp. 451–458, 2015.

[11] J. Rocabert, A. Luna, F. Blaabjerg, and P. Rodríguez, "Control of power converters in ac microgrids," *IEEE Transactions on Power Electronics*, vol. 27, no. 11, pp. 4734–4749, November 2012.

[12] J. M. Guerrero, M. Chandorkar, T. L. Lee, and P. C. Loh, "Advanced control architectures for intelligent microgrids—part i: Decentralized and hierarchical control," *IEEE Transactions on Industrial Electronics*, vol. 60, no. 4, pp. 1254–1262, April 2013.

[13] Y. Li, Y. Gu, and T. C. Green, "Revisiting grid-forming and grid-following inverters: A duality theory," *IEEE Transactions on Power Systems*, vol. 37, no. 6, pp. 4541–4554, November 2022.

[14] S. M. Muyeen, R. Takahashi, T. Murata, and J. Tamura, "A variable speed wind turbine control strategy to meet wind farm grid code requirements," *IEEE Transactions on Power Systems*, vol. 25, no. 1, pp. 331–340, February 2010.

[15] I. A. G. f. I. S. 1547, "Ieee guide for using ieee std 1547 for interconnection of energy storage distributed energy resources with electric power systems," IEEE, Tech. Rep. IEEE Std 1547.9-2022, August 2022.

[16] H. R. Enslin and P. J. M. Heskes, "Harmonic interaction between a large number of distributed power inverters and the distribution network," *IEEE Transactions on Power Electronics*, vol. 19, no. 6, pp. 1586–1593, Nov 2004.

Chapter 6. Conclusions and Future Scopes

[17] R. K. Varma and S. Auddy, "Mitigation of subsynchronous oscillations in a series compensated wind farm with static var compensator," in *2006 IEEE Power Engineering Society General Meeting*, 2006, pp. 7 pp.–.

[18] A. F. Zobaa and M. Jovanovic, "A comprehensive overview on reactive power compensation technologies for wind power applications," in *2006 12th International Power Electronics and Motion Control Conference*, 2006, pp. 1848–1852.

[19] E. Muljadi, C. P. Butterfield, B. Parsons, and A. Ellis, "Characteristics of variable speed wind turbines under normal and fault conditions," in *2007 IEEE Power Engineering Society General Meeting*, 2007, pp. 1–7.

[20] L. T. Ha and T. K. Saha, "Investigation of power loss and voltage stability limits for large wind farm connections to a subtransmission network," in *IEEE Power Engineering Society General Meeting, 2004*, 2004, pp. 2251–2256 Vol. 2.

[21] J. Fang, H. Li, Y. Tang, and F. Blaabjerg, "Distributed power system virtual inertia implemented by grid-connected power converters," *IEEE Transactions on Power Electronics*, vol. 33, no. 10, pp. 8488–8499, 2018.

[22] S. Hajiaghasi, A. Salemnia, and M. Hamzeh, "Hybrid energy storage system for microgrids applications: A review," *Journal of Energy Storage*, vol. 21, pp. 543–570, 2019.

[23] P. J. d. S. Neto, T. A. d. S. Barros, J. P. C. Silveira, E. R. Filho, J. C. Vasquez, and J. M. Guerrero, "Power management strategy based on virtual inertia for dc microgrids," *IEEE Transactions on Power Electronics*, vol. 35, no. 11, pp. 12 472–12 485, Nov 2020.

[24] J. Meng *et al.*, "An overview and comparison of online implementable soc estimation methods for lithium-ion battery," *IEEE Transactions on Industry Applications*, vol. 54, no. 2, pp. 1583–1591, 2018.

[25] E. Rakhshani and P. Rodriguez, "Inertia emulation in ac/dc interconnected power systems using derivative technique considering frequency measurement effects," *IEEE Transactions on Power Systems*, vol. 32, no. 5, pp. 3338–3351, Sept 2017.

[26] Q. Peng, J. Fang, Y. Yang, T. Liu, and F. Blaabjerg, "Maximum virtual inertia from dc-link capacitors considering system stability at voltage control timescale," *IEEE Journal on Emerging and Selected Topics in Circuits and Systems*, vol. 11, no. 1, pp. 79–89, March 2021.

[27] S. K. Singh, R. Singh, H. Ashfaq, and R. Kumar, "Virtual inertia emulation of inverter interfaced distributed generation (iidg) for dynamic frequency stability & damping enhancement through bfoa tuned optimal controller," *Arabian Journal for Science and Engineering*, vol. 47, no. 3, pp. 3293–3310, 2021.

[28] J. Fang, H. Li, Y. Tang, and F. Blaabjerg, "Distributed power system virtual inertia implemented by grid-connected power converters," *IEEE Transactions on Power Electronics*, vol. 33, no. 10, pp. 8488–8499, Oct 2018.

[29] Y. Ma, W. Cao, L. Yang, F. Wang, and L. Tolbert, "Virtual synchronous generator control of full converter wind turbines with short-term energy storage," *IEEE Transactions on Industrial Electronics*, vol. 64, no. 11, pp. 8821–8831, 2017.

[30] L. Ruttledge and D. Flynn, "Emulated inertial response from wind turbines: Gain scheduling and resource coordination," *IEEE Transactions on Power Systems*, vol. 31, no. 5, pp. 3747–3755, Sept 2016.

[31] K. Gu *et al.*, "Ssr analysis of dfig-based wind farm with vsm control strategy," *IEEE Access*, vol. 7, pp. 118 702–118 711, 2019.

[32] M. A. T. L., L. A. C. Lopes, L. A. M. T., and J. R. E. C., "Self-tuning virtual synchronous machine: A control strategy for energy storage systems to support dynamic frequency control," *IEEE Transactions on Energy Conversion*, vol. 29, no. 4, pp. 833–840, Dec 2014.

[33] A. S. Mir and N. Senroy, "Self-tuning neural predictive control scheme for ultrabattery to emulate a virtual synchronous machine in autonomous power systems," *IEEE Transactions on Neural Networks and Learning Systems*, vol. 31, no. 1, pp. 136–147, Jan 2020.

[34] W. Song, Z. Deng, S. Wang, and X. Feng, "A simple model predictive power control strategy for single-phase pwm converters with modulation function

Chapter 6. Conclusions and Future Scopes

optimization," *IEEE Transactions on Power Electronics*, vol. 31, no. 7, pp. 5279–5289, July 2016.

[35] Li *et al.*, "Model predictive control of grid-connected converter based on virtual synchronous machine," in *2019 IEEE 8th International Conference on Advanced Power System Automation and Protection (APAP)*, 2019, pp. 1294–1298.

[36] M. Soshinskaya, W. Crijns-Graus, J. M. Guerrero, and J. C. Vasquez, "Microgrids: experiences, barriers and success factors," *Renewable and Sustainable Energy Reviews*, vol. 40, pp. 659–672, 2014.

[37] K. Liu, Y. Qu, H.-M. Kim, and H.-J. Song, "Avoiding frequency second dip in power unreserved control during wind power rotational speed recovery," *IEEE Transactions on Power Systems*, vol. 33, no. 3, pp. 3097–3106, May 2018.

[38] G. Delille, B. Francois, and G. Malarange, "Dynamic frequency control support by energy storage to reduce the impact of wind and solar generation on isolated power system's inertia," *IEEE Transactions on Sustainable Energy*, vol. 3, no. 4, pp. 931–939, Oct 2012.

[39] F. Blaabjerg, R. Teodorescu, M. Liserre, and A. Timbus, "Overview of control and grid synchronization for distributed power generation systems," *IEEE Transactions on Industrial Electronics*, vol. 53, no. 5, pp. 1398–1409, Oct 2006.

[40] N. Hatziargyriou, "Contribution to bulk system control and stability by distributed energy resources connected at distribution network," in *IEEE Power Energy Society*.   Piscataway, NJ, USA: IEEE, 2017.

[41] H. Golpira, H. Seifi, A. R. Messina, and M. R. Haghifam, "Maximum penetration level of microgrids in large-scale power systems: frequency stability viewpoint," *IEEE Transactions on Power Systems*, vol. 31, no. 6, pp. 5163–5171, Nov 2016.

[42] P. Ferraro, E. Crisostomi, M. Raugi, and F. Milano, "Analysis of the impact of microgrid penetration on power system dynamics," *IEEE Transactions on Power Systems*, vol. 32, no. 5, pp. 4101–4109, Sep 2017.

[43] J. Varela, N. Hatziargyriou, L. J. Puglisi, M. Rossi, A. Abart, and B. Bletterie, "The igreengrid project: increasing hosting capacity in distribution grids," *IEEE Power and Energy Magazine*, vol. 15, no. 3, pp. 30–40, 2017.

[44] G. Pandove and M. Singh, "Robust repetitive control design for a three-phase four wire shunt active power filter," *IEEE Transactions on Industrial Informatics*, vol. 15, no. 5, pp. 2810–2818, May 2019.

[45] M. N. Mandis, "Management of low- and high-frequency power components in demand-generation fluctuations of a dfig-based wind-dominated raps system using hybrid energy storage," *IEEE Transactions on Industry Applications*, vol. 50, pp. 2258–2268, 2014.

[46] B. Long, X. Liu, R. Jiang, G. Ma, T. K, and C. C, "Frequency stability enhancement of an islanded microgrid: a fractional-order virtual synchronous generator," *International Journal of Electrical Power and Energy Systems*, vol. 147, 2023.

[47] S. Stephan, "Load frequency control of hybrid hydro systems using tuned pid controller and fuzzy logic controller," *International Journal of Engineering Research and Development*, vol. 5, March 2016.

[48] W. Khaled, A. Mohamed, and P. Vasant, "Fuzzy fractional-order pid control for pmsg-based wind energy conversion system with sparse matrix converter topology," *International Transactions on Electrical Energy Systems*, vol. 2022, pp. 1–18, 2022.

[49] N. Paliwal, L. Sharma, and M. Pandey, "Application of grey wolf optimization algorithm for load frequency control in multi-source single area power system," *Evolutionary Intelligence*, vol. 10, 2020.

[50] K. Parmar, S. Majhi, and D. Kothari, "Lfc of an interconnected power system with multi-source power generation in deregulated power environment," *International Journal of Electrical Power & Energy Systems*, vol. 57, pp. 277–286, 2014.

[51] G. da Silva, E. de Oliveira, L. de Oliveira, A. de Paula, J. Ferreira, and L. Honório, "Load frequency control and tie-line damping via virtual

synchronous generator," *International Journal of Electrical Power & Energy Systems*, vol. 132, pp. 1–10, 2021.

[52] G. Song, X. Liu, J. Tian, and P. Wang, "An improved fuzzy voltage compensation control strategy for parallel inverter," *International Transactions on Electrical Energy Systems*, vol. 2022, pp. 1–20, 2022.

[53] J. Fang, Z. Zhang, L. Liu, M. Ma, Q. Kang, and G. Zhang, "An improved virtual synchronous generator power control strategy considering time-varying characteristics of soc," *International Journal of Electrical Power & Energy Systems*, vol. 144, 2023.

[54] B. He, Y. Ren, Y. Xue, C. Fang, Z. Hu, and X. Dong, "Research on the frequency regulation strategy of large-scale battery energy storage in the power grid system," *International Transactions on Electrical Energy Systems*, vol. 2022, pp. 1–13, 2022.

[55] S. Maleki, H. Niknam, and H. Tabrizizadeh, "Robust frequency control of microgrids: a mixed h2/h virtual inertia emulation," *International Transactions on Electrical Energy Systems*, vol. 2023, pp. 1–14, 2023.

[56] M. A. Arasomwan and A. O. Adewumi, "On the performance of linear decreasing inertia weight particle swarm optimization for global optimization," *The Scientific World Journal*, vol. 2013, pp. 1–12, 2013.

[57] S. Oladipo, Y. Sun, and O. Adeleke, "An improved particle swarm optimization and adaptive neuro-fuzzy inference system for predicting the energy consumption of university residence," *International Transactions on Electrical Energy Systems*, vol. 2023, pp. 1–16, 2023.

[58] T. Wen, "Tuning of pid load frequency controller for power system," *Energy Conversion and Management*, vol. 50, pp. 1465–1472, 2009.

[59] H. Sadat, *Power System Analysis*. New York, NY, USA: McGraw-Hill, 1999.

[60] R. E. J. Kennedy, "Particle swarm optimization," in *Proceedings of the IEEE International Conference on Neural Network*, Orlando, FL, USA, June 1995, pp. 1942–1948.

[61] Z.-L. Gaing, "A particle swarm optimization approach for optimum design of pid controller in avr system," *IEEE Transactions on Energy Conversion*, vol. 19, no. 2, pp. 384–391, 2004.

[62] H. Bevrani, F. Habibi, P. Babahajyani, M. Watanabe, and Y. Mitani, "Intelligent frequency control in an ac microgrid: online pso-based fuzzy tuning approach," *IEEE Transactions on Smart Grid*, vol. 3, no. 4, pp. 1935–1944, 2012.

[63] X. H. J. M. G. Chen, "Natural exponential inertia weight strategy in particle swarm optimization," in *Proceedings of the Congress on Intelligent Control and Automation*, vol. 1, 2006, pp. 3672–3675.

[64] K. C. R. Mandal, "Virtual inertia emulation and rocof control of a microgrid with high renewable power penetration," *Electric Power Systems Research*, vol. 194, pp. 1–11, 2021.

[65] A. Jayachitra and R. Vinodha, "Genetic algorithm based pid controller tuning approach for continuous stirred tank reactor," *Advances in Artificial Intelligence*, vol. 2014, p. 8, 2014.

[66] T. Kerdphol, M. Watanabe, K. Hongesombut, and Y. Mitani, "Self-adaptive virtual inertia control-based fuzzy logic to improve frequency stability of microgrid with high renewable penetration," *IEEE Access*, vol. 7, pp. 76 071–76 083, 2019.

[67] S. Vachirasricirikul and I. Ngamroo, "Robust lfc in a smart grid with wind power penetration by coordinated v2g control and frequency controller," *IEEE Transactions on Smart Grid*, vol. 5, no. 1, pp. 371–380, 2014.

[68] C. L. Yuan, C. Liu, X. Zhang, T. Zhao, X. Xiao, and N. Tang, "Comparison of dynamic characteristics between virtual synchronous machines adopting different active power droop controls," *Journal of Power Electronics*, vol. 17, no. 3, pp. 766–776, 2017.

[69] E. Rakhshani, D. Remon, A. M. Cantarellas, and P. Rodriguez, "Analysis of derivative control based virtual inertia in multi-area high-voltage direct

current interconnected power systems," *IET Generation, Transmission & Distribution*, vol. 10, no. 6, pp. 1458–1469, 2016.

[70] D. S. Naresh and N. T. Malla, "Supplementary control for virtual synchronous machine based on adaptive dynamic programming," in *Proceedings of the IEEE Congress on Evolutionary Computation*, July 2016.

[71] L. S. Paliwal and N. Paliwal, "Application of grey wolf optimization algorithm for load frequency control in multi-source single area power system," *Evolutionary Intelligence*, vol. 12, 2019.

[72] L.-R. Chang-Chien, L. N. Anh, T.-W. Lin, and W. Lee, "Incorporating demand response with spinning reserve to realize an adaptive frequency restoration plan for system contingencies," *IEEE Transactions on Smart Grid*, vol. 3, no. 3, pp. 1145–1153, 2012. [Online]. Available: https://doi.org/10.1109/TSG.2012.2192297

[73] L. Huang, H. Xin, and Z. Wang, "Damping low-frequency oscillations through vsc-hvdc stations operated as virtual synchronous machines," *IEEE Transactions on Power Electronics*, vol. 34, no. 6, pp. 5803–5818, 2019. [Online]. Available: https://doi.org/10.1109/TPEL.2018.2866523

[74] N. Soni, S. S. Doolla, and M. C. Chandorkar, "Inertia design methods for islanded microgrids having static and rotating energy sources," *IEEE Transactions on Industry Applications*, vol. 52, no. 6, pp. 5165–5174, 2016. [Online]. Available: https://doi.org/10.1109/TIA.2016.2597281

[75] C. Yuan, D. Yang, J. Feng, and C. Liu, "Constrained operation zone of a vsg considering the dc-side power margin," *The Journal of Engineering*, vol. 2019, no. 16, pp. 2563–2568, 2019. [Online]. Available: https://doi.org/10.1049/joe.2018.8679

[76] S. Chapaloglou, E. Alves, V. Trovato, and E. Tedeschi, "Optimal energy management in autonomous power systems with probabilistic security constraints and adaptive frequency control," *IEEE Transactions on Power Systems*, vol. 39, no. 1, pp. 1543–1554, 2024.

[77] C. Bhattar and M. Chaudhari, "Centralized energy management scheme for grid connected dc microgrid," *IEEE Systems Journal*, vol. 17, no. 3, pp. 3741–3751, 2023.

[78] A. Ikram, A. Ullah, D. Datta, A. Islam, and T. Ahmed, "Optimizing energy consumption in smart homes: Load scheduling approaches," *IET Power Electronics*, pp. 1–13, 2024.

[79] Y. Chen, J. Meng, Y. Yan, and L. Zhong, "Quasi-z based adaptive sliding mode control for three-phase photovoltaic grid-connected system," *IET Power Electronics*, vol. 16, no. 15, pp. 2577–2591, 2023.

[80] M. Majeed, S. Phichisawat, F. Asghar, and U. Hussan, "Optimal energy management system for grid-tied microgrid: An improved adaptive genetic algorithm," *IEEE Access*, vol. 11, pp. 117 351–117 361, 2023.

[81] M. Joshi and S. Samanta, "Energy management with improved frequency sharing based control for battery/ultracapacitor hybrid energy system in the presence of delay," *IET Power Electronics*, vol. 13, no. 10, pp. 2019–2028, 2020.

[82] L. Guo, Z. Xu, N. Jin, Y. Li, and W. Wang, "A weighted voltage model predictive control method for a virtual synchronous generator with enhanced parameter robustness," *Protection and Control of Modern Power Systems*, vol. 6, no. 1, pp. 1–11, 2021.

[83] M. Elwakil, H. Zoghaby, S. Sharaf, and M. Mosa, "Adaptive virtual synchronous generator control using optimized bang-bang for islanded microgrid stability improvement," *Protection and Control of Modern Power Systems*, vol. 8, no. 1, p. 57, 2023.

[84] T. Shi, J. Sun, X. Han, and C. Tang, "Research on adaptive optimal control strategy of virtual synchronous generator inertia and damping parameters," *IET Power Electronics*, vol. 17, no. 1, pp. 121–133, 2024.

[85] V. Skiparev *et al.*, "Virtual inertia control of isolated microgrids using an nn-based vfopid controller," *IEEE Transactions on Sustainable Energy*, vol. 14, no. 3, pp. 1558–1568, 2023.

Chapter 6. Conclusions and Future Scopes

[86] D. Leng and S. Polmai, "Virtual synchronous generator based on hybrid energy storage system for pv power fluctuation mitigation," *Applied Sciences*, vol. 9, no. 23, pp. 1–18, 2019.

[87] D. Li, Q. Zhu, S. Lin, and X. Bian, "A self-adaptive inertia and damping combination control of vsg to support frequency stability," *IEEE Transactions on Energy Conversion*, vol. 32, no. 1, pp. 397–398, 2017.

[88] Y. Hu, W. Wei, Y. Peng, and J. Lei, "Fuzzy virtual inertia control for virtual synchronous generator," in *Chinese Control Conference (CCC), 2016.* IEEE, August 2016, pp. 8523–8527.

[89] M. Mohamed, H. El Zoghby, S. Sharaf, and M. Mosa, "Optimal virtual synchronous generator control of battery/supercapacitor hybrid energy storage system for frequency response enhancement of photovoltaic/diesel microgrid," *Journal of Energy Storage*, vol. 51, p. 104317, 2022.

[90] L. Chong, Y. Wong, R. Rajkumar, and D. Isa, "An optimal control strategy for standalone pv system with battery-supercapacitor hybrid energy storage system," *Journal of Power Sources*, vol. 331, pp. 553–565, 2016.

[91] V. Le Nguyen, "Stability analysis of an isolated microgrid with the presence of the hybrid energy storage system-based virtual synchronous generator," *Journal of Science and Technology*, pp. 46–51, 2020.

[92] K. Li, P. Cheng, L. Wang, X. Tian, J. Ma, and L. Jia, "Improved active power control of virtual synchronous generator for enhancing transient stability," *IET Power Electronics*, vol. 16, no. 1, pp. 157–167, 2023.

[93] Y. Oh, O. Kwon, and J. Kwon, "Bidirectional push–pull/h-bridge converter for low-voltage energy storage system," *IET Power Electronics*, vol. 17, no. 1, pp. 1–9, 2024.

[94] P. Yegon and M. Singh, "Frequency stability enhancement of microgrid using optimization techniques-based adaptive virtual inertia control," *International Transactions on Electrical Energy Systems*, vol. 1, 2023.

[95] G. Chen, X. Huang, J. Jin, and Z. Ma, "Natural exponential inertia weight strategy in particle swarm optimization," in *Proceedings of the World Congress on Intelligent Control and Automation*, vol. 1, 2006, pp. 3672–3675.

[96] Z. Zhang, J. Fang, C. Dong, C. Jin, and Y. Tang, "Enhanced grid frequency and dc-link voltage regulation in hybrid ac/dc microgrids through bidirectional virtual inertia support," *IEEE Transactions on Industrial Electronics*, vol. 70, no. 7, pp. 6931–6940, 2023.

[97] P. Kundur, *Power System Stability and Control*. McGraw Hill Education, 2007.

[98] H. Guentri, T. Allaoui, M. Mekki, and M. Denai, "Power management and control of a photovoltaic system with hybrid battery-supercapacitor energy storage based on heuristics methods," *Journal of Energy Storage*, vol. 39, p. 102578, 2021.

[99] N. Paliwal, L. Srivastava, and M. Pandit, "Application of grey wolf optimization algorithm for load frequency control in multi-source single area power system," *Evolutionary Intelligence*, vol. 15, no. 1, pp. 563–584, 2022.

[100] S. K. Singh, R. Singh, H. Ashfaq, and R. Kumar, "Virtual inertia emulation of inverter interfaced distributed generation (iidg) for dynamic frequency stability & damping enhancement through bfoa tuned optimal controller," *Arabian Journal for Science and Engineering*, vol. 47, no. 3, pp. 3293–3310, 2022.

[101] T. Gupta, G. K. Pandit, B. Sharan, H. Mishra, S. Singh, and R. Dewan, "A robust approach for analysis and visualization of co2 and greenhouse gas emission and its effect," in *Proceedings of the 17th INDIACom; 2023 10th International Conference on Computing for Sustainable Global Development (INDIACom 2023)*, 2023, pp. 238–243.

[102] V. Gupta, S. R. Konda, R. Kumar, and B. K. Panigrahi, "Electric vehicle driver response evaluation in multiaggregator charging management with ev routing," *IEEE Transactions on Industry Applications*, vol. 56, no. 6, pp. 6914–6924, 2020.

Chapter 6. Conclusions and Future Scopes

[103] M. A. Islam, J. G. Singh, I. Jahan, M. S. H. Lipu, T. Jamal, R. M. Elavarasan *et al.*, "Modeling and performance evaluation of anfis controller-based bidirectional power management scheme in plug-in electric vehicles integrated with electric grid," *IEEE Access*, vol. 9, pp. 166 762–166 780, 2021.

[104] M. Yilmaz and P. T. Krein, "Review of the impact of vehicle-to-grid technologies on distribution systems and utility interfaces," *IEEE Transactions on Power Electronics*, vol. 28, no. 12, pp. 5673–5689, 2013.

[105] X. Ren, Z. W. Xu, Z. Zhang, H. Li, M. He, J. Tang *et al.*, "A 1-kv input sic llc converter with split resonant tanks and matrix transformers," *IEEE Transactions on Power Electronics*, vol. 34, no. 11, pp. 10 446–10 457, 2019.

[106] S. A. Zaid, H. Albalawi, K. S. Alatawi, H. W. El-Rab, M. E. El-Shimy, A. Lakhouit *et al.*, "Novel fuzzy controller for a standalone electric vehicle charging station supplied by photovoltaic energy," *Applied Systems Innovation*, vol. 4, no. 3, pp. 1–14, 2021.

[107] H. N. D. Melo, J. P. F. Trovão, P. G. Pereirinha, H. M. Jorge, and C. H. Antunes, "A controllable bidirectional battery charger for electric vehicles with vehicle-to-grid capability," *IEEE Transactions on Vehicular Technology*, vol. 67, no. 1, pp. 114–123, 2018.

[108] M. Ansari, G. Yadav, and M. Singh, "Modified bidirectional llc converter for electric vehicle application," in *Proceedings of the 2023 2nd International Conference on Electrical, Electronics, Information, and Communication Technology (ICEEICT)*, 2023, pp. 1–7.

[109] S. Pirouzi, J. Aghaei, T. Niknam, M. H. Khooban, T. Dragicevic, H. Farahmand *et al.*, "Power conditioning of distribution networks via single-phase electric vehicles equipped," *IEEE Systems Journal*, vol. 13, no. 3, pp. 3433–3442, 2019.

[110] J. Saroha, M. Singh, and D. K. Jain, "Anfis-based add-on controller for unbalanced voltage compensation in a low-voltage microgrid," *IEEE Transactions on Industrial Informatics*, vol. 14, no. 12, pp. 5338–5345, 2018.

[111] S.-i. Amari, "Backpropagation and stochastic gradient descent method," *Neurocomputing*, vol. 5, no. 4-5, pp. 185–196, 1993.

[112] A. Seth and M. Singh, "Unified adaptive neuro-fuzzy inference system control for off board electric vehicle charger," *International Journal of Electrical Power & Energy Systems*, vol. 130, p. 106896, 2021. [Online]. Available: https://doi.org/10.1016/j.ijepes.2021.106896

[113] W. Wei, Y. Zhou, J. Zhu, K. Hou, H. Zhao, Z. Li *et al.*, "Reliability assessment for ac/dc hybrid distribution network with high penetration of renewable energy," *IEEE Access*, vol. 7, pp. 153 141–153 150, 2019.

[114] D. Liang, C. Qin, S. Wang, and H. Guo, "Reliability evaluation of dc distribution power network," in *China International Conference on Electricity Distribution (CICED)*, 2018, pp. 654–658.

[115] S. K. Kim, D. K. Choi, K. B. Lee, and Y. I. Lee, "Offset-free model predictive control for the power control of three-phase ac/dc converters," *IEEE Transactions on Industrial Electronics*, vol. 62, no. 11, pp. 7114–7126, 2015.

[116] X. Chen, M. Shi, J. Zhou, Y. Chen, W. Zuo, J. Wen *et al.*, "Distributed cooperative control of multiple hybrid energy storage systems in a dc microgrid using consensus protocol," *IEEE Transactions on Industrial Electronics*, vol. 67, no. 3, pp. 1968–1979, 2020.

[117] S. K. Kollimalla, M. K. Mishra, A. Ukil, and H. B. Gooi, "Dc grid voltage regulation using new hess control strategy," *IEEE Transactions on Sustainable Energy*, vol. 8, no. 2, pp. 772–781, 2017.

[118] R. Kadri, J. P. Gaubert, and G. Champenois, "An improved maximum power point tracking for photovoltaic grid-connected inverter based on voltage-oriented control," *IEEE Transactions on Industrial Electronics*, vol. 58, no. 1, pp. 66–75, 2011.

[119] D. B. Wickramasinghe Abeywardana, B. Hredzak, and V. G. Agelidis, "A fixed-frequency sliding mode controller for a boost-inverter-based battery-supercapacitor hybrid energy storage system," *IEEE Transactions on Power Electronics*, vol. 32, no. 1, pp. 668–680, 2017.

Chapter 6. Conclusions and Future Scopes

[120] Y. Shan, J. Hu, Z. Li, and J. M. Guerrero, "A model predictive control for renewable energy based ac microgrids without any pid regulators," *IEEE Transactions on Power Electronics*, vol. 33, no. 11, pp. 9122–9126, 2018.

[121] X. Zhang, B. Wang, U. Manandhar, H. B. Gooi, and G. Foo, "A model predictive current controlled bidirectional three-level dc/dc converter for hybrid energy storage system in dc microgrids," *IEEE Transactions on Power Electronics*, vol. 34, no. 5, pp. 4025–4030, 2019.

[122] Y. Shan, J. Hu, K. W. Chan, Q. Fu, and J. M. Guerrero, "Model predictive control of bidirectional dc-dc converters and ac/dc interlinking converters: A new control method for pv-wind-battery microgrids," *IEEE Transactions on Sustainable Energy*, vol. 10, no. 4, pp. 1823–1833, 2019.

[123] J. R. P. A. M. K. Patricio Cortés, "Direct power control of an afe using predictive control," *IEEE Transactions on Power Electronics*, vol. 23, no. 5, pp. 2516–2523, Sep 2008.

[124] A. K. A. R. M. A. S. S. O. Mohamed Lasheen, "Adaptive reference voltage-based mppt technique for pv applications," *IET Renewable Power Generation*, vol. 11, no. 5, pp. 715–722, Mar 2017.

[125] M. Saitou, N. Matsui, and T. Shimizu, "A control strategy of single-phase active filter using a novel d-q transformation," in *Conference Record - IAS Annual Meeting (IEEE Industry Applications Society)*, vol. 2, 2003, pp. 1222–1227.

137

Appendix A

Laboratory setup details

A scaled experimental hardware prototype was developed in the laboratory to execute the proposed control schemes. The design and development of the proposed controller were conducted for validation using experimental methods.Subsequent to software simulation, the VSM control algorithms were assessed and confirmed on a small-scale hardware test-bed, functioning as a real-time application.Simulator in rapid control prototype (RCP) evaluation. The hardware setup includes the following components:

1. Grid power source

2. A transformer AC source voltage

3. Voltage and current sensors

4. A diode rectifier is employed to convert the alternating output voltage into a direct current link voltage.

5. Three phase converters

6. three-phase resistive loads designated for step load testing

7. A real-time simulator executing the control algorithms for the comprehensive test-bed using dSPACE

8. Real-Time Simulator OPAL-RT (OP-4510)

9. Battery bank

10. Solar panel

Appendix A. Laboratory setup details

FIGURE A.1: Laboratory setup

11. PMSG wind emulator

12. Regenerative grid simulator

13. Bidirectional DC power supply

PMSG Wind Emulator–The system includes a front-end converter (FEC) that draws power from the mains and maintains the DC output at a predetermined V_{DC} set value. The inverter uses this DC output from the FEC to supply two machines: inverter-1, which is connected to an induction motor, and inverter-2, which is connected to a PMSM. The induction motor can be controlled either

in open-loop V/F mode or closed-loop vector control using inverter-1, while the PMSM operates in closed-loop vector control using inverter-2.

When functioning as a wind emulator, the induction motor driven by inverter-1 simulates wind turbine characteristics. In this configuration, inverter-1 is set to motoring mode with the wind emulator mode enabled, and inverter-2 is set to generating mode with MPPT mode enabled. The process begins by starting inverter-1 with a preset wind speed value. Without a load, the induction motor gradually accelerates to the maximum speed (as referenced in inverter-1). When inverter-2 is activated, it operates at the optimal speed due to the wind speed information and draws power accordingly. The wind speed can be adjusted within a range of 3 m/s to 8 m/s, even while the system is running.

OPAL-RT (OP-4510)–OPAL-RT (OP-4510) has been used for real-time simulation in Chapter 2 and Chapter 3 to validate MATLAB simulations. The simulator is used for real-time control of power electronic converters. The real-time simulator has multiple probes for input and output channels connected to the host computer and the hardware. The PWM signals are generated to drive the power electronic converter. The control technique is implemented using OPAL-RT software and executed on the central processing unit (CPU) cores of the real-time simulator.

dSPACE–utilizes a digital signal processor (DSP) for the continuous control of inverters. A quick experimentation controller board from dSPACE, the DS1104, is utilized for the hardware design. The DS1104 facilitates the real-time execution of MATLAB/Simulink models. The combination of MATLAB/Simulink with dSPACE allows for quick implementation of changes or entirely new control algorithms in real-time. The DS1104 board also comprises 8 analogue-to-digital conversion (ADC), 8 digital-to-analogue conversion (DAC) channels respectively, 20-bit input/output (I/O) ports,timers,and interrupt controllers. The interface of hardware and software is outlined as follows:

- MATLAB/Simulink functions as an offline simulation tool for the design,modeling, and analysis of controllers.

- The Real-Time Interface augments the Simulink block library by incorporating blocks that enable the integration of Simulink with real-time hardware.

140

FIGURE A.2: dSPACE

Battery Pack

- The Simulink model is converted into real-time code through the Real-Time Workshop (RTW), which automatically produces C-code for the created model.

- The C-code is subsequently uploaded to the dSPACE master or slave unit, preparing it for job execution.

Battery bank–A laboratory bench test experiment is conducted to investigate the behavior of a battery pack when integrated with other energy sources to create a microgrid, utilizing a stack of eight batteries. Each battery is a 12-volt, 7 amp-hour lead-acid type. The batteries are configured in series to create a 96 V large battery. Each battery has a standby voltage between 13.50 V to 13.80 V at the room temperature of 20°C, with a charging voltage between 14.4 V to 15 V for constant voltage charging.

List of Publications

Papers in Refereed Journals

[1] Philemon Yegon and Mukhtiar Singh. Frequency stability enhancement of microgrid using optimization techniques-based adaptive virtual inertia control. *International Transactions on Electrical Energy Systems*, 2023:1–19, 2023. doi: 10.1155/2023/2121721.

[2] Philemon Yegon and Mukhtiar Singh. Optimization of battery/ultra-capacitor hybrid energy storage system for frequency response support in low-inertia microgrid. *IET Power Electronics*, pages 1–15, 2024. doi: 10.1049/pel2.12723.

National and International Conference Proceedings

[1] Philemon Yegon and Mukhtiar Singh. Comparison of control strategies pi, fopid, and anfis controllers in ev system for microgrid interactive system. In *2024 IEEE Third International Conference on Power Electronics, Intelligent Control and Energy Systems (ICPEICES)*, pages 274–279, 2024. doi: 10.1109/ICPEICES62430.2024.10719352.

[2] Philemon Yegon and Mukhtiar Singh. Application of optimization techniques for frequency stability improvement in microgrid. In *2024 International Conference on Electrical Electronics and Computing Technologies (ICEECT)*, pages 1–5, 2024. doi: 10.1109/ICEECT61758.2024.10739301.

[3] Philemon Yegon and Mukhtiar Singh. Unveiling enhanced model predictive control for power regulation in single phase ac/dc converter. In *2024*

142

International Conference on Electrical Electronics and Computing Technologies (ICEECT), pages 1–5, 2024. doi: 10.1109/ICEECT61758.2024.10738998.

[4] Philemon Yegon and Mukhtiar Singh. Performance analysis of adaptive genetic algorithm-based pi and conventional pi for evs integrated to microgrid. In *2024 6th International Conference on Emerging Technologies: Micro to Nano (ETMN)*, pages 1–5, 2024.